University of Milano-Bicocca
Department of Mathematics and Applications

Induction effects of torus knots and unknots

Chiara Oberti

Supervisor:

Professor Renzo L. Ricca

Examination Committee:

Professor Carlo Barenghi
Professor Gunnar Hornig
Doctor Daniel Peralta-Salas

In partial fulfillment of the requirements for the
Degree of Doctor of Philosophy (Dottorato di Ricerca)

September 21, 2015

Abstract

The induction effects due to a steady source field in the shape of a torus knot or unknot filament are analysed in detail. Similar studies for rectilinear, circular or helical geometries have been done in the past, but very little is known for more complex geometries and topologies. Torus knots provide a rare example of closed, space curves of non-trivial topology, that admit a mathematically simple description; for this reason they represent an interesting case study to consider. Moreover, since torus knots are also a good mathematical model for studying braided field line structures, the present work provides useful information for a wide range of possible applications, from physical sciences (solar physics and astrophysics, vortex dynamics, fusion physics) to technology (telecommunication, new materials design, data analysis). The work is organized in 4 chapters.

In chapter 1 we present a comprehensive study of geometric and topological properties of torus knots and unknots. By using a standard parametrization, we demonstrate the existence, and determine the location, of inflection points for a given critical configuration, and prescribe the condition for removing the singularity associated with torsion at the inflection point. We show that, to first approximation, total length grows linearly with the number of coils, and it is proportional to the minimum crossing number of the knot type. By taking the winding number, given by the ratio between meridian and longitudinal wraps, as measure of topological complexity of the knot, we analyse its influence on several global quantities, such as total length, curvature, torsion and writhe.

In chapter 2 we analyse the influence of the winding number and other geometric properties on induction, energy and helicity. This is done by assuming the physical filament of infinitesimally small cross-section and by using the Biot-Savart law adapted for the particular parametrization chosen. Field line patterns of the induced field are obtained for a large family of knots/unknots on several cross-sectional planes. The intensity of the induced field is shown to depend linearly on the number of toroidal coils. We provide bounds on energy, and an estimate of helicity in terms of writhe.

In chapter 3 we compare local and global induction contributions in relation to the winding number, by providing asymptotic expansions of the integrand function. We show that in general local leading order terms are not sufficient to provide accurate global information; nevertheless, for some values of the winding number local and global behaviours are found to be in good agreement.

In chapter 4 we investigate the influence of the winding number on the binormal component of the self-induction a point asymptotically near to the source field. Since in the limit the Biot-Savart integral becomes singular, we apply the analytical prescription of Moore and Saffman (1972) to regularize it. While to leading order the self-induction is proportional to local curvature, we derive an integral formula for next terms, including higher order local terms together with non-local terms, and we study its dependence on the winding number by showing that the dominant contribution is generally given by non-local terms.

Acknowledgements

I thank Professor Renzo Ricca, my supervisor, for his guidance: leading a PhD student, I have understood, is not only teaching how he should do things, but also allowing him to find his own way of expression. Thanks for introducing me to a varied and stimulating scientific community; thanks for giving me the possibility to attend the Intensive Research Period "Knots & Applications" in Pisa, my first international research program, and then many others. My gratitude to the members of my Examination Committee, Professors Carlo Barenghi, Gunnar Hornig and Daniel Peralta-Salas, for the willing time they have dedicated to my work, for their genuine interest and for their comments. I thank De Witt Sumners for some useful mails we exchanged on self-linking and for pointing out reference [22]. I thank Mitch Berger for his routine *Tuba* which I used to plot torus knots, and for his routine on writhe (with Chris Prior) which was useful to check my own calculations.

Thanks to Professors Gianmario Tessitore and Roberto Paoletti, directors of the PhD program in Pure & Applied Mathematics at U. Milano-Bicocca, for their assistance and help. A special thank to Professor Franco Magri, who had been the advisor for my Bachelor Degree's thesis and the first one to show me how much passion a scientist can have for his work; I thank him for his inborn intellectual honesty and for still caring about my progresses. My appreciation to my colleagues at U. Milano-Bicocca, in particular to Simone Camosso and Iman Mehrabi Nezhad.

I kindly acknowledge U. Milano-Bicocca for financial support, and the universities and research institutions I visited during research programs and conferences for their hospitality and support: the Mathematical Research Centre Ennio De Giorgi, Pisa (Italy); the Centre International de Rencontres Mathématiques, Marseilles (France); the Isaac Newton Institute for Mathematical Sciences, Cambridge (UK); the Institute of Theoretical and Applied Physics, Turunç-Marmaris (Turkey); the International Centre for Mathematical Sciences, Edinburgh (UK); the Max Planck Institute for Mathematics in the Sciences, Leipzig (Germany); the University of Glasgow (UK); the Independent University & the Laboratoire Poncelet, Moscow (Russia); the University of Basel (Switzerland).

A heartfelt thank to my family and to Michaël for their constant support, for walking next to me during my ups but also during my downs, and for loving and taking care of me, as simple as that. A sincere thank to Marco for his help as mathematician and as friend. A kind thank to Enza for her friendship.

Contents

Introduction

The first mathematical formulation of the physical law giving the magnetic effects due to an infinitely long, rectilinear, electric wire dates October 30, 1820, when Biot and Savart read in front of the French Royal Academy of Sciences the *Mémoire sur la mesure de l'action exercée à distance sur une particule de magnétisme, par un fil conjonctif* [12]. In this one-page note they state that the measured effects are proportional to the distance from the wire and directed orthogonally to it, acknowledging the first experimental observations by Oersted [42] and the work by Ampère on mutual effects of two straight electric wires, a wire and a magnet, and two magnets [5, 6]. Other communications by Biot and Savart then followed to add further information to their very first statement [13], together with supplementary comments by other scientists, such as Laplace and Ampère, but some of these communications were never published (see [56] pp. 80–127 and 128–140 for a posthumous collection of two extensive communications by Biot & Savart and Ampère, respectively).

A challenging programme on magnetic effects induced by more complex geometries and topologies was undertaken by Tait in the late 1870s. Inspired and motivated by Lord Kelvin's theory of vortex atoms to describe natural laws of physics and energy quantizations in terms of topological properties, he began a tabulation of knots and links ordered according to their minimal number of crossings. Since he was in search for a discriminant to identify different knot-types, he began to investigate the effects of currents in electric wires in the shape of knots, trying to detect the knot-type of the source in terms of its magnetic effects. In particular, he thought that "we might possibly obtain a definite measurement of beknottedness in terms of the work necessary to carry a magnetic pole along the curve, the curve being supposed to be traversed by an electric current: as it obviously must be always the same for the same knot, and must vanish when there is no beknottedness" [57]. After several efforts, on April 3, 1882 Tait had to communicate, in a short note to the Royal Society of Edinburgh, his failed attempts; nevertheless, he managed to classify knots up to 7 crossings (1877, [58]; see [59], plate 44), and then alternating knots up to 10 crossings (1885, [60], plates 80 and 81).

The possibility of extracting geometric and topological properties of an object from emitted signals interested scientists of different areas, being this part of

the general inverse problem to infer information on a source from analysis of its effects; for example Kac addresses the problem of detecting the geometric shape of an elastic membrane with fixed boundary from the algebraic analysis of the eigenvalues of the acoustic wave equation [25]. A similar problem was firstly addressed by Weyl in [62], where he proved a relation between eigenvalues and area of the membrane. Manuar & Jaggar use wave scattering techniques to examine the geometry and topology of a thin scattered wire [32, 33]. In particular they analyse the backscattering of 4 different objects: the trefoil and its related unknot (obtained by local switching of a crossing), and their respective mirror image, finding that the difference in the backscattering is larger between the knot and its unknot (which share the same geometry, except for a neighbourhood of the switched crossing), than between the knot and its mirror image (which share the same topology). Werner, by looking for applications to communication devices, considers small torus knotted electric wires and finds that the far electro-magnetic field is equivalent to that produced by a circular loop [63]. Peralta-Salas *et al.* examine the structure and properties of the induced magnetic field-lines due to several current distributions [23, 3, 2].

Detailed studies of the Biot-Savart induction effects due to circular or helical geometries have been done in the past, but to the best of our knowledge the problem for more complex geometries and topologies is still open. In this thesis, by taking advantage of the rather simple mathematical description of torus knots and unknots, we analyse the geometric and topological effects on the Biot-Savart induction due to a steady field in the shape of a torus knot/unknot. Since circular configurations, as well as non-planar deformations of the circle, can be obtained as degenerate cases from the standard parametrization of torus knots/unknots, it is reasonable to think that this problem falls into the class of elliptic integral problems, to which the Biot-Savart integral on a circular support belongs. Since in ideal flows the Biot-Savart law gives the velocity field induced by vorticity, or, by analogy, the magnetic field induced by an electric current, this work is of interest for applications in fluid dynamics as well as magnetohydrodynamics.

Chapter 1

The geometry of torus knots and unknots

In this chapter we present a comprehensive study of geometric and topological properties of torus knots and unknots. By using a standard parametrization, new results on local and global properties are found. In Sections 1.3–1.5 we present a detailed analysis of local properties. The existence of inflectional configurations for every torus knot/unknot is proven, and we determine the location of the inflection points. We prescribe the condition for removing the singularity associated with torsion at the inflection point and we revise a result on zeros of torsion for knots/unknots in inflectional state. Global properties are discussed in Sections 1.6–1.13. We show that to first approximation total length grows linearly with the number of coils, and it is proportional to the minimum crossing number of the knot type. The dependence on knot complexity, measured by the winding number, of several global quantities such as total curvature and torsion, writhing number, total squared curvature and torsion is investigated. By using the concept of tangent indicatrix, we relate the development of inflectional configurations to the growth in writhing number, and we show how the passage through inflectional state is responsible for the jump of the intrinsic twist of framed torus knots/unknots.

1.1 Torus knots and unknots

By torus knots and unknots we mean particularly symmetric, closed curves, that lie on the surface of a mathematical torus, wrapped uniformly around it. A torus knot or unknot $\mathcal{T}_{p,q}$ wraps p times along the longitudinal (or toroidal) direction and q times along the meridian (or poloidal) direction. Torus knots are obtained by taking $p > 1$, $q > 1$ and p, q co-prime integers [34] (Figure 1.1a). If either p or q is equal to 1, we do *not* have knots, but multiply coiled curves, topologically equivalent to the unknot (Figure 1.1b). The ratio $w = q/p$ is called

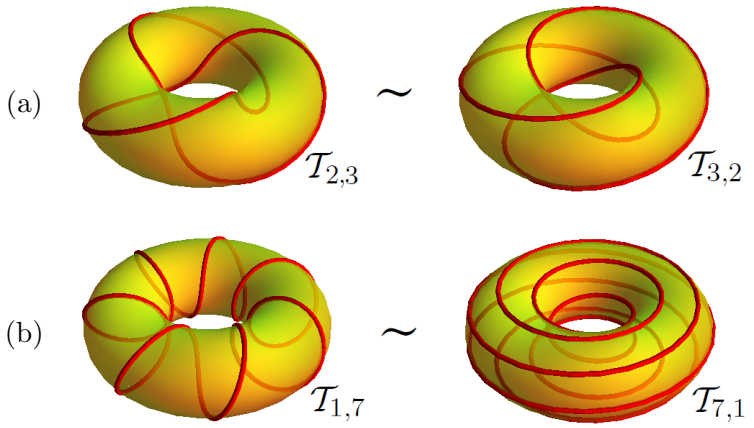

Figure 1.1: (a) Two geometrically different presentations of the same topological knot type. The trefoil knot $\mathcal{T}_{2,3}$ on the left can be deformed to the $\mathcal{T}_{3,2}$ on the right by a continuous deformation, and vice-versa. (b) A poloidal coil $\mathcal{T}_{1,7}$ (left) and a toroidal coil $\mathcal{T}_{7,1}$ (right). These two curves are both topologically equivalent to the unknot.

the *winding number* of $\mathcal{T}_{p,q}$, and it is a rational, positive number, taken here as a measure of the geometric and topological complexity of the knot (or unknot).
For a given, finite value of p, by letting $q \to \infty$, the curve covers entirely the mathematical torus with infinitely many poloidal turns and, in the limit, we obtain a *poloidal hollow ring*. For a given, finite value of q, by letting $p \to \infty$, the curve covers entirely the torus with infinitely many toroidal turns and, in the limit, we obtain a *toroidal hollow ring*.
For given p and q, torus knots $\mathcal{T}_{p,q}$ and $\mathcal{T}_{q,p}$ are topologically equivalent [34], that is, it is possible to deform each knot into the other by continuous deformations and vice-versa; however they have different geometries and they are defined by different equations (Figure 1.1a).
A natural parametrization of a torus knot or unknot with winding number w is given by

$$\mathbf{x}(R, r, w; \alpha) : \begin{cases} x = (R + r\cos w\alpha)\cos\alpha \\ y = (R + r\cos w\alpha)\sin\alpha, \\ z = r\sin w\alpha \end{cases} \qquad \alpha \in [0, 2\pi p) \ , \tag{1.1}$$

where α is the parameter of the curve, R and r are respectively the toroidal and the poloidal radii of the torus. We require $0 < r < R$ in order to avoid degenerate configurations (for $r = 0$ the torus degenerates into a planar circumference of radius R, and for $r \geq R$ the torus self-intersects).
By introducing the non-dimensional quantity $\lambda = r/R$, $\lambda \in (0, 1)$, eqs. (1.1) be-

come

$$\mathbf{x}(R,\lambda,w;\alpha):\begin{cases} x = R(1+\lambda\cos w\alpha)\cos\alpha \\ y = R(1+\lambda\cos w\alpha)\sin\alpha, \\ z = R\lambda\sin w\alpha \end{cases} \qquad \alpha\in[0,2\pi p)\ , \tag{1.2}$$

where λ is the *aspect ratio* of the torus.
For every R and λ, every torus knot and unknot parametrized by eqs. (1.2) is a smooth (i.e C^∞) and simple (i.e. without self-intersections) curve in $\mathbb{R}^3$.

1.2 The symmetry of torus knots and unknots

A torus knot/unknot $\mathcal{T}_{p,q}$ parametrized by eqs. (1.2) can be thought of as generated under the action of a rotational symmetry group by a $(q-1)$-times rigid rotation (around the z-axis and parallel to the (xy)-plane) of the section

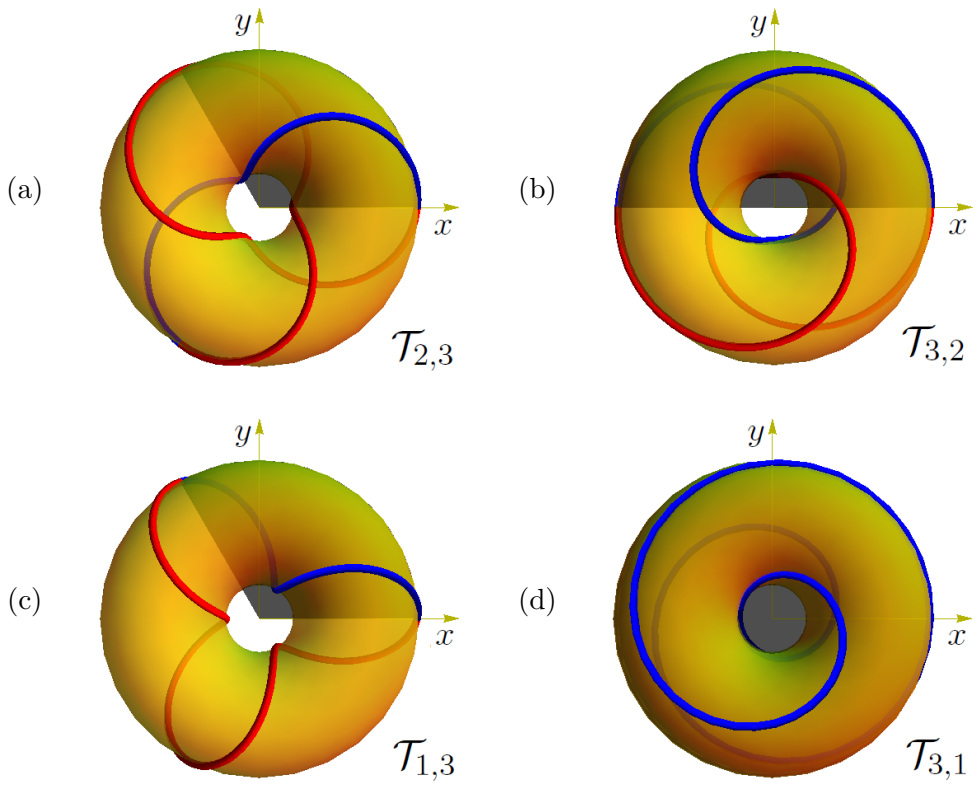

Figure 1.2: Fundamental sections (in blue) and fundamental sectors (darker regions) of torus knots (a) $\mathcal{T}_{2,3}$ and (b) $\mathcal{T}_{3,2}$ and torus unknots (c) $\mathcal{T}_{1,3}$ and (d) $\mathcal{T}_{3,1}$.

of the curve given by $\alpha \in [0, 2\pi/w)$. We shall call this section *fundamental section*. The whole closed curve is therefore recovered from the fundamental section (Figure 1.2). For every torus knot and unknot, its fundamental section presents a central symmetry at $\alpha = \pi/w$, with the two halves of the fundamental section wrapping up and down around the torus anti-symmetrically. Hence, the geometry of the curve, given for example by curvature and torsion information, can be studied on the fundamental section and extended to the whole curve with period $2\pi/w$. Moreover, the central symmetry of the fundamental section implies the axial symmetry of both pointwise curvature and torsion.
Since a torus knot/unknot $\mathcal{T}_{p,q}$ parametrized by eqs. (1.2) appears the same from each of the cross-sectional half-planes at $2k\pi/q$, with $k = 0, ..., q-1$, we can also identify a *fundamental sector* between the half-planes at 0 and $2\pi/q$ (Figure 1.2), a property that will be exploited in the analysis done later on.

1.3 Regularity

Let us consider now a smooth curve γ in $\mathbb{R}^3$, parametrized by $\mathbf{r}(t)$, $t \in [a, b]$. We shall denote by $\dot{\mathbf{r}}(t)$, $\ddot{\mathbf{r}}(t)$ and $\dddot{\mathbf{r}}(t)$ the first, second and third derivative, respectively, of the parametrization with respect to t. The pointwise curvature and torsion of γ are defined by

$$c(t) = \frac{|\dot{\mathbf{r}}(t) \times \ddot{\mathbf{r}}(t)|}{|\dot{\mathbf{r}}(t)|^3} \ , \tag{1.3}$$

$$\tau(t) = \frac{(\dot{\mathbf{r}}(t) \times \ddot{\mathbf{r}}(t)) \cdot \dddot{\mathbf{r}}(t)}{|\dot{\mathbf{r}}(t) \times \ddot{\mathbf{r}}(t)|^2} \ . \tag{1.4}$$

A smooth curve γ with parametrization $\mathbf{r}(t)$ is said to be *regular* if its tangent vector $\dot{\mathbf{r}}(t)$ never vanishes for all $t \in [a, b]$. A point where $\dot{\mathbf{r}}(t_0) = 0$ is said to be a *singular point of order* 0. A point where $\ddot{\mathbf{r}}(t_1) = 0$ in isolation, but $\dot{\mathbf{r}}(t_1) \neq 0$, is said to be a *singular point of order* 1 or an *inflection point*. Equivalently, a point of a smooth and regular curve where curvature vanishes in isolation is called an inflection point. Indeed, non vanishing $\dot{\mathbf{r}}(t)$ and $\ddot{\mathbf{r}}(t)$ are linearly independent for all t, hence, the curvature of a regular curve is zero at a point $r(t_1)$ if and only if $\ddot{\mathbf{r}}(t_1) = 0$. At an inflection point, torsion is singular (where the singularity is integrable [51]). The simplest inflection point is when the singularity of the torsion is removable by continuity, that is when the left and right limit of torsion at the inflection point have finite and equal values. For a regular curve with everywhere non vanishing curvature, the vectors $\dot{\mathbf{r}}(t)$, $\ddot{\mathbf{r}}(t)$ and $\dddot{\mathbf{r}}(t)$ are linearly independent if and only if $(\dot{\mathbf{r}}(t) \times \ddot{\mathbf{r}}(t)) \cdot \dddot{\mathbf{r}}(t) \neq 0$. Hence, the torsion of a regular curve with everywhere non vanishing curvature is zero at a point $r(t_3)$ if and only if $\dot{\mathbf{r}}(t_3)$, $\ddot{\mathbf{r}}(t_3)$ and $\dddot{\mathbf{r}}(t_3)$ are linearly dependent. The case when $\dddot{\mathbf{r}}(t_3) = 0$ is just a special case for which $\dot{\mathbf{r}}(t_3)$, $\ddot{\mathbf{r}}(t_3)$ and $\dddot{\mathbf{r}}(t_3)$ are linearly dependent.

For torus knots and unknots parametrized by eqs. (1.2), we have:

$$\begin{aligned}
\dot{\mathbf{x}}(R,\lambda,w;\alpha) =& R\begin{pmatrix} -(1+\lambda\cos w\alpha)\sin\alpha - \lambda w\cos\alpha\sin w\alpha \\ (1+\lambda\cos w\alpha)\cos\alpha - \lambda w\sin\alpha\sin w\alpha \\ \lambda w\cos w\alpha \end{pmatrix}, \\
\ddot{\mathbf{x}}(R,\lambda,w;\alpha) =& R\begin{pmatrix} -(1+\lambda\cos w\alpha+\lambda w^2\cos w\alpha)\cos\alpha + 2\lambda w\sin\alpha\sin w\alpha \\ -(1+\lambda\cos w\alpha+\lambda w^2\cos w\alpha)\sin\alpha - 2\lambda w\cos\alpha\sin w\alpha \\ -\lambda w^2\sin w\alpha \end{pmatrix}, \\
\dddot{\mathbf{x}}(R,\lambda,w;\alpha) =& R\begin{pmatrix} (1+\lambda\cos w\alpha+3\lambda w^2\cos w\alpha)\sin\alpha + (3+w^2)\lambda w\cos\alpha\sin w\alpha \\ -(1+\lambda\cos w\alpha+3\lambda w^2\cos w\alpha)\cos\alpha + (3+w^2)\lambda w\sin\alpha\sin w\alpha \\ -\lambda w^3\cos w\alpha \end{pmatrix}.
\end{aligned} \tag{1.5}$$

We can prove the following result:

Proposition 1.1. *Every torus knot and unknot parametrized by* eqs. (1.2)*, is a regular curve.*

Proof. For considerations on the symmetry of torus knots/unknots, it is sufficient to prove that, for every $w \in (0,+\infty)\cap\mathbb{Q}$, $R \in (0,+\infty)$ and $\lambda \in (0,1)$,

$$\dot{\mathbf{x}}(R,\lambda,w;\alpha) = R\begin{pmatrix} -(1+\lambda\cos w\alpha)\sin\alpha - \lambda w\cos\alpha\sin w\alpha \\ (1+\lambda\cos w\alpha)\cos\alpha - \lambda w\sin\alpha\sin w\alpha \\ \lambda w\cos w\alpha \end{pmatrix} \neq 0 \ \ \forall\ \alpha \in \left[0, \frac{2\pi}{w}\right). \tag{1.6}$$

Let us assume the first and second components of $\dot{\mathbf{x}}$ to vanish: we prove that the third is never zero. From the second component we have

$$1+\lambda\cos w\alpha = \frac{\lambda w\sin\alpha\sin w\alpha}{\cos\alpha} \quad \text{for} \quad \alpha \neq \frac{\pi}{2} + k\pi,\ k\in\mathbb{Z}\ . \tag{1.7}$$

By substituting eq. (1.7) into the first component, we have

$$\lambda w\sin w\alpha = 0\ . \tag{1.8}$$

Solutions to eq. (1.8) are given by $\alpha = 0$ and $\alpha = \dfrac{\pi}{w}$; for both of these values, the third component never vanishes.
For $\alpha = \dfrac{\pi}{2} + k\pi, k\in\mathbb{Z}$, the first component becomes

$$\left[-\sin\left(\frac{\pi}{2}+k\pi\right)\right]\cdot\left[1+\lambda\cos\left(w\left(\frac{\pi}{2}+k\pi\right)\right)\right] = 0\ , \tag{1.9}$$

and since

$$\sin\left(\frac{\pi}{2}+k\pi\right) \neq\ 0 \quad \forall\ k\in\mathbb{Z}\ , \tag{1.10}$$

we have

$$\cos\left(w\left(\frac{\pi}{2}+k\pi\right)\right) = -\frac{1}{\lambda}\ . \tag{1.11}$$

By eq. (1.11) the third component evaluated at $\alpha = \dfrac{\pi}{2} + k\pi, k\in\mathbb{Z}$, never vanishes. □

1.4 Curvature

The study of the existence of inflectional configurations is interesting for the geometric characterization of torus knots and unknots as curves in $\mathbb{R}^3$ as well as for applications. Given a $\mathcal{T}_{p,q}$ of winding number w, its geometric shape depends on the supporting torus by changing the values of the aspect ratio λ. The following result states that there exists a unique torus of aspect ratio $\lambda = \lambda(w)$ on which $\mathcal{T}_{p,q}$ has inflection point in isolation.

Theorem 1.2 (Fuller Jr, [21, 22])**.** *Let $\mathcal{T}_{p,q}$ be a torus knot or unknot with winding number w on a torus of aspect ratio λ. Then $\mathcal{T}_{p,q}$ has points of zero curvature (in isolation) for only one value of $\lambda = \lambda_{cr} = \dfrac{1}{1+w^2}$. For $\lambda = \lambda_{cr}$ there are exactly q points of vanishing curvature on $\mathcal{T}_{p,q}$, all lying on the innermost longitudinal circle of the torus.*

We shall call $\lambda_{cr} = \lambda_{cr}(w)$ the *critical aspect ratio* for $\mathcal{T}_{p,q}$. By considering λ as a kinematic parameter, eqs. (1.2) provide a kinematic description of a deformation process of the curve through an inflectional configuration.
The existence of a critical aspect ratio λ_{cr} for $\mathcal{T}_{p,q}$ (and hence for $\lambda = \lambda_{cr}$, the existence of q inflection points on $\mathcal{T}_{p,q}$) can be easily proved. By evaluating the curvature of $\mathcal{T}_{p,q}$ (see the definition given by eq. (1.3)) at the point $\mathbf{Q}$ for $\alpha = \pi/w$, we have

$$c\left(R, \lambda, w; \frac{\pi}{w}\right) = \frac{1 - \lambda - \lambda w^2}{R(1-\lambda)^2 + \lambda^2 w^2} \ . \tag{1.12}$$

Hence,

$$c\left(R, \lambda, w; \frac{\pi}{w}\right) = 0 \quad \Leftrightarrow \quad 1 - \lambda - \lambda w^2 = 0 \quad \Leftrightarrow \quad \lambda = \lambda_{cr} = \frac{1}{1+w^2} \ . \tag{1.13}$$

The point $\mathbf{Q}$ is in the fundamental section, which has $q-1$ repeats along the closed curve, and is defined for $\alpha \in [0, 2\pi/w)$, hence the points at

$$\alpha = \frac{\pi}{w} + \frac{2k\pi}{w} \ , \quad k = 0, 1, ..., q-1 \ , \tag{1.14}$$

are the q inflection points of $\mathcal{T}_{p,q}$.
The result of Theorem 1.2 is proven if and only if:

1. for $\lambda = \lambda_{cr}$, $\mathcal{T}_{p,q}$ has no more than q inflection points;
2. $\lambda = \lambda_{cr}$ is the only critical aspect ratio for $\mathcal{T}_{p,q}$.

Fuller Jr's proof of Theorem 1.2 relies on the geodesic and normal components of curvature.
Because of symmetry considerations, the position of the inflection points on $\mathcal{T}_{p,q}$ can be determined according to the following result.

Corollary 1.3. *Every critical torus knot/unknot $\mathcal{T}_{p,q}$ with $\lambda = \lambda_{cr}(w)$ has an inflection point at $\alpha = \pi/w$ in the middle of the fundamental section, and $q-1$ repeats obtained by rotating $q-1$ times the fundamental section along the torus.*

In Figure 1.3 and Figure 1.4 we show the curvature period for several torus knots and unknots ($R = 1$) with different λ. The curvature of every torus knot/unknot with $\lambda \neq \lambda_{cr}$ never vanishes. The pair (λ, α) for which curvature vanishes in the fundamental section is given by

$$(\lambda, \alpha) = \left(\frac{1}{1+w^2}, \frac{\pi}{w} \right) \ , \tag{1.15}$$

and the inflection point is placed at the middle of the curvature period. For example, the torus knot $\mathcal{T}_{2,3}$ (Figure 1.3a) has $\lambda_{cr} = 4/13$ with inflection point at $\alpha = 2\pi/3$ (in the middle of the curvature period of $4\pi/3$); there are 3 inflection points in total, the other two are at $\alpha = 2\pi$ and $\alpha = 10\pi/3$.
As $\lambda \to \lambda_{cr}$, the curvature c develops two maxima. When $\lambda \to 0$, the torus collapses to the standard circle of radius $R = 1$. Hence, when toroidal wraps dominate, $c \to 1/R$ when $\lambda \to 0$ (see, for example, in the right-hand side diagrams of Figure 1.3 and 1.4, when $\lambda = 0.1$ (red)). When poloidal wraps dominates, when $\lambda \to 1$, then the curvature approximates that of the cross-sectional circle of radius λ, that is $c \to 1/\lambda$ (see Figure 1.3e and 1.4e for $\lambda = 0.9$ (blue)).

1.5 Torsion

We are interested in the behaviour of torsion in the neighbourhood of the inflection point. For this it is sufficient to study the torsion in the fundamental section. Let us denote by $\alpha_{cr}(w) = \pi/w$ the value of α for which a $\mathcal{T}_{p,q}$ with $\lambda = \lambda_{cr}(w)$ has an inflection point. As expected, the denominator of

$$\tau\left(R, \lambda_{cr}, w; \alpha_{cr}\right) \tag{1.16}$$

vanishes and torsion is singular. Note that, since $\lambda_{cr}(w)$ and $\alpha_{cr}(w)$ are only functions of w, $\tau\left(R, \lambda_{cr}, w; \alpha_{cr}\right)$ is only a function of R and w as well.

Theorem 1.4. *For every $\mathcal{T}_{p,q}$ of winding number w with $\lambda = \lambda_{cr}(w)$, the singularity of the torsion at the inflection point is removable by continuity by setting*

$$\tau\left(R, \lambda_{cr}, w; \alpha_{cr}\right) := -\frac{\left(10 + 7w^2 + w^4\right)\left(1 + w^2\right)}{2Rw\left(2 + w^2\right)^2} \ . \tag{1.17}$$

Proof. Taylor's expansion of the numerator $N_\tau\left(R, \lambda_{cr}, w; \alpha\right)$ and denominator $D_\tau\left(R, \lambda_{cr}, w; \alpha\right)$ of $\tau\left(R, \lambda_{cr}, w, \alpha\right)$ near $\alpha = \alpha_{cr}$ gives

$$\begin{aligned} N_\tau\left(R, \lambda_{cr}, w; \alpha\right) &= n_2 \left(\alpha - \frac{\pi}{w}\right)^2 + n_4 \left(\alpha - \frac{\pi}{w}\right)^4 + \ldots \ , \\ D_\tau\left(R, \lambda_{cr}, w; \alpha\right) &= d_2 \left(\alpha - \frac{\pi}{w}\right)^2 + d_4 \left(\alpha - \frac{\pi}{w}\right)^4 + \ldots \ , \end{aligned} \tag{1.18}$$

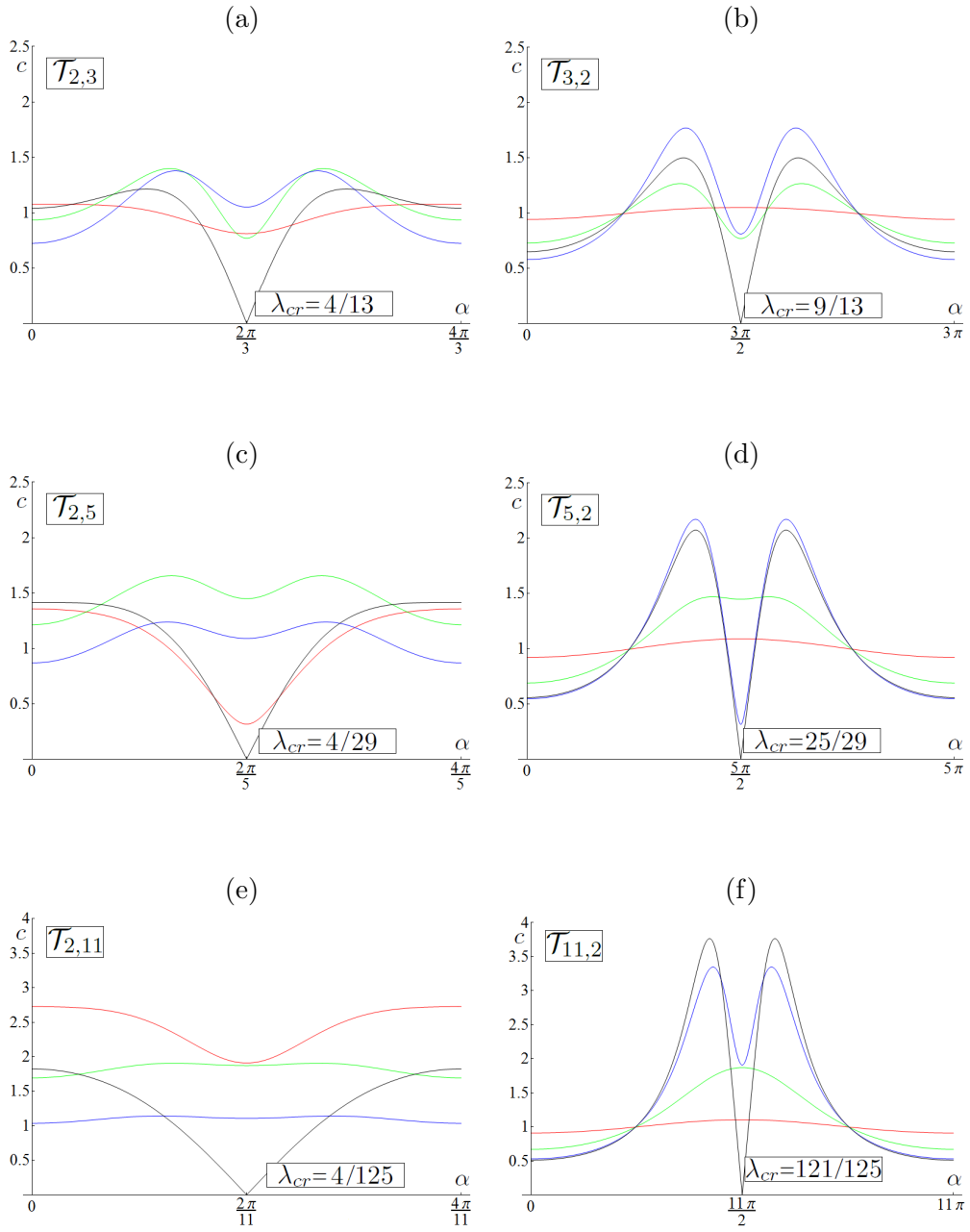

Figure 1.3: One period of curvature c versus α, for several knot types ($R = 1$); $\lambda = 0.1$ (red), $\lambda = 0.5$ (green), $\lambda = 0.9$ (blue) and $\lambda = \lambda_{cr}$ (black).

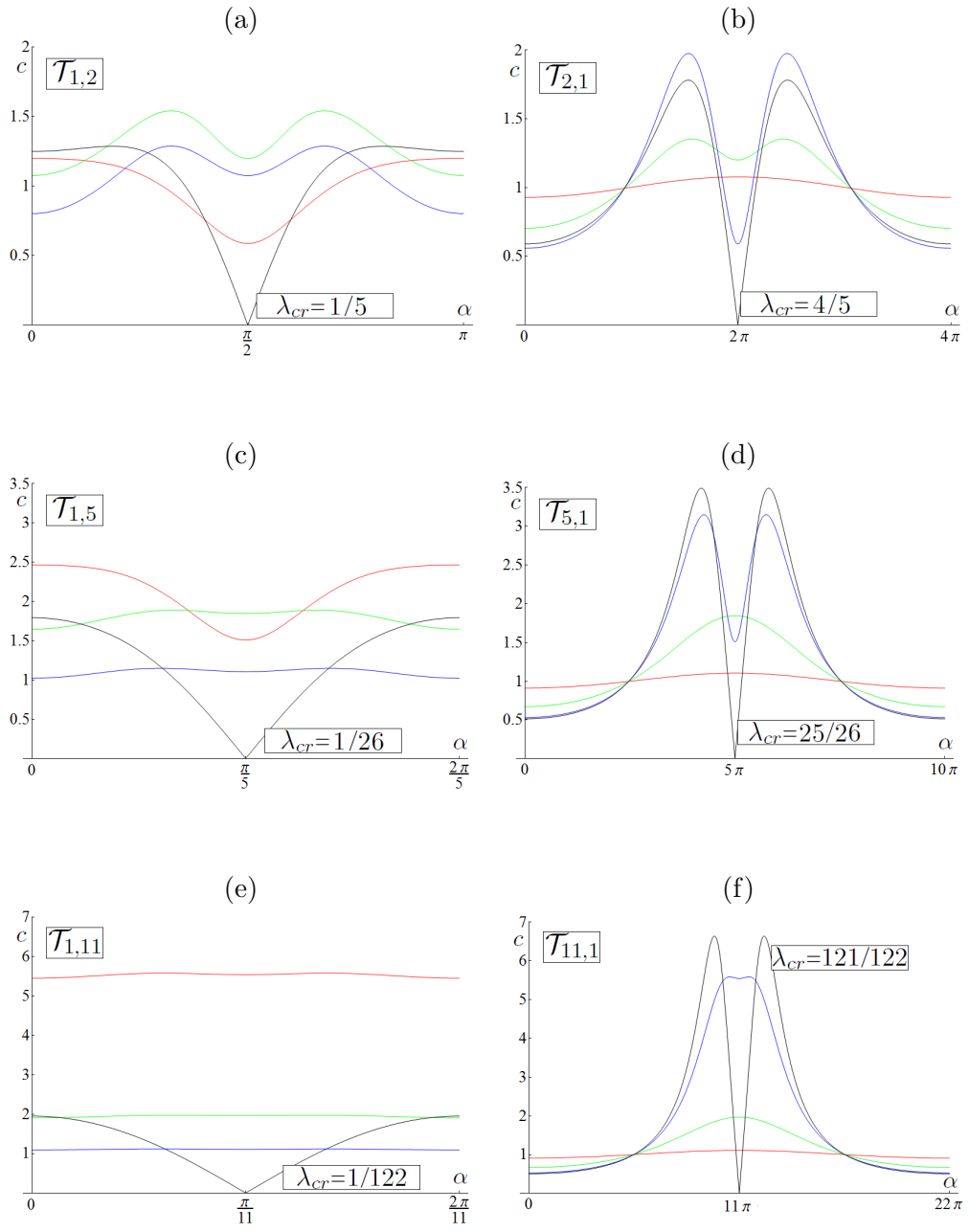

Figure 1.4: One period of curvature c versus α, for several unknot types ($R = 1$); $\lambda = 0.1$ (red), $\lambda = 0.5$ (green), $\lambda = 0.9$ (blue) and $\lambda = \lambda_{cr}$ (black).

where

$$n_2 = -\frac{R^3 w^5 \left(10 + 7w^2 + w^4\right)}{2\left(1 + w^2\right)^3} \ , \quad n_4 = \frac{R^3 w^5 \left(-6 + 64w^2 + 31w^4 + w^6\right)}{24\left(1 + w^2\right)^3} \ ,$$
$$d_2 = \frac{R^4 w^6 \left(2 + w^2\right)^2}{\left(1 + w^2\right)^4} \ , \qquad d_4 = \frac{R^4 w^6 \left(3 + 29w^2 + 5w^4 - w^6\right)}{12\left(1 + w^2\right)^4} \ . \tag{1.19}$$

Hence,

$$\tau\left(R, \lambda_{cr}, w; \alpha\right) = \frac{n_2 \left(\alpha - \frac{\pi}{w}\right)^2 \left(1 + \frac{n_4}{n_2}\left(\alpha - \frac{\pi}{w}\right)^2 + ...\right)}{d_2 \left(\alpha - \frac{\pi}{w}\right)^2 \left(1 + \frac{d_4}{d_2}\left(\alpha - \frac{\pi}{w}\right)^2 + ...\right)} \underset{\alpha \to \frac{\pi}{w}}{\longrightarrow} \frac{n_2}{d_2} \ , \tag{1.20}$$

where

$$\frac{n_2}{d_2} = -\frac{\left(10 + 7w^2 + w^4\right)\left(1 + w^2\right)}{2Rw\left(2 + w^2\right)^2} \tag{1.21}$$

and since the denominator of eq. (1.21) never vanishes, the limit is finite. Thus, the singularity of torsion for $\alpha = \alpha_{cr}$ can be removed by continuity by setting

$$\tau\left(R, \lambda_{cr}, w; \alpha_{cr}\right) := -\frac{\left(10 + 7w^2 + w^4\right)\left(1 + w^2\right)}{2Rw\left(2 + w^2\right)^2} \ . \tag{1.22}$$

□

Since eq. (1.17) never vanishes for all w, we have:

Corollary 1.5. *For every $\mathcal{T}_{p,q}$ of winding number w with $\lambda = \lambda_{cr}(w)$, the value of torsion at the inflection point (*eq. (1.17)*) is never zero.*

In Figure 1.5 and Figure 1.6 we show the diagrams of one period of torsion versus α for several knot/unknot types ($R = 1$). For each knot/unknot in inflectional configuration, the singularity of torsion at the inflection point is removed by applying eq. (1.17). The negative value of torsion is due to the parametrization chosen. By replacing the third equation of the parametrization eqs. (1.2) with $z = -R\lambda \sin w\alpha$, we obtain graphs that are axially symmetric with respect to the x-axis.
The more the aspect ratio approaches λ_{cr}, the more marked becomes the variation in the values of torsion with respect to α. If $\lambda \to \lambda_{cr}^-$ then torsion has a positive, global maximum value; if $\lambda \to \lambda_{cr}^+$ then torsion has a negative, global minimum value (λ_{cr}^- and λ_{cr}^+ denote the left- and right-hand limit respectively). The maximum (or minimum) is reached at $\alpha = \pi/w$, which is the α_{cr} in the limit $\lambda = \lambda_{cr}$. When considering the deformation with kinematic parameter λ of a $\mathcal{T}_{p,q}$, this behaviour of the torsion for $\lambda \approx \lambda_{cr}$ is responsible to the jump discontinuity

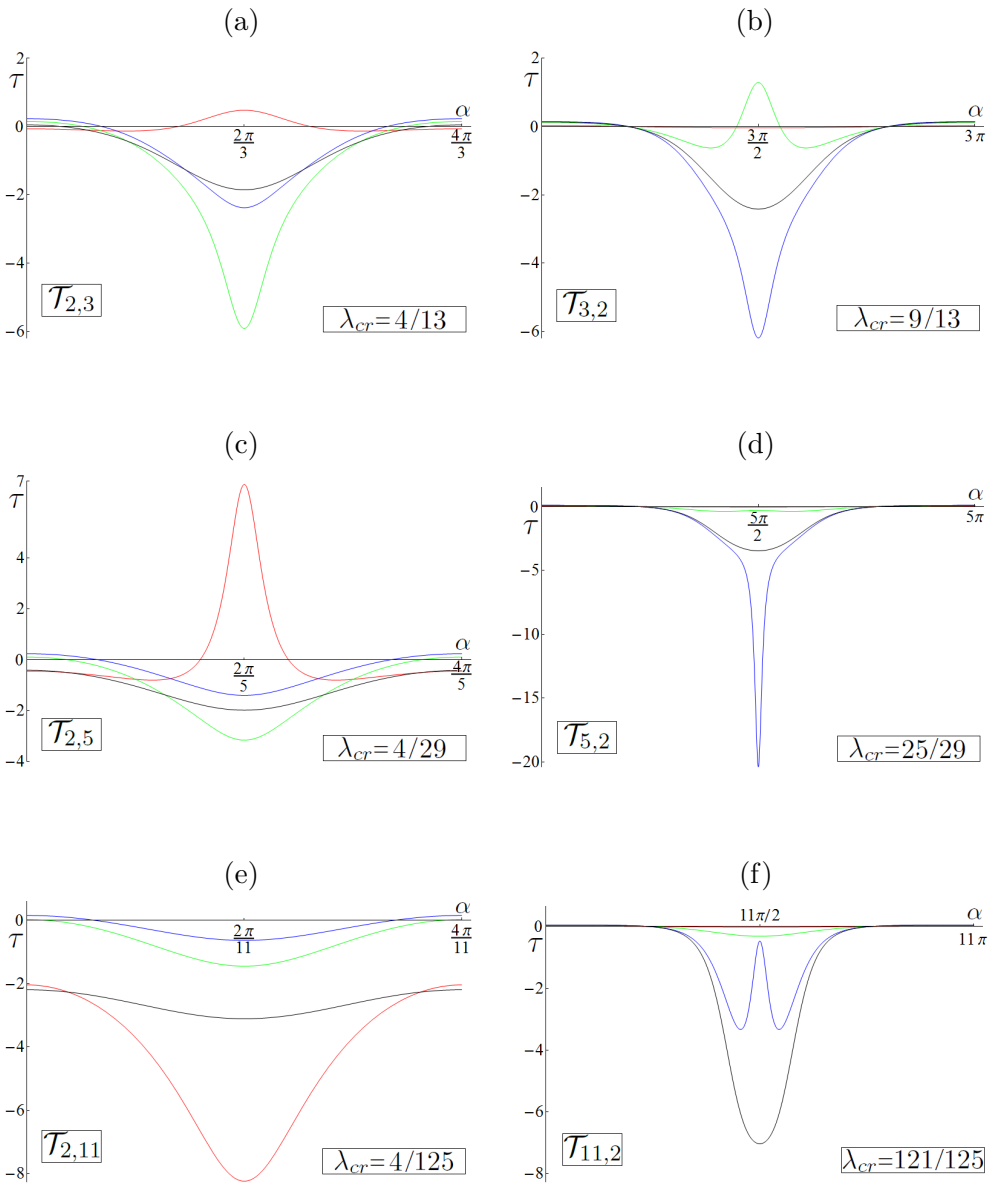

Figure 1.5: One period of torsion τ versus α, for several knot types ($R = 1$); $\lambda = 0.1$ (red), $\lambda = 0.5$ (green), $\lambda = 0.9$ (blue) and $\lambda = \lambda_{cr}$ (black).

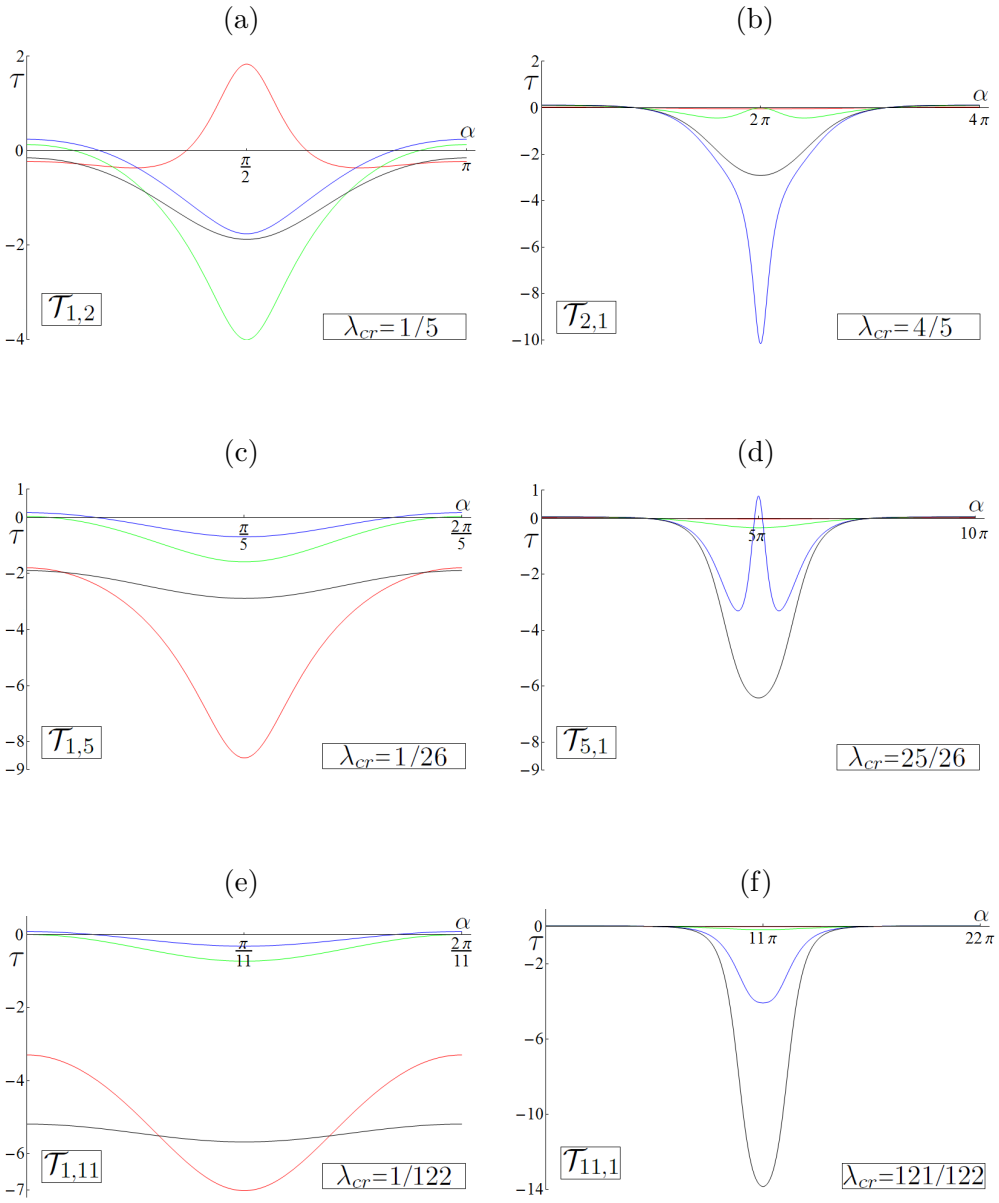

Figure 1.6: One period of torsion τ versus α, for several unknot types ($R = 1$); $\lambda = 0.1$ (red), $\lambda = 0.5$ (green), $\lambda = 0.9$ (blue) and $\lambda = \lambda_{cr}$ (black).

of the total torsion as a function of λ as $\mathcal{T}_{p,q}$ passes through the inflectional configuration (see [39]).
Torus knots/unknots with dominant toroidal wraps for λ small are almost planar curves, hence torsion is nearly zero everywhere (right columns of Figure 1.5 and 1.6, in red). For torus knots/unknots with dominant poloidal wraps for λ large since each poloidal turn lies almost in the cross-sectional plane, torsion assumes values next to zero (Figure 1.5e and 1.6e, in blue).
When torus knots/unknots have dominant toroidal wraps, then they have points of zero torsion for every λ (right columns of Figure 1.5 and 1.6). On the contrary, there exist some torus knots/unknots with dominant poloidal wraps with nowhere vanishing torsion (Figure 1.5e and 1.6c and e).

Theorem 1.6 (Rodriguez Costa, [53])**.** *A torus knot or unknot $\mathcal{T}_{p,q}$ of winding number w with aspect ratio λ, is of non-vanishing torsion if and only if the following two conditions are both satisfied:*

$$\begin{aligned} &\text{(i)} \quad w^2 > 1 \ , \\ &\text{(ii)} \quad \frac{1}{w^2+1} < \lambda < \frac{w^2-1}{2w^2+1} \ . \end{aligned} \tag{1.23}$$

In [53] Rodriguez Costa considers also open, dense curves on the torus (that is when w is irrational). Note that the lower bound in (ii) is the critical aspect ratio $\lambda_{cr}(w)$. Clearly, from

$$\frac{1}{w^2+1} < \frac{w^2-1}{2w^2+1} \ , \tag{1.24}$$

we must have

$$w^4 - 2w^2 - 2 > 0 \ . \tag{1.25}$$

By solving eq. (1.25), we obtain:

Corollary 1.7 (Rodriguez Costa, [53])**.** *A torus knot/unknot $\mathcal{T}_{p,q}$ of winding number w admits configurations of non-vanishing torsion for some aspect ratio λ if and only if*

$$w^2 > 1 + \sqrt{3} \ . \tag{1.26}$$

The knot $\mathcal{T}_{2,11}$, for example, has $w = 11/2 > \sqrt{1+\sqrt{3}}$ and hence admits configurations of non-vanishing torsion for $4/125 < \lambda < 39/82$. A realization is given by $\lambda = 0.1$ (Figure 1.5e, red). However, the torsion of $\mathcal{T}_{2,11}$ is non-vanishing also for $\lambda = \lambda_{cr} = 4/125$ (black), while the left inequality in (ii) is strict.
Rodriguez Costa proves Theorem 1.6 by searching the conditions on λ and w for which the vectors $\dot{\mathbf{x}}(R,\lambda,w;\alpha)$, $\ddot{\mathbf{x}}(R,\lambda,w;\alpha)$ and $\dddot{\mathbf{x}}(R,\lambda,w;\alpha)$ are linearly independent for all α. However, the statement "$\dot{\mathbf{x}}(R,\lambda,w;\alpha)$, $\ddot{\mathbf{x}}(R,\lambda,w;\alpha)$ and $\dddot{\mathbf{x}}(R,\lambda,w;\alpha)$ are linearly independent for all α" is equivalent to "torsion never

vanishes for all α" if and only if $\ddot{\mathbf{x}}(R, \lambda, w; \alpha) \neq 0$ for every α. From section 1.4 we know that for every w and $\lambda = \lambda_{cr}(w)$ there exists $\alpha = \alpha_{cr}(w)$ for which $\ddot{\mathbf{x}}(R, \lambda_{cr}, w; \alpha_{cr}) = 0$. Thus, Theorem 1.6 and Corollary 1.7 hold true if and only if $\lambda \neq \lambda_{cr}$; for $\lambda = \lambda_{cr}$ possible zeros of $\tau(R, \lambda_{cr}, w; \alpha)$ should be studied by a different approach. We can prove the following result:

Proposition 1.8. *A $\mathcal{T}_{p,q}$ with winding number w and $\lambda = \lambda_{cr}$ has everywhere non-vanishing torsion if and only if*

$$w^2 > 1 + \sqrt{3} \ . \tag{1.27}$$

Proof. The numerator $N_\tau(R, \lambda_{cr}, w; \alpha)$ of torsion is

$$4w^2 + 6w^4 + 2w^6 - \cos w\alpha \left(2 + 14w^2 + 8w^4\right) + \cos^2 w\alpha \left(-2 + 2w^2\right) \ ; \tag{1.28}$$

We search conditions on w for which $N_\tau(R, \lambda_{cr}, w; \alpha) = 0$ for some α. By setting $t = \cos w\alpha$, $-1 \leq t \leq 1$, we obtain a polynomial of degree at most two in t. If $w = \pm 1$, the polynomial is reduced to

$$12 - 24t = 0 \ , \tag{1.29}$$

and the solution is $t = 1/2$.
Let us now assume $w \neq \pm 1$; the polynomial is given by

$$4w^2 + 6w^4 + 2w^6 - t\left(2 + 14w^2 + 8w^4\right) + t^2\left(-2 + 2w^2\right) = 0 \ , \tag{1.30}$$

and solutions are given by

$$t_{+,-} = \frac{1 + 7w^2 + 4w^4}{2\left(-1 + w^2\right)} \pm \frac{\sqrt{1 + 22w^2 + 61w^4 + 48w^6 + 12w^8}}{2\left(-1 + w^2\right)} \ . \tag{1.31}$$

We admit only those solutions for which

$$-1 \leq t_{+,-} \leq 1 \ . \tag{1.32}$$

Let us first consider

$$-1 \leq t_{+} \leq 1 \ . \tag{1.33}$$

Solutions to the left-hand side inequality are $w \in \mathbb{R} \setminus \{-1, 1\}$. Solutions to the right-hand side inequality are $-1 < w < 1$. Hence, solutions to eq. (1.33) are $-1 < w < 1$.
Let us now consider

$$-1 \leq t_{-} \leq 1 \ . \tag{1.34}$$

Solutions to the left-hand side inequality are $w < -1$, $w > 1$ or $w = 0$. Solutions to the right-hand side inequality are $-\sqrt{1 + \sqrt{3}} \leq w < -1$ or $1 < w \leq \sqrt{1 + \sqrt{3}}$. Hence, solutions to eq. (1.34) are $-\sqrt{1 + \sqrt{3}} \leq w < -1$ or $1 < w \leq \sqrt{1 + \sqrt{3}}$.
Thus, among the solutions eq. (1.31) we can admit only those for $-\sqrt{1 + \sqrt{3}} \leq w \leq \sqrt{1 + \sqrt{3}}$, $w \neq \pm 1$. Hence, $N_\tau(R, \lambda_{cr}, w; \alpha) = 0$ for some α if and only if $-\sqrt{1 + \sqrt{3}} \leq w \leq \sqrt{1 + \sqrt{3}}$. Thus, $\tau(R, \lambda_{cr}, w; \alpha)$ never vanishes if and only if $w < -\sqrt{1 + \sqrt{3}}$ or $w > \sqrt{1 + \sqrt{3}}$. □

By Proposition 1.8, the revised version of Theorem 1.6 and Corollary 1.7 is:

Theorem 1.9. *A torus knot/unknot $\mathcal{T}_{p,q}$ admits configurations of non-vanishing torsion if and only if its winding number satisfies*

$$w^2 > 1 + \sqrt{3} \ , \tag{1.35}$$

and its aspect ratio satisfies

$$\lambda_{cr} \leq \lambda < \frac{w^2 - 1}{2w^2 + 1} \ . \tag{1.36}$$

1.6 Total length

In this section and in the following ones we investigate the relationship between global geometric quantities and torus knots/unknots complexity, given by the winding number.
The total length of a torus knot/unknot $\mathcal{T}_{p,q}$ is given by

$$L = \int_0^{2\pi p} |\dot{\mathbf{x}}(R, \lambda, w; \alpha)| d\alpha = R \int_0^{2\pi p} \sqrt{(1 + \lambda \cos w\alpha)^2 + \lambda^2 w^2} \ d\alpha \ . \tag{1.37}$$

We non-dimensionalize eq. (1.37) by normalizing it with respect to a reference total length, which we choose to be $L_0 = 2\pi R$, the total length of the centreline of the mathematical torus. The non-dimensional total length is given by

$$\overline{L} = \frac{1}{2\pi} \int_0^{2\pi p} \sqrt{(1 + \lambda \cos w\alpha)^2 + \lambda^2 w^2} \ d\alpha \ . \tag{1.38}$$

Theorem 1.10. *Let $\mathcal{T}_{p,q}$ be a torus knot/unknot of non-dimensional length $\overline{L}$ given by* eq. (1.38)*. We have:*

$$\begin{aligned} &\text{(i)} \quad \textit{for given } p, \textit{ if } q \gg p, \textit{ then } \overline{L} \approx \lambda q \ ; \\ &\text{(ii)} \quad \textit{for given } q, \textit{ if } p \gg q, \textit{ then } \overline{L} \approx (1 + \lambda) p \ . \end{aligned} \tag{1.39}$$

Proof. By writing $w = q/p$ in eq. (1.38), we obtain

$$\overline{L} = \frac{1}{2\pi} \int_0^{2\pi p} \sqrt{\left(1 + \lambda \cos\left(\frac{q}{p}\alpha\right)\right)^2 + \lambda^2 \frac{q^2}{p^2}} \ d\alpha \ . \tag{1.40}$$

Let us fix p; for $q \gg p$ we have

$$\overline{L} \approx \frac{1}{2\pi} \int_0^{2\pi p} \lambda \frac{q}{p} \ d\alpha = \lambda q \ . \tag{1.41}$$

Let us fix q; for $p \gg q$, we have

$$\overline{L} \approx \frac{1}{2\pi} \int_0^{2\pi p} (1 + \lambda) \, d\alpha = (1 + \lambda) \, p \ . \tag{1.42}$$

□

In Figure 1.7 we show the non-dimensional total length of several torus knots for different aspect ratios. If the number q of poloidal wraps is fixed, then $\overline{L}$ grows linearly with p. Conversely, if p is kept fixed, then $\overline{L}$ grows linearly with q. $\overline{L}$ of a $\mathcal{T}_{p,q}$ with $w < 1$ is larger than $\overline{L}$ of its isotope, with $w > 1$. This is justified by the presence of a further positive addendum in eq. (1.42) in comparison with eq. (1.41). For torus knots with dominant poloidal wraps $\overline{L}$ is strongly influenced by variation in λ, whereas for torus knots with dominant toroidal wraps it is almost uninfluenced. The same holds true for torus unknots as well.

The minimum crossing number $c_{\min}$ of torus knots is simply given by [41]

$$c_{\min}(\mathcal{T}_{p,q}) = \min\left(p(q-1), q(p-1)\right) \ . \tag{1.43}$$

It is a topological invariant of torus knots (for example, $c_{\min}(\mathcal{T}_{2,3}) = c_{\min}(\mathcal{T}_{3,2}) = 3$) and it provides a useful measure of the topological complexity of torus knots. For torus knots with $q > p$, it is $q(p-1) < p(q-1)$; hence $c_{\min} = q(p-1)$. For torus knots with $p > q$, it is $p(q-1) < q(p-1)$; hence $c_{\min} = p(q-1)$. Let us fix p; for $q \gg p$, by combining eq. (1.41) and $c_{\min} = q(p-1)$, we obtain

$$\overline{L} \approx \frac{\lambda}{p-1}\, c_{\min} \ . \tag{1.44}$$

Let us fix q; for $p \gg q$, by combining eq. (1.42) and $c_{\min} = p(q-1)$, we obtain

$$\overline{L} \approx \frac{1+\lambda}{q-1}\, c_{\min} \ . \tag{1.45}$$

Eqs. (1.44) and (1.45) provide a very simple linear relation between $\overline{L}$ and $c_{\min}$ of torus knots (the linearity coefficients depending on the respective prevalence of poloidal or toroidal wraps).

In Fig 1.8 we show $\overline{L}$ against w of several torus knots/unknots, for different values of λ. Torus knots/unknots $\mathcal{T}_{p,q}$ are divided in two families, with $w < 1$ and $w > 1$.

Lower and upper bounds on $\overline{L}$ are given here. Since, for every α and w, $-1 \le \cos w\alpha \le 1$, we have

$$\sqrt{(1-\lambda)^2 + \lambda^2 w^2} \le \sqrt{(1+\lambda\cos w\alpha)^2 + \lambda^2 w^2} \le \sqrt{(1+\lambda)^2 + \lambda^2 w^2} \ . \tag{1.46}$$

Hence, by eqs. (1.46) and (1.38), we obtain

$$\frac{1}{2\pi}\int_0^{2\pi p} \sqrt{(1-\lambda)^2 + \lambda^2 w^2}\, d\alpha \le \overline{L} \le \frac{1}{2\pi}\int_0^{2\pi p} \sqrt{(1+\lambda)^2 + \lambda^2 w^2}\, d\alpha \ . \tag{1.47}$$

By direct integration of the left-hand side and right-hand side of eq. (1.47), we have

$$p\sqrt{(1-\lambda)^2 + \lambda^2 w^2} \le \overline{L} \le p\sqrt{(1+\lambda)^2 + \lambda^2 w^2} \ , \tag{1.48}$$

and, by writing $w = q/p$, we obtain

$$\sqrt{(1-\lambda)^2 p^2 + \lambda^2 q^2} \le \overline{L} \le \sqrt{(1+\lambda)^2 p^2 + \lambda^2 q^2} \ . \tag{1.49}$$

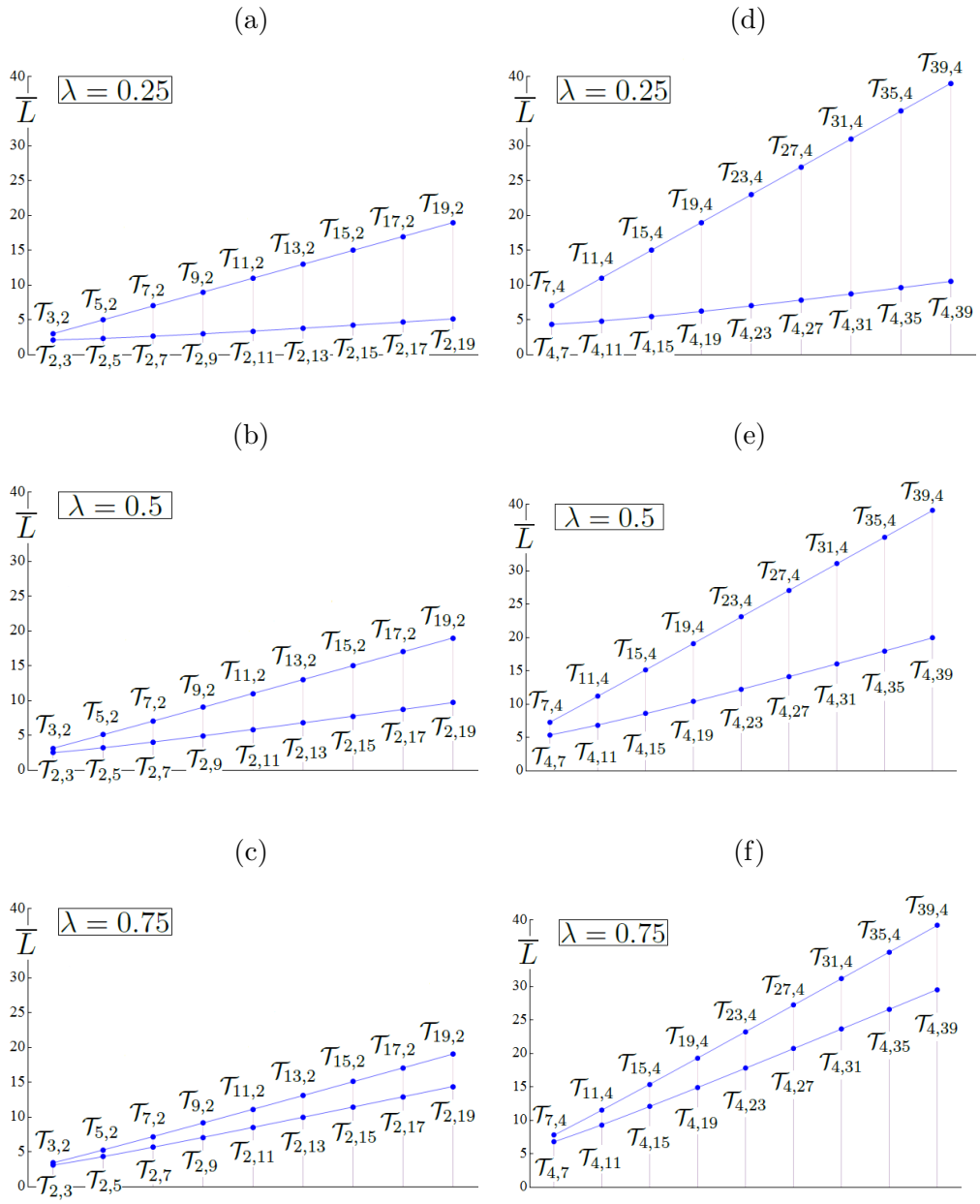

Figure 1.7: Non-dimensional total length $\overline{L}$ of torus knots $\mathcal{T}_{p,2}$ and $\mathcal{T}_{2,q}$ (left column), and $\mathcal{T}_{p,4}$ and $\mathcal{T}_{4,q}$ (right columnn). Knots are equally spaced on the x-axis. Interpolation is for visualization purposes only.

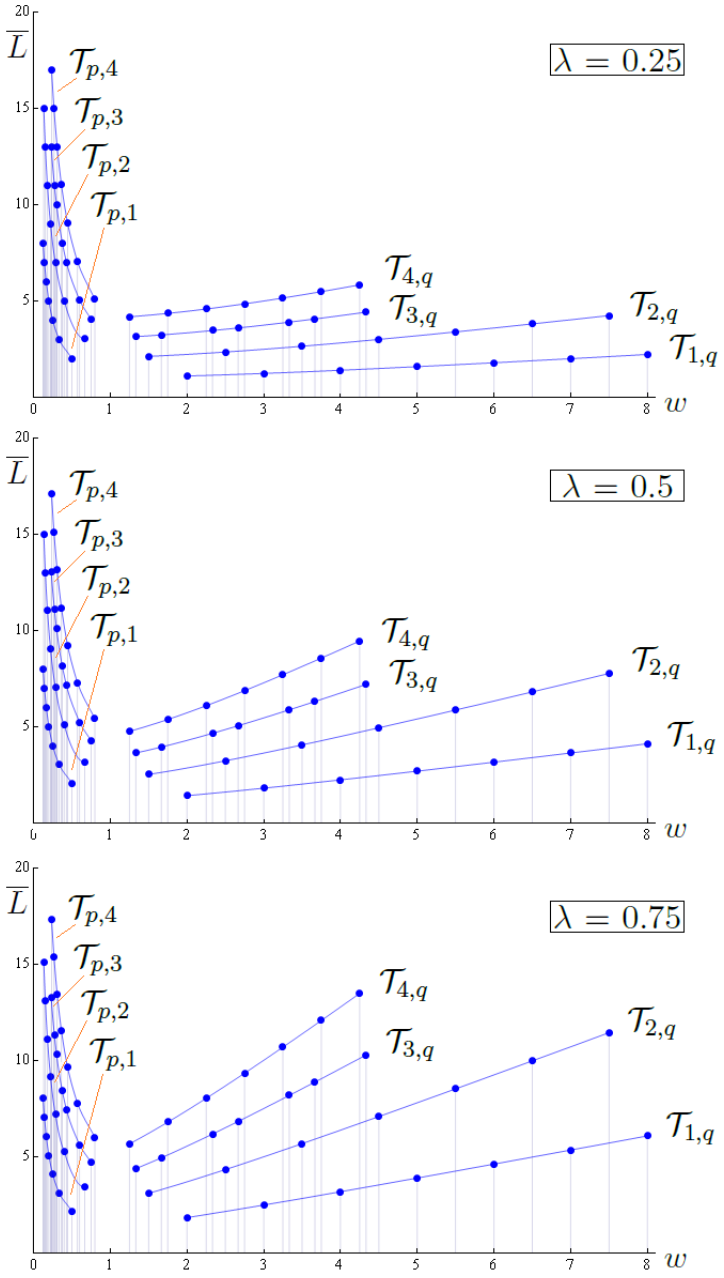

Figure 1.8: Non-dimensional total length $\overline{L}$ against winding number w for several torus knots/unknots with (a) $\lambda = 0.25$, (b) $\lambda = 0.5$ and (c) $\lambda = 0.75$. $\mathcal{T}_{p,1}$ and $\mathcal{T}_{1,q}$ $(p, q = 2, 3, 4, 5, 6, 7, 8)$; $\mathcal{T}_{p,2}$ and $\mathcal{T}_{2,q}$ $(p, q = 3, 5, 7, 9, 11, 13, 15)$; $\mathcal{T}_{p,3}$ and $\mathcal{T}_{3,q}$ $(p, q = 4, 5, 7, 8, 10, 11, 13)$; $\mathcal{T}_{p,4}$ and $\mathcal{T}_{4,q}$ $(p, q = 5, 7, 9, 11, 13, 15, 17)$. Interpolation is for visualization purposes only.

1.7 Total curvature

The total curvature of a torus knot/unknot $\mathcal{T}_{p,q}$ is given by

$$K = \int_0^{2\pi p} c(R, \lambda, w; \alpha) \; |\dot{\mathbf{x}}(R, \lambda, w; \alpha)| d\alpha \; , \tag{1.50}$$

where $c(R, \lambda, w; \alpha)$ is the pointwise curvature, defined in eq. (1.3). K is naturally non-dimensional, since it is given by the integration of the pointwise curvature, that is dimensionally an the inverse of a length, over the entire length.

In Figure 1.9 we show the total curvature against the winding number of several torus knots/unknots, for different values of the aspect ratio. The variation of λ influences K when poloidal wraps are dominant, whereas it leaves mostly

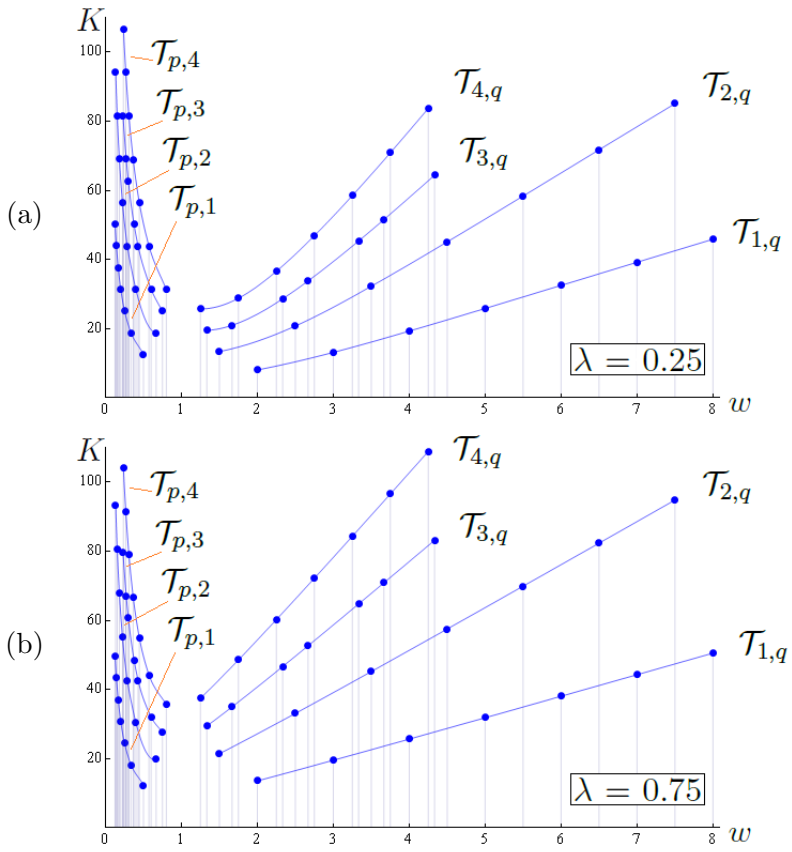

Figure 1.9: Total curvature K against winding number w of several torus knots/unknots ($R = 1$) with (a) $\lambda = 0.25$ and (b) $\lambda = 0.75$. $\mathcal{T}_{p,1}$ and $\mathcal{T}_{1,q}$ $(p, q = 2, 3, 4, 5, 6, 7, 8)$; $\mathcal{T}_{p,2}$ and $\mathcal{T}_{2,q}$ $(p, q = 3, 5, 7, 9, 11, 13, 15)$; $\mathcal{T}_{p,3}$ and $\mathcal{T}_{3,q}$ $(p, q = 4, 5, 7, 8, 10, 11, 13)$; $\mathcal{T}_{p,4}$ and $\mathcal{T}_{4,q}$ $(p, q = 5, 7, 9, 11, 13, 15, 17)$. Interpolation is only for visualization purposes.

unchanged K when toroidal wraps are dominant. For λ small, poloidal wraps contribute less to K than toroidal wraps (Figure 1.9a). The gradual increase of λ leads to a gradual increase of the contribution from poloidal wraps and, for large λ, poloidal wraps contribute most to K (Figure 1.9b).

A major contribution to K comes from L. For example, let us consider $\mathcal{T}_{p,q_1}$ and $\mathcal{T}_{p,q_2}$, with $p \ll q_1 < q_2$, with λ large. As we observed in section 1.4, their respective curvatures are almost constant (the constant value given by $1/\lambda$). However, $K(\mathcal{T}_{p,q_2}) > K(\mathcal{T}_{p,q_1})$, due to the contribution of L, that grows linearly with q. Thus, let us consider the *total curvature per unit length* (also a dimensionless quantity)

$$\overline{K}(\mathcal{T}_{p,q}) = \frac{K(\mathcal{T}_{p,q})}{\overline{L}(\mathcal{T}_{p,q})} \ . \tag{1.51}$$

In Figure 1.10 we plot $\overline{K}$ against w for $\lambda = 0.5$ and $R = 1$. Note that the values of all knots/unknots of a given family ($w < 1$ and $w > 1$) collapse to a single curve; this behaviour is generic and independent of λ. When $w \to 0$, $\overline{K} \to 2\pi$, that is the total curvature per unit length of the torus axis. When $w \to \infty$, $\overline{K} \to 4\pi$, that is the total curvature per unit length of the cross-sectional circle of the torus.

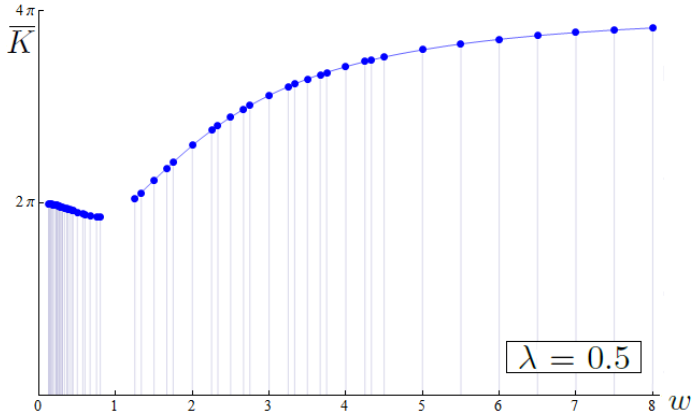

Figure 1.10: Total curvature per unit length $\overline{K}$ against winding number w of the torus knots/unknots considered in Figure 1.9, for $\lambda = 0.5$ and $R = 1$. Interpolation is for visualization purposes only.

1.8 Total torsion

The total torsion of a torus knot/unknot $\mathcal{T}_{p,q}$ is given by

$$T = \int_0^{2\pi p} \tau(R, \lambda, w; \alpha) \ |\dot{\mathbf{x}}(R, \lambda, w; \alpha)| d\alpha \tag{1.52}$$

where $\tau(R, \lambda, w; \alpha)$ is the pointwise torsion (eq. (1.4)). T is non-dimensional, since it is given by the integration of the pointwise torsion, that dimensionally is an

inverse of a length, over the entire length.

In Figure 1.11 we show T against w of several torus knots/unknots, organized in two families, with $w < 1$ (Figure 1.11a) and $w > 1$ (Figure 1.11b), for $\lambda = 0.5$. Poloidal wraps generally contribute the most to total torsion (in absolute values), except for a few torus knots/unknots of particular geometry. Indeed, for a very thin or very thick torus, there exist pairs of isotopes whose total torsion has almost the same value. As number of wraps increases, T tends to a constant.

In Figure 1.12 we show the *total torsion per unit length* $\overline{T}$ against the winding number of all torus knots/unknots considered in Figure 1.11, according to the

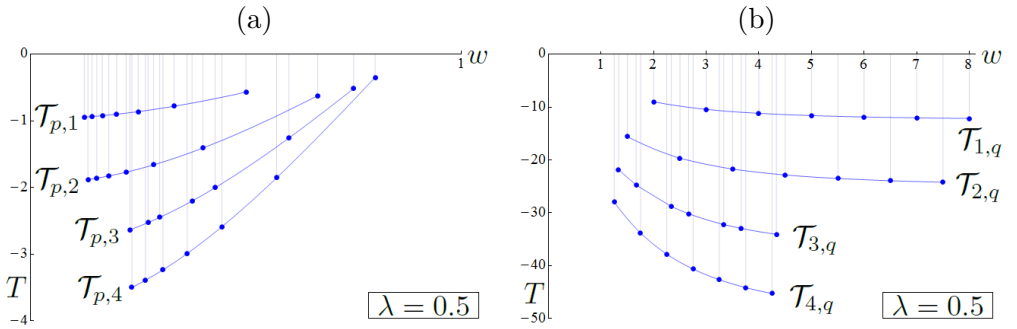

Figure 1.11: Total torsion T against winding number w of several torus knots/unknots ($R = 1$) with (a) $w < 1$ and (b) $w > 1$. $\mathcal{T}_{p,1}$ and $\mathcal{T}_{1,q}$ ($p, q = 2, 3, 4, 5, 6, 7, 8$); $\mathcal{T}_{p,2}$ and $\mathcal{T}_{2,q}$ ($p, q = 3, 5, 7, 9, 11, 13, 15$); $\mathcal{T}_{p,3}$ and $\mathcal{T}_{3,q}$ ($p, q = 4, 5, 7, 8, 10, 11, 13$); $\mathcal{T}_{p,4}$ and $\mathcal{T}_{4,q}$ ($p, q = 5, 7, 9, 11, 13, 15, 17$). Interpolation is for visualization purposes only.

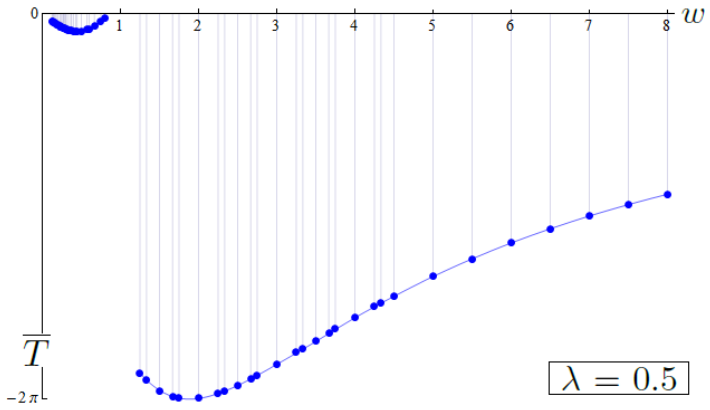

Figure 1.12: Total torsion per unit length $\overline{T}$ against winding number w of the torus knots/unknots considered in Figure 1.11, for $\lambda = 0.5$ and $R = 1$. Interpolation is for visualization purposes only.

following definition:

$$\overline{T}(\mathcal{T}_{p,q}) = \frac{T(\mathcal{T}_{p,q})}{\overline{L}(\mathcal{T}_{p,q})} \ . \tag{1.53}$$

The values of $\overline{T}$ for knots/unknots within each family $w < 1$ and $w > 1$ follow the same power law, represented by the single interpolation curve. When $w \to 0$ and $w \to \infty$, $\overline{T} \to 0$; this behaviour is generic and independent of λ. The presence of a minimum in the interpolation curves (for both $w < 1$ and $w > 1$) is also an interesting generic feature, observed for all λ considered. The position and the value of the minimum, for both $w < 1$ and $w > 1$, are function of λ (see Figure 1.13).

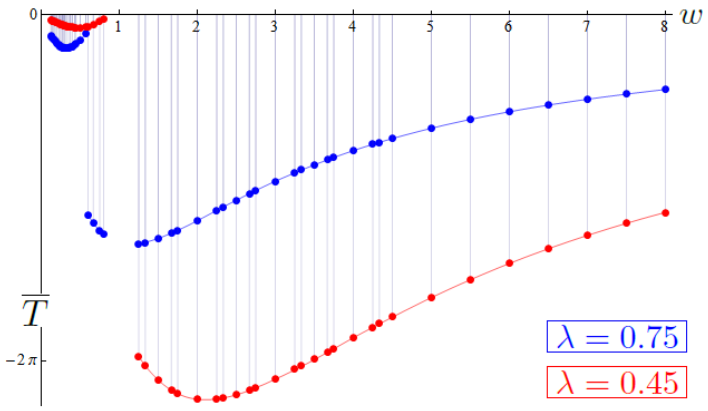

Figure 1.13: Total torsion per unit length $\overline{T}$ against winding number w of the torus knots/unknots considered in Figure 1.11, for $\lambda = 0.45$ (red) and $\lambda = 0.75$ (blue); $R = 1$. Interpolation is for visualization purposes only.

1.9 Total squared curvature and torsion

Global functionals of curvature and torsion have been widely studied both in differential geometry and topology [17, 35, 1], and in applications to many different fields of natural sciences, when the curve is the skeleton of a tube-like structure [43, 61, 47, 50]. In this section we shall consider the total squared curvature and torsion of a $\mathcal{T}_{p,q}$, that in first approximation are directly related to bending and torsional energy of elastic filaments [16, 29], and are given by

$$E_b = \int_0^{2\pi p} c^2(\alpha)\ |\dot{\mathbf{x}}(\alpha)| d\alpha \ , \qquad E_\tau = \int_0^{2\pi p} \tau^2(\alpha)\ |\dot{\mathbf{x}}(\alpha)| d\alpha \ , \tag{1.54}$$

where, for simplicity, we have omitted the dependence of c, τ and $\dot{\mathbf{x}}$ on the parameters R, λ and w.
In order to have non-dimensional quantities it is convenient to normalize both E_b and E_τ a reference quantity E_0, given by the total squared curvature of a circle of

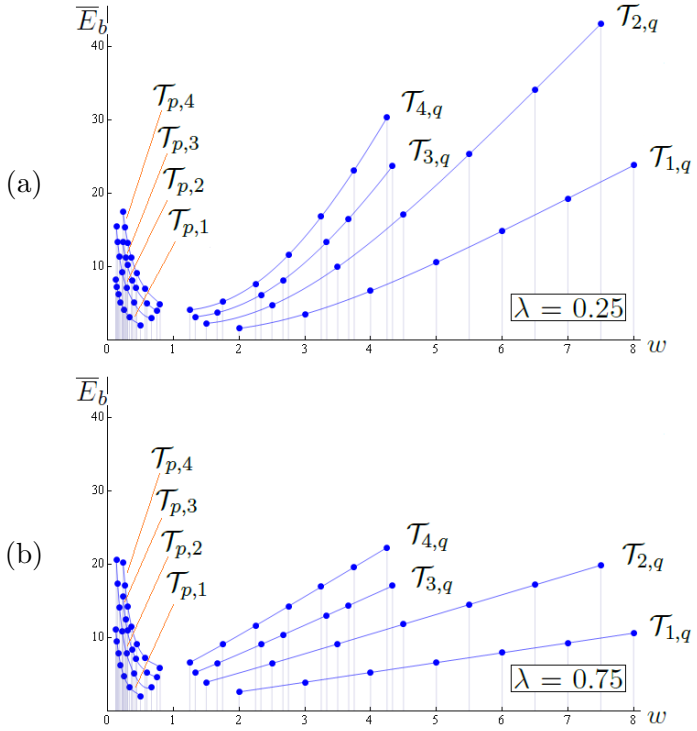

Figure 1.14: Non-dimensional total squared curvature $\overline{E}_b$ against winding number w of several torus knots/unknots ($R = 1$) with (a) $\lambda = 0.25$ and (b) $\lambda = 0.75$. $\mathcal{T}_{p,1}$ and $\mathcal{T}_{1,q}$ $(p, q = 2, 3, 4, 5, 6, 7, 8)$; $\mathcal{T}_{p,2}$ and $\mathcal{T}_{2,q}$ $(p, q = 3, 5, 7, 9, 11, 13, 15)$; $\mathcal{T}_{p,3}$ and $\mathcal{T}_{3,q}$ $(p, q = 4, 5, 7, 8, 10, 11, 13)$; $\mathcal{T}_{p,4}$ and $\mathcal{T}_{4,q}$ $(p, q = 5, 7, 9, 11, 13, 15, 17)$. Interpolation is for visualization purposes only.

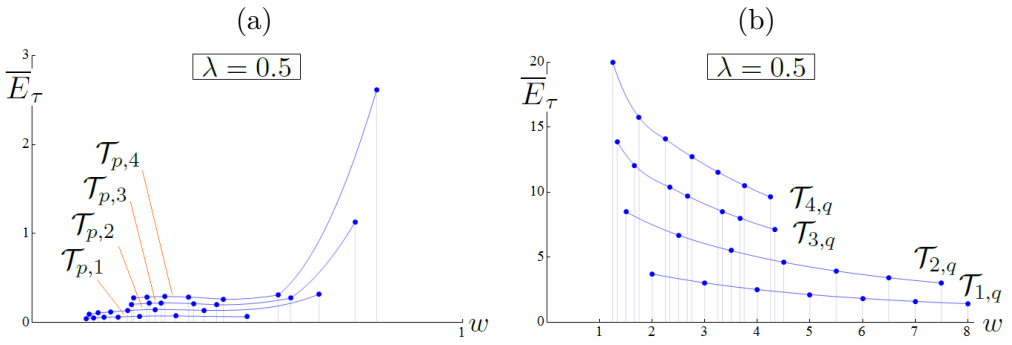

Figure 1.15: Non-dimensional total squared torsion $\overline{E}_\tau$ against the winding number w of several torus knots/unknots with (a) $w < 1$ and (b) $w > 1$, for $\lambda = 0.5$ and $R = 1$. $\mathcal{T}_{p,1}$ and $\mathcal{T}_{1,q}$ $(p, q = 2, 3, 4, 5, 6, 7, 8)$; $\mathcal{T}_{p,2}$ and $\mathcal{T}_{2,q}$ $(p, q = 3, 5, 7, 9, 11, 13, 15)$; $\mathcal{T}_{p,3}$ and $\mathcal{T}_{3,q}$ $(p, q = 4, 5, 7, 8, 10, 11, 13)$; $\mathcal{T}_{p,4}$ and $\mathcal{T}_{4,q}$ $(p, q = 5, 7, 9, 11, 13, 15, 17)$. Interpolation is only for visualization purposes.

radius $R = 1$, that is $E_0 = 2\pi$. Thus, the non-dimensional total squared curvature and torsion are given by

$$\overline{E}_b = \frac{E_b}{E_0} = \frac{1}{2\pi}\int_0^{2\pi p} c^2(\alpha)\,|\dot{\mathbf{x}}(\alpha)|d\alpha\ ,\quad \overline{E}_\tau = \frac{E_\tau}{E_0} = \frac{1}{2\pi}\int_0^{2\pi p} \tau^2(\alpha)\,|\dot{\mathbf{x}}(\alpha)|d\alpha\ . \quad (1.55)$$

In Figure 1.14 we show $\overline{E}_b$ against w of several torus knots/unknots. The relative contribution of toroidal/poloidal wraps to $\overline{E}_b$ depends on λ, so that two topologically equivalent torus knots/unknots with different aspect ratio may have the same $\overline{E}_b$. For $\mathcal{T}_{p,q}$ in the same family, say $w > 1$, it is *not* generally true that higher values of $\overline{E}_b$ are attained for larger λ.

In Figure 1.15 we show $\overline{E}_\tau$ against w of several torus knots/unknots, with $w < 1$ and $w > 1$. When $w \to 0$ and $w \to \infty$, $\overline{E}_\tau \to 0$, in analogy with the total torsion per unit length $\overline{T}$. Generally poloidal wraps give the dominant contribution to $\overline{E}_\tau$, except for a few torus knots/unknots with large aspect ratio (for example with $\lambda = 0.75$, not shown here). The contribution from $\overline{E}_\tau$ of $\mathcal{T}_{p,1}$–$\mathcal{T}_{p,4}$ is one order of magnitude smaller than that from $\overline{E}_b$.

1.10 Writhing number

The writhing number Wr of $\mathcal{T}_{p,q}$ is given by

$$Wr = \frac{1}{4\pi}\int_0^{2\pi p}\int_0^{2\pi p} \frac{(\dot{\mathbf{x}}(\alpha)\times\dot{\mathbf{x}}(\alpha^*))\cdot(\mathbf{x}(\alpha)-\mathbf{x}(\alpha^*))}{|\mathbf{x}(\alpha)-\mathbf{x}(\alpha^*)|^3}\,d\alpha d\alpha^*\ , \quad (1.56)$$

where $\mathbf{x}(\alpha)$ and $\mathbf{x}(\alpha^*)$ are two points on $\mathcal{T}_{p,q}$. The writhing number is a non-dimensional, global geometric quantity associated with a closed, simple curve and

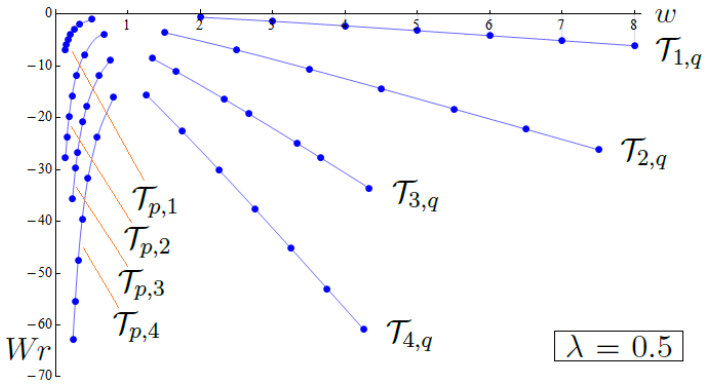

Figure 1.16: Writhing number Wr against the winding number w of several torus knots/unknots with $\lambda = 0.5$ and $R = 1$. $\mathcal{T}_{p,1}$ and $\mathcal{T}_{1,q}$ $(p, q = 2, 3, 4, 5, 6, 7, 8)$; $\mathcal{T}_{p,2}$ and $\mathcal{T}_{2,q}$ $(p, q = 3, 5, 7, 9, 11, 13, 15)$; $\mathcal{T}_{p,3}$ and $\mathcal{T}_{3,q}$ $(p, q = 4, 5, 7, 8, 10, 11, 13)$; $\mathcal{T}_{p,4}$ and $\mathcal{T}_{4,q}$ $(p, q = 5, 7, 9, 11, 13, 15, 17)$. Interpolation is only for visualization purposes.

it is a measure of the coiling of the curve.

In Figure 1.16 we show Wr against w of several torus knots/unknots with $\lambda = 0.5$ and $R = 1$. The negative value of Wr is due to the parametrization chosen. By replacing the third equation of eqs. (1.2) with $z = -R\lambda \sin w\alpha$, we obtain diagrams that are axially symmetric with respect to the x-axis. Generally a variation in λ produce a modest variation in the writhing number values, especially for torus knots/unknots with $w < 1$. Topologically equivalent torus knots/unknots have almost the same writhing number for $\lambda \approx 0.75$.

1.11 Spherical indicatrices

Let $\mathcal{C}$ be a regular, closed curve in $\mathbb{R}^3$ of class C^3, with arc-length s and Frenet frame $(\mathbf{t}, \mathbf{n}, \mathbf{b})$ defined everywhere. Each of the three vectors of the Frenet frame maps points of the curve $\mathcal{C}$ to points on the unit sphere. In particular, the tip of the tangent vector describes with the variation of s a closed curve on the sphere. This curve is called spherical indicatrix of the tangent vector or *tangent indicatrix* (tantrix). In the same way the normal and binormal vectors describe two closed curves on the sphere, called spherical indicatrices of the normal and binormal vectors, or *normal and binormal indicatrices*. We shall denote these three curves with $I_{\mathbf{t}}$, $I_{\mathbf{n}}$ and $I_{\mathbf{b}}$, respectively (see Figure 1.17, where $\mathcal{C} = \mathcal{T}_{2,3}$). Note that the tangent vector of the tantrix is $\mathbf{n}$.
Information on the local and global geometry of the curve $\mathcal{C}$ can be deduced from information on the spherical indicatrices. We have (see, for example, [17, 35])

$$L(I_{\mathbf{t}}) = \int_{\mathcal{C}} c(s)\, ds \ , \tag{1.57}$$

$$L(I_{\mathbf{n}}) = \int_{\mathcal{C}} |\tau(s)|\, ds \ , \tag{1.58}$$

$$L(I_{\mathbf{b}}) = \int_{\mathcal{C}} \sqrt{c^2(s) + \tau^2(s)}\, ds \ . \tag{1.59}$$

where c and τ are the pointwise curvature and torsion of $\mathcal{C}$ and $L(I_{\mathbf{j}})$ is the total length of $I_{\mathbf{j}}$, $\mathbf{j} = \mathbf{t}, \mathbf{n}, \mathbf{b}$.
If $\mathcal{C}$ has inflection point, $I_{\mathbf{t}}$ is still well-defined. A point of $\mathcal{C}$ with $c = 0$ corresponds to a cusp of $I_{\mathbf{t}}$ (see Figure 1.18b). A point of $\mathcal{C}$ with $\tau = 0$ corresponds to an inflection of $I_{\mathbf{t}}$ and to a cusp of $I_{\mathbf{b}}$ (see Figure 1.17c). The curve $I_{\mathbf{n}}$ has no cusps. See, for example, [18] and references within.
Let us define the spherical area A enclosed by the tantrix by the following procedure (see also [4]). The tantrix $I_{\mathbf{t}}$ naturally inherits an orientation from the arc-length parametrization of $\mathcal{C}$ and generally present points of self-intersection. Let us divide $I_{\mathbf{t}}$ into a finite family of non self-intersecting, coherently-oriented, closed curves. Let us consider the *geodesic normal vector* $\mathbf{U}$ of the Darboux frame $(\mathbf{T}, \mathbf{U}, \mathbf{N})$ of $I_{\mathbf{t}}$, where $\mathbf{T}$ is the unit tangent to $I_{\mathbf{t}}$, $\mathbf{N}$ is the outer-pointing unit

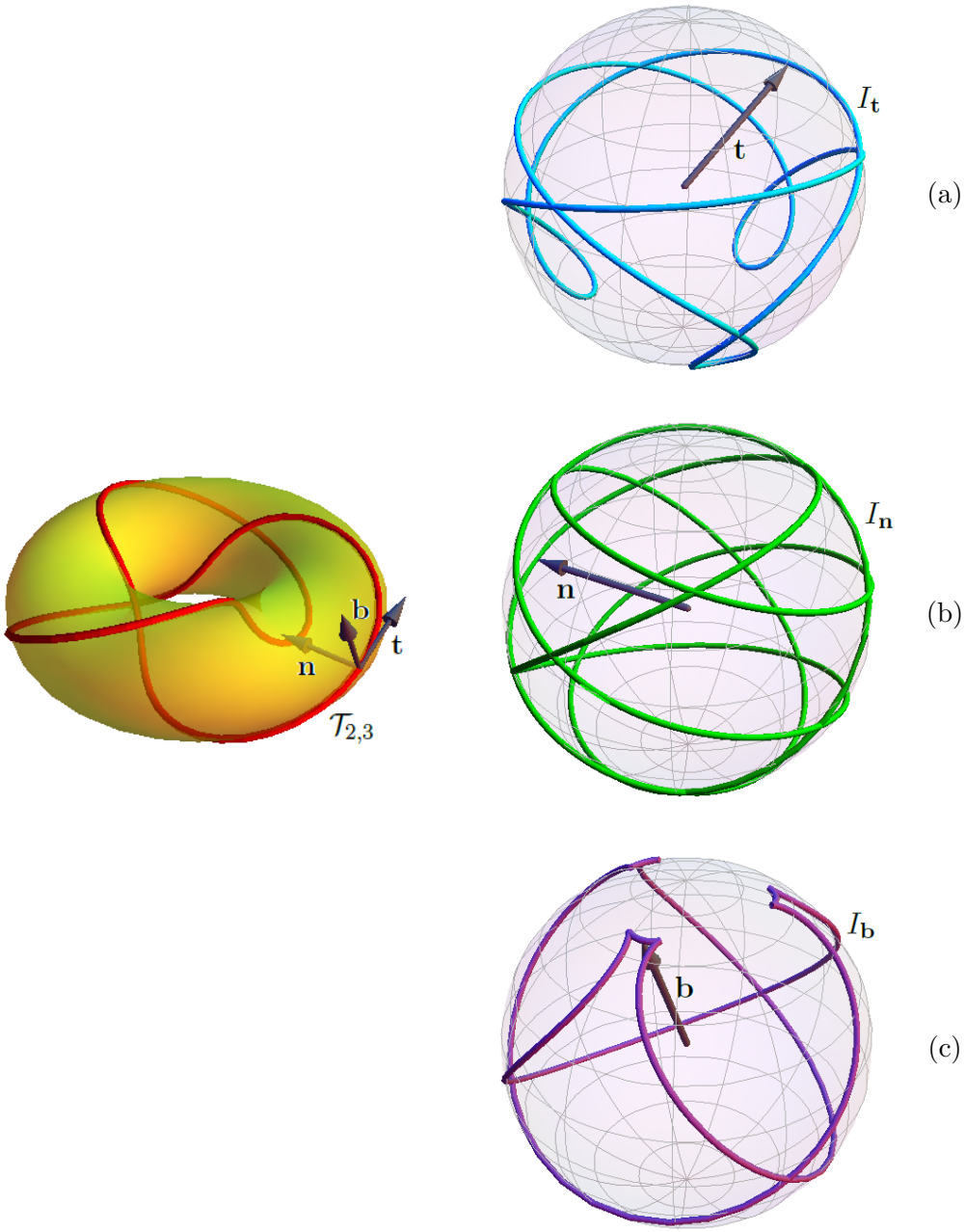

Figure 1.17: Spherical indicatrices of (a) the tangent, (b) the normal and (c) the binormal vectors of $\mathcal{T}_{2,3}$ with $\lambda = 0.5$ and $R = 1$.

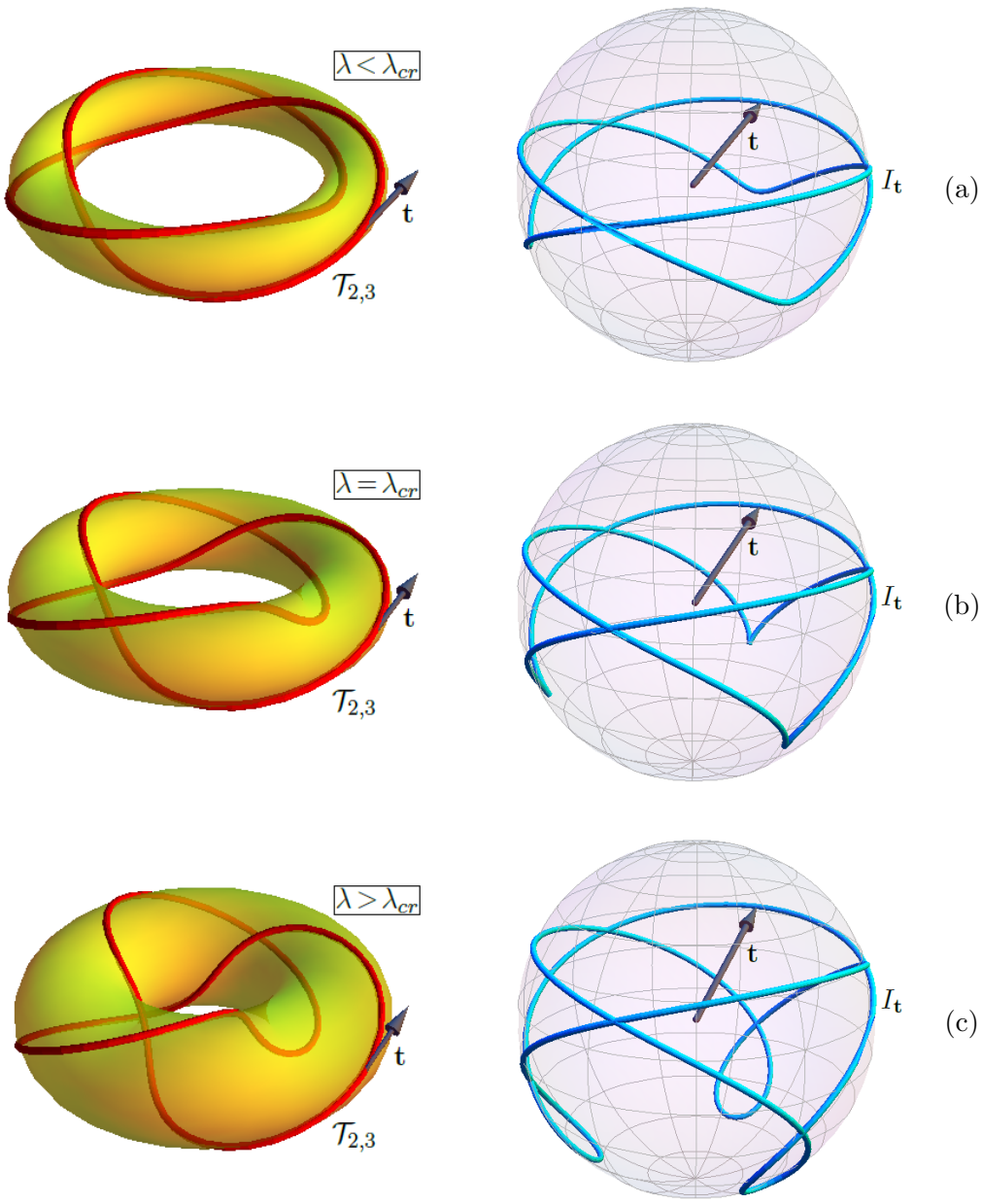

Figure 1.18: Tantrix of $\mathcal{T}_{2,3}$ ($R = 1$) with (a) $\lambda = 0.2 < \lambda_{cr}$, (b) $\lambda = 4/13 = \lambda_{cr}$ and (c) $\lambda = 0.5 > \lambda_{cr}$.

normal to the sphere and $\mathbf{U} = \mathbf{N} \times \mathbf{T}$. Note that $\mathbf{U}$ varies continuously as it pass through an inflection of $I_{\mathbf{t}}$. For each curve of the family choose the enclosed spherical region such that $\mathbf{U}$ is directed towards its interior. Let A be the sum of the areas of these regions. Note that two regions can intersect and the area of their intersection has to be counted once for each region (see, for example, the top row of Figure 1.19). Moreover, if a region is encircled more than once by its enclosing curve, then its area has to be counted with multiplicity given by the number of times the curve encircles the region. The spherical area of the tantrix is related to the writhing number Wr of $\mathcal{C}$, according to

Theorem 1.11 (Fuller, [20]). *Let A be the spherical area enclosed by the tantrix of $\mathcal{C}$, as defined above. Then the writhing number of $\mathcal{C}$ is given by*

$$Wr \equiv \frac{A}{2\pi} + 1 \mod 2 \,. \tag{1.60}$$

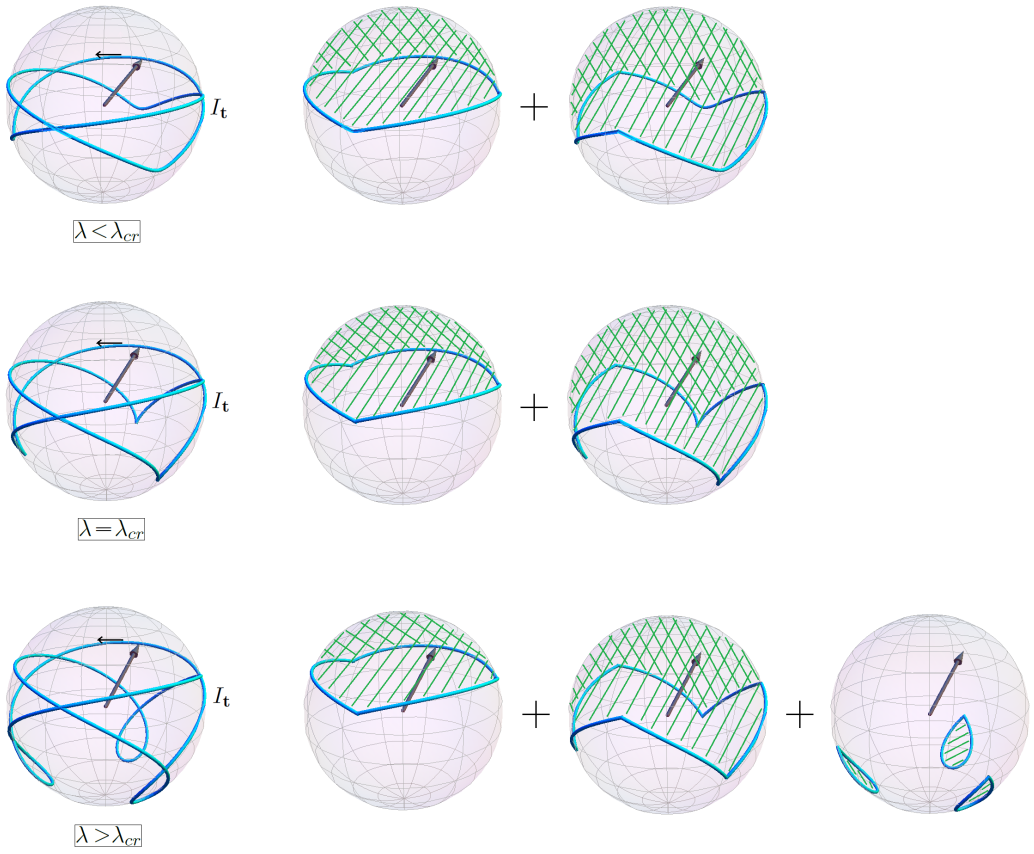

Figure 1.19: Tantrix area contributing to Wr of the torus knot $\mathcal{T}_{2,3}$ with $R = 1$ and (top row) $\lambda = 0.2 < \lambda_{cr}$, (central row) $\lambda = 4/13 = \lambda_{cr}$ and (bottom row) $\lambda = 0.5 > \lambda_{cr}$.

Let us consider $\mathcal{C} = \mathcal{T}_{p,q}$. The presence of inflectional configurations has consequences for writhe, which become evident by its interpretation in terms of tantrix area. Since the unit tangent $\mathbf{T}$ to the tantrix is the unit normal vector $\mathbf{n}$ to $\mathcal{T}_{p,q}$, q inflection points on $\mathcal{T}_{p,q}$ are mapped to q cusps on the corresponding tantrix. By considering the deformation of the tantrix as λ increases, first we see the development of q cusps (at $\lambda = \lambda_{cr}$, Figure 1.18b), then the development of q loops (for $\lambda > \lambda_{cr}$, Figure 1.18c), enclosing a larger spherical region as $\lambda \to 1$, whose additional total area contributes to the writhe according to eq. (1.60), as visualized in the bottom row of Figure 1.19.

1.12 Pohl self-linking number

Let us consider the quantity

$$SL = Wr + \mathscr{T} \ , \tag{1.61}$$

where Wr and $\mathscr{T} = T/2\pi$ are the writhing number and the normalized total torsion of a closed curve $\mathcal{C}$ of class C^3, free from cusps and self-intersections; let us call SL the *Pohl self-linking number* of $\mathcal{C}$. SL is an integer and is invariant for continuous deformations of $\mathcal{C}$ that do *not* pass through inflectional configurations [14, 45]. Notice that both Wr and $\mathscr{T}$ are neither integers, nor invariant under such deformations.
When $\mathcal{C} = \mathcal{T}_{p,q}$ we have the following result.

Theorem 1.12 (Fuller Jr, [21, 22])**.** *Let $\mathcal{T}_{p,q}$ be a torus knot/unknot with $\lambda \neq \lambda_{cr}$. Then*

$$SL = \begin{cases} -q(p-1) & \text{if } 0 < \lambda < \lambda_{cr} \\ -pq & \text{if } \lambda_{cr} < \lambda < 1 \end{cases} \ . \tag{1.62}$$

The negative values of SL are given by the parametrization associated with the handedness of $\mathcal{T}_{p,q}$. Direct computation of Wr and $\mathscr{T}$ for all knots/unknots considered in sections 1.8 and 1.10 are in good agreement with the results of Theorem 1.12.

By considering the deformation of $\mathcal{T}_{p,q}$ as λ increases, when $\mathcal{T}_{p,q}$ goes through the inflectional configuration at $\lambda = \lambda_{cr}$, SL jumps from $-q(p-1)$ to $-pq$ and the jump is given by $\lfloor SL \rfloor = -pq + [q(p-1)] = -q$. Conversely, by considering the deformation of $\mathcal{T}_{p,q}$ as λ decreases, the jump in SL is given by $\lfloor SL \rfloor = -[q(p-1)] + pq = q$. This jump discontinuity is due to the jump discontinuity of $\mathscr{T}$ as $\mathcal{T}_{p,q}$ passes through the inflectional state.

Since for $w > 1$ it is $\lambda_{cr}(w) < 1/2$, whereas for $w < 1$ it is $\lambda_{cr}(w) > 1/2$, the following result is straightforward:

Corollary 1.13. *Let $\mathcal{T}_{p,q}$ be a torus knot/unknot with $\lambda = 1/2$. Then*

$$SL = \begin{cases} -q(p-1) & \text{if } w < 1 \\ -pq & \text{if } w > 1 \end{cases} . \tag{1.63}$$

1.13 Framed curves and Călugăreanu invariant

Let us consider a $\mathcal{T}_{p,q}$ endowed with a framing (given by a ribbon unit vector field $\mathbf{N} = \mathbf{N}(\alpha)$, pointwise normal to the curve). The *Călugăreanu self-linking number* Lk of the framed $\mathcal{T}_{p,q}$ is defined as [15]

$$Lk(\mathcal{T}_{p,q}) = \lim_{\varepsilon \to 0} Lk(\mathcal{T}_{p,q}, \mathcal{T}_{p,q} + \varepsilon \mathbf{N}) , \tag{1.64}$$

where $Lk(\mathcal{T}_{p,q}, \mathcal{T}_{p,q} + \varepsilon\mathbf{N})$ is the Gauss linking number between $\mathcal{T}_{p,q}$ and $\mathcal{T}_{p,q} + \varepsilon\mathbf{N}$; the limit exists finite and is an integer, and $Lk(\mathcal{T}_{p,q})$ is an isotopy invariant of the framed $\mathcal{T}_{p,q}$ [15].
The Călugăreanu-White-Fuller theorem [15, 64, 19] relates the Pohl's geometric self-linking number to the Călugăreanu's topological self-linking number Lk by

$$Lk = Wr + \mathscr{T} + \mathscr{N} = SL + \mathscr{N} , \tag{1.65}$$

where the *intrinsic twist* $\mathscr{N}$ is the number of full rotations of $\mathbf{N}$ around the base curve of the ribbon, all along the curve (since $\mathcal{T}_{p,q}$ is a closed curve, $\mathscr{N}$ is an integer). The quantity $\mathscr{T} + \mathscr{N} = Tw$ is the *total twist number*.
The role of $\mathscr{N}$ when the framed $\mathcal{T}_{p,q}$ passes through the inflectional state at $\lambda = \lambda_{cr}$ is made clear by comparing the right-hand side of eq. (1.65) to eq. (1.62). Since Lk is a topological invariant of the framed $\mathcal{T}_{p,q}$, it remains unchanged when $\mathcal{T}_{p,q}$ goes through the inflectional configuration. This, however, produces a jump in SL, given by $\lfloor SL \rfloor = \pm q$, that must be compensate by an equal and opposite jump in $\mathscr{N}$, given by $\lfloor \mathscr{N} \rfloor = \mp q$, according to

$$Lk - SL = \mathscr{N} . \tag{1.66}$$

Hence, we can state the following:

Corollary 1.14. *For any $\mathcal{T}_{p,q}$ parametrized by* eqs. (1.2) *and endowed with a framing, the jump in the intrinsic twist, given when $\mathcal{T}_{p,q}$ goes through the inflectional configuration at $\lambda = \lambda_{cr}$, is equal to $\lfloor \mathscr{N} \rfloor = \mp q$, where q is the number of poloidal wraps.*

This result justifies the conjecture made by Moffatt & Ricca ([39], p. 426), as regards the transition of a torus unknot through an inflectional state given by a critical aspect ratio.

Let us show that the normal and binormal framing are two natural choices for

which $\mathscr{N} = 0$. For this purpose, let us generally consider a framed closed curve $\mathcal{C}$. Let s be the arc-length of $\mathcal{C}$ and $(\mathbf{t}, \mathbf{n}, \mathbf{b})$ its Frenet frame, satisfying the Frenet equations (prime denotes derivative with respect to s)

$$\begin{cases} \mathbf{t}' = c\mathbf{n} \\ \mathbf{n}' = -c\mathbf{t} + \tau\mathbf{b} \\ \mathbf{b}' = -\tau\mathbf{n} \end{cases}, \tag{1.67}$$

and let $\mathbf{N} = \mathbf{N}(s) = \mathbf{n}\cos\Theta + \mathbf{b}\sin\Theta$ be the framing unit vector field, with $\Theta = \Theta(s) \in [0, 2\pi)$. By choosing $\Theta(s)$ at each point of the base curve, we have a unique choice of framing. Following [19, 39], the total twist number is given by

$$Tw = \frac{1}{2\pi}\int_{\mathcal{C}} (\mathbf{N} \times \mathbf{N}') \cdot \mathbf{t}\, ds\ . \tag{1.68}$$

Let us suppose $\mathbf{N} = \mathbf{n}$ (that is, $\Theta = 0$). By the Frenet equations (1.67) we obtain $\mathbf{N}' = -c\mathbf{t} + \tau\mathbf{b}$. Hence, $\mathbf{N} \times \mathbf{N}' = \tau\mathbf{t} + c\mathbf{b}$ and $(\mathbf{N} \times \mathbf{N}') \cdot \mathbf{t} = \tau$. Thus,

$$Tw = \frac{1}{2\pi}\int_{\mathcal{C}} \tau\, ds = \mathscr{T}\ . \tag{1.69}$$

Let us suppose $\mathbf{N} = \mathbf{b}$ (that is, $\Theta = \pi/2$). By the Frenet equations (1.67) we obtain $\mathbf{N}' = -\tau\mathbf{n}$. Hence, $\mathbf{N} \times \mathbf{N}' = \tau\mathbf{t}$ and $(\mathbf{N} \times \mathbf{N}') \cdot \mathbf{t} = \tau$. Thus, the total twist number is reduced to normalized total torsion only, as in eq. (1.69).
In general, if $\Theta = \text{const}$, then $\mathscr{N} = 0$ and $Lk = SL$. In order to have non zero intrinsic twist, Θ needs to be a non trivial function of s.

Chapter 2

The Biot-Savart integral: winding number effects, helicity and energy

In this chapter we present new numerical results on the Biot-Savart induction effects of a steady field in the shape of a torus knot/unknot. Field patterns of the induced field represented on cross-sectional planes are shown in Section 2.4, where their dependence on knot complexity is analysed. The influence of winding number on the induction is investigated in Section 2.5, where we show that the intensity of the induced field at the origin of the reference system is linearly dependent on the number of toroidal coils and dominated by length contribution. In Section 2.6 we discuss the presence of maxima in the mean intensity of the induced field (analysed over families of knots/unknots) for induction points inside the mathematical torus, near to the boundary. Three different approaches to calculate helicity are compared in Section 2.7, where we show that helicity of toroidal knots/unknots is dominated by writhe contribution. In Section 2.8 we find estimates for the magnetic energy of magnetic torus knot/unknot and an analytic lower bound, in terms of helicity and a quantity that depends only on the geometry of the torus knot/unknot.

2.1 The Biot-Savart induction law

Given a steady vector field $\mathbf{j} = \mathbf{j}(\mathbf{x})$, $\mathbf{x} \in \mathbb{R}^3$, defined over a volume $V = V(\mathbf{x})$ in a domain $\mathcal{D} \subseteq \mathbb{R}^3$, we want to find a vector field $\mathbf{B}$ such that

$$\nabla \times \mathbf{B} = \mathbf{j} \ , \quad \nabla \cdot \mathbf{B} = 0 \ . \tag{2.1}$$

We shall call $\mathbf{j}$ the *source field* and $\mathbf{B}$ the *induced field*. To do this we must invert the curl operator of eq. (2.1) and express $\mathbf{B}$ in terms of $\mathbf{j}$. Let us suppose satisfied the list of sufficient conditions for which the inversion is possible [54] and

B uniquely determined.
The solenoidal condition on **B** implies that there exists a vector field $\mathbf{A} = \mathbf{A}(\mathbf{x})$, called *vector potential* of **B**, such that

$$\mathbf{B} = \nabla \times \mathbf{A} \ , \quad \nabla \cdot \mathbf{A} = 0 \ , \tag{2.2}$$

where the second equation is a choice of gauge. Thus, from eq. (2.1) and (2.2) we have

$$\mathbf{j} = \nabla \times (\nabla \times \mathbf{A}) = \nabla(\nabla \cdot \mathbf{A}) - \nabla \cdot (\nabla \mathbf{A}) = -\nabla^2 \mathbf{A} \ . \tag{2.3}$$

Equation (2.3) is the *Poisson equation* for **j** and has a well-known solution (see, for example, [54]) given by

$$\mathbf{A}(\mathbf{x}) = -\frac{1}{4\pi} \int_{V(\mathbf{x}^*)} \frac{\mathbf{j}(\mathbf{x}^*)}{|\mathbf{x} - \mathbf{x}^*|} \, d\mathbf{x}^* \ . \tag{2.4}$$

By taking the curl of eq. (2.4), we have

$$\mathbf{B}(\mathbf{x}) = \frac{1}{4\pi} \int_{V(\mathbf{x}^*)} \frac{\mathbf{j}(\mathbf{x}^*) \times (\mathbf{x} - \mathbf{x}^*)}{|\mathbf{x} - \mathbf{x}^*|^3} \, d\mathbf{x}^* \ . \tag{2.5}$$

For brevity, let us call the right-hand side of eq. (2.5) $\mathcal{BS}(\mathbf{j})(\mathbf{x})$. Equation (2.5) is the inverse of the curl operator and gives the law of induction for the field **B** by the source field **j**. Note that $\mathcal{BS}$ is a three-component vector with integrand singular when the *induction point* **x** reaches the source point $\mathbf{x}^*$.
In ideal MHD theory (electrically neutral, incompressible medium, with zero resistivity) **B** is the magnetic field induced by a given electric current distribution **j**. The first of eqs. (2.1) is the Ampère's law (where the magnetic permeability $\mu = 1$). In ideal, classical fluid mechanics (incompressible, inviscid fluid), given a non-zero vorticity field $\boldsymbol{\omega}$, by the analogy $\boldsymbol{\omega} \leftrightarrow \mathbf{j}$, the rotational velocity field **u** induced by $\boldsymbol{\omega}$ is simply obtained by replacing **B** with **u**. Equations (2.1) become $\boldsymbol{\omega} = \nabla \times \mathbf{u}$ and $\nabla \cdot \mathbf{u} = 0$, and we obtain $\mathbf{u} = \mathcal{BS}(\boldsymbol{\omega})$. Likewise, by the analogy $\boldsymbol{\omega} \leftrightarrow \mathbf{B}$, the vector potential **A** associated with the magnetic field **B** is simply given by $\mathbf{A} = \mathcal{BS}(\mathbf{B})$.

2.2 Reduction to a line integral

Let us suppose that the source field **j** is confined to a thin tube of circular, infinitesimal cross-section $\mathcal{S}$ and centreline $\mathcal{C}$. Let us suppose that **j** is uniform over $\mathcal{S}$ and directed along the unit tangent **t** to $\mathcal{C}$. The flux of **j** through $\mathcal{S}$ is given by

$$\Phi = \int_{\mathcal{S}} \mathbf{j} \cdot \mathbf{t} \, dA \ . \tag{2.6}$$

Since $\mathcal{S}$ is very small, we identify the thin tube with its centreline. Under these assumptions the Biot-Savart integral of eq. (2.5) can be reduced to the line integral along $\mathcal{C}$, given by

$$\mathbf{B}(\mathbf{x}) = \frac{\Phi}{4\pi} \int_{\mathcal{C}(\mathbf{x}^*)} \frac{\mathbf{t}(\mathbf{x}^*) \times (\mathbf{x} - \mathbf{x}^*)}{|\mathbf{x} - \mathbf{x}^*|^3} d\mathbf{x}^* \ . \tag{2.7}$$

2.3 Source field in the shape of a torus knot/unknot

Now, let us take $\mathcal{C} = \mathcal{T}_{p,q}$, where $\mathcal{T}_{p,q}$ is the torus knot/unknot parametrized by eqs. (1.2). Let us denote by $\mathbf{x}_k$ a point on $\mathcal{T}_{p,q}$ and by $\mathbf{x}_o$ the induction point. The Biot-Savart line integral takes the form

$$\mathbf{B}(\mathbf{x}_o) = \frac{\Phi}{4\pi} \int_0^{2\pi p} \frac{\mathbf{t}(\alpha) \times (\mathbf{x}_o - \mathbf{x}_k(\alpha))}{|\mathbf{x}_o - \mathbf{x}_k(\alpha)|^3} \ |\dot{\mathbf{x}}_k(\alpha)| d\alpha \ , \tag{2.8}$$

where $\mathbf{t} = \dot{\mathbf{x}}_k / |\dot{\mathbf{x}}_k|$ is the unit tangent vector to $\mathcal{T}_{p,q}$, $\dot{\mathbf{x}}_k$ denotes derivative with respect to α; note that $\mathbf{x}_k$, $\dot{\mathbf{x}}_k$ and $\mathbf{t}$ depend on R, λ and w. The integrand is singular when $\mathbf{x}_o \in \mathcal{T}_{p,q}$. For simplicity, let us set $\Phi/4\pi = 1$.

2.4 Field lines patterns of the induced field

By performing numerical integration of eq. (2.8), we obtain visualizations of the field lines patterns of the induced field $\mathbf{B}$ due to the source field $\mathbf{j}$ on $\mathcal{T}_{p,q}$ in different cross-sectional planes. The visualizations are obtained by the following steps:

- we numerically solve each of the three components of the right-hand side of eq. (2.8) for a given $\mathcal{T}_{p,q}$, thus obtaining the vector field $\mathbf{B} = \mathbf{B}(\mathbf{x}_o)$;
- we project $\mathbf{B}$ onto a given cross-sectional plane;
- we compute the field lines of the projection of $\mathbf{B}$ on the cross-sectional plane.

2.4.1 Numerical computation and visualization

The numerical computation of the field lines has been performed by using Mathematica [65]. In particular, the $\mathbf{B}$-field lines are visualized by the routine `StreamPlot`, which takes as arguments a vector field $\mathbf{v} = (v_x(x,y), v_y(x,y))$ in $\mathbb{R}^2$ and intervals for x and y, and returns the plot of the $\mathbf{v}$-field lines, drawn as the envelope of the vectors obtained by appropriate evaluations of $\mathbf{v}$ at points $(x,y) \in \mathbb{R}^2$ within the given intervals.
The routine plots the $\mathbf{B}$-field lines straightforwardly onto the cross-sectional planes (x,z) and (y,z). Indeed, let $\mathbf{B} = (B_x, B_y, B_z)$ and consider, for example, the plot onto the (y,z)-plane. The projection of $\mathbf{B}$ onto this plane is given by $P(\mathbf{B}) =$

$(0, B_y, B_z)$, hence we can set $\mathbf{v} = (B_y, B_z)$, to be evaluated at points $(0, y, z)$ in the (y, z)-plane, for given intervals of y and z. Plots in other cross-sectional planes are not straightforward, since $P(\mathbf{B})$ on other planes has *three* non zero components. In this case a standard rendering procedure is needed. Let us denote by

$$R(\phi) = \begin{pmatrix} \cos\phi & -\sin\phi & 0 \\ \sin\phi & \cos\phi & 0 \\ 0 & 0 & 1 \end{pmatrix} \tag{2.9}$$

the matrix performing a counter-clockwise rotation of angle ϕ about the z-axis, and by θ the angle by which a cross-sectional plane is rotated with respect to the (x, z)-plane. Let us consider, as example, the plot on the cross-sectional plane at $\theta = \pi/6$:

1. We rotate a point in the (y, z)-plane by $\phi = \theta - \pi/2$, so that it lies on the cross-sectional plane at $\theta = \pi/6$, obtaining the new point

$$\mathbf{x}_\theta = \left(\frac{\sqrt{3}}{2}\, y, \frac{1}{2}\, y, z \right) \ . \tag{2.10}$$

2. We project $\mathbf{B}$ onto the plane at $\theta = \pi/6$, with orthonormal basis vectors $\mathbf{w}_1 = (\sqrt{3}/2, 1/2, 0)$ and $\mathbf{w}_2 = (0, 0, 1)$, obtaining

$$\begin{aligned} P(\mathbf{B}) &= (\mathbf{B} \cdot \mathbf{w}_1)\, \mathbf{w}_1 + (\mathbf{B} \cdot \mathbf{w}_2)\, \mathbf{w}_2 \\ &= \left(\frac{3}{4}\, B_x + \frac{\sqrt{3}}{4}\, B_y,\ \frac{\sqrt{3}}{4}\, B_x + \frac{1}{4}\, B_y,\ B_z \right) \ , \end{aligned} \tag{2.11}$$

   where $\mathbf{B} \cdot \mathbf{w}_i$ denotes the standard scalar product.

3. We rotate $P(\mathbf{B})$ by $\pi/2 - \theta$, so that it lies on the (y, z)-plane, obtaining the new vector

$$\mathbf{B}_\theta = \left(0,\ \frac{\sqrt{3}}{2}\, B_x + \frac{1}{2}\, B_y,\ B_z \right) \ . \tag{2.12}$$

4. The arguments for `StreamPlot` are thus given by

$$\mathbf{v} = \left(\frac{\sqrt{3}}{2}\, B_x(\mathbf{x}_\theta) + \frac{1}{2}\, B_y(\mathbf{x}_\theta),\ B_z(\mathbf{x}_\theta) \right) \ , \tag{2.13}$$

   with appropriate intervals of variation for y and z.

2.4.2 Numerical results

In Figure 2.1 we show the **B**-field lines on the cross-sectional plane at $\theta = \pi/6$ for several torus knots/unknots ($R = 1$ and $\lambda = 0.75$). The geometric reference system (cross-sectional axes and torus) and the cross-section of $\mathcal{T}_{p,q}$ ($2p$ points) are shown in yellow and red, respectively. For induction points at a distance of $O(\lambda)$ or greater, the field lines configuration resembles that of the field induced by a circular electric wire (electric dipole). Thus, from a distance of $O(\lambda)$ or greater there is no possibility to detect the geometric and topological complexity of the source field by means of information from the induced field.
Let us consider the field lines patterns in a neighbourhood of the source field. When p is small the **B**-field lines configuration is analogous to that of the field induced by a system of $2p$ (parallel and anti-parallel) straight lines orthogonal to the cross-sectional plane (Figure 2.1a–e). In this case the local contribution of the source field to the cross-sectional components of **B** is dominant with respect to the global contribution. Conversely, when p is large the global contribution of the source field dominates: the **B**-field line are like those of the field induced by a toroidal hollow ring and the poloidal component of **B** is dominant (Figure 2.1f). The poloidal wraps q do not give an evident contribution to the components of **B** in the cross-sectional plane (compare Figure 2.1c with e and Figure 2.1b with d). This is due to the fact that a dominant poloidal source field induces a dominant toroidal field and the toroidal component of **B** is stronger in the direction orthogonal to the cross-sectional plane.

In Figure 2.2 we show visualizations of the **B**-field lines for the torus knot $\mathcal{T}_{2,3}$ ($R = 1$ and $\lambda = 0.75$) in several cross-sectional planes. The field-lines pattern not only translates along the torus central axis as we move along this axis, but also turns about this axis. The morphism relating the field lines on two different cross-sectional planes is not simply a rotation, but is also function of the reciprocal positions of the cross-sectional points of $\mathcal{T}_{p,q}$. When p is larger, field lines on different cross-sections show the same pattern. Indeed, the larger is the number of toroidal wraps, the more the source field tends to a configuration with circular symmetry in cross-section.

2.5 Influence of winding number

In Figure 2.3 we show the norm (intensity) $|\mathbf{B}|$ of the induced field against the winding number w of several torus knots/unknots ($R = 1$ and $\lambda = 0.75$) at the induction point $\mathbf{x}_o = (x_o, 0, 0)$ for different positions on the x-axis. Let $\mathbf{x}_o$ be at the origin of the reference system; for a toroidal source field $|\mathbf{B}|$ grows with the number of toroidal wraps, whereas for a poloidal source field it is almost constant (Figure 2.3a). When $\mathbf{x}_o$ is moved away from this symmetric position, for unknots $\mathcal{T}_{p,1}$ $|\mathbf{B}|$ shows a different behaviour depending on the parity of p and the interpolation curve splits into two different branches (Figure 2.3b and c). This is

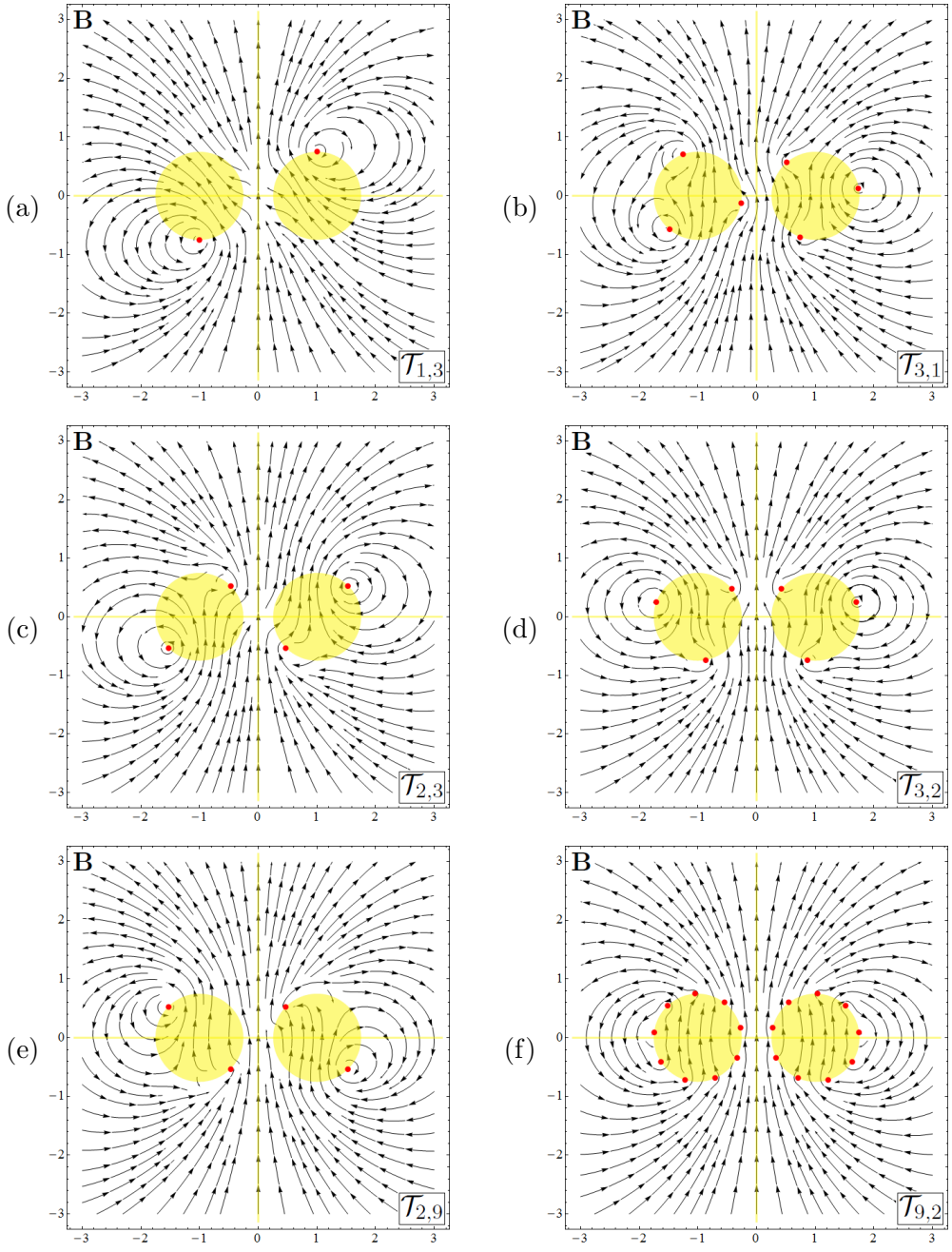

Figure 2.1: **B**-field lines on the cross-sectional plane at $\theta = \pi/6$ for several torus knots/unknots ($R = 1$ and $\lambda = 0.75$). The geometric reference system and the cross-section of $\mathcal{T}_{p,q}$ are shown in yellow and red colours, respectively.

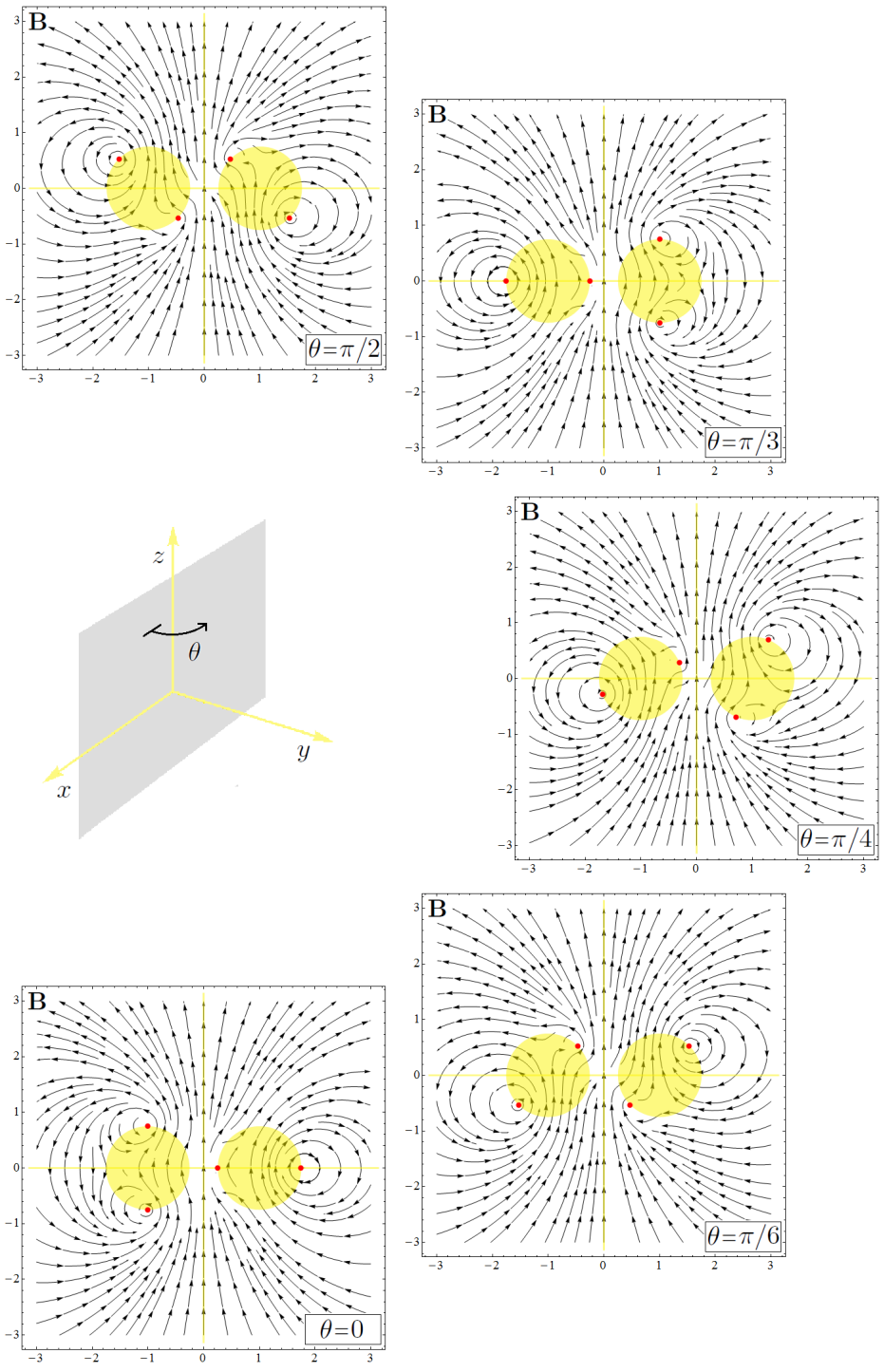

Figure 2.2: **B**-field lines for $\mathcal{T}_{2,3}$ ($R = 1$ and $\lambda = 0.75$) on several cross-sectional planes. The geometric reference system and the cross-section of $\mathcal{T}_{p,q}$ are shown in yellow and red, respectively.

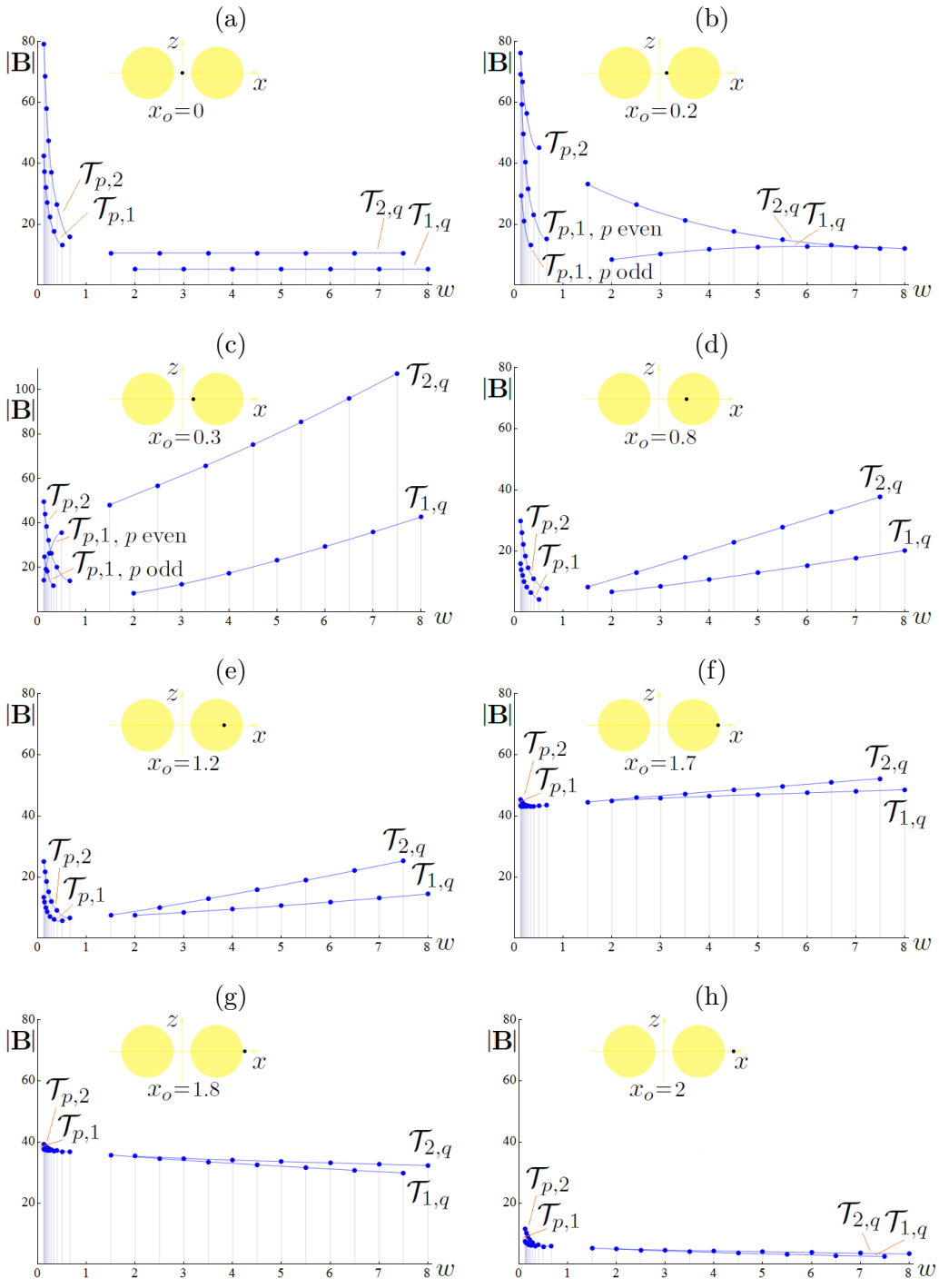

Figure 2.3: Intensity $|\mathbf{B}|$ of the induced field against winding number w. Torus knots/unknots with $R = 1$ and $\lambda = 0.75$. $\mathcal{T}_{p,1}$ and $\mathcal{T}_{1,q}$ $(p, q = \{2, 3, 4, 5, 6, 7, 8\})$; $\mathcal{T}_{p,2}$ and $\mathcal{T}_{2,q}$ $(p, q = \{3, 5, 7, 9, 11, 13, 15\})$. Induction points $\mathbf{x}_o = (x_o, 0, 0)$ at different positions on the x-axis. Interpolation is for visualization purposes only.

essentially due to the different local geometry of $\mathcal{T}_{p,1}$ in a neighbourhood of $\mathbf{x}_o$. As $\mathbf{x}_o$ is in the region occupied by the mathematical torus (next to its boundary), also $|\mathbf{B}|$ of a poloidal source field grows with the number of poloidal wraps and can reach very high values (Figure 2.3c). In general, if the source field is toroidal, the induced field is weaker inside the torus than on the outside, whereas if the source field is poloidal, the induced field is weaker outside the torus. The more $\mathbf{x}_o$ moves away along on the x-axis, the lower $|\mathbf{B}|$ becomes. For $\mathbf{x}_o$ in a neighbourhood of the centre of the torus, $|\mathbf{B}|$ for toroidal and poloidal source fields is of the same order (Figure 2.3d and e). As $\mathbf{x}_o$ approaches the torus boundary from the interior, $|\mathbf{B}|$ suddenly increases (Figure 2.3f) and then gradually decreases as $\mathbf{x}_o$ is

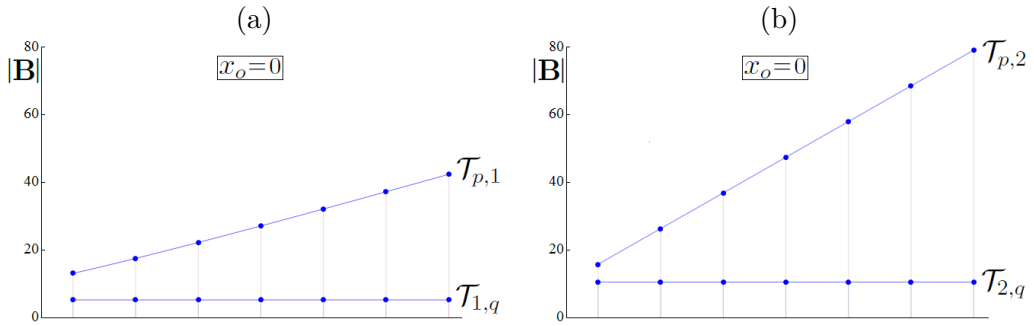

Figure 2.4: Intensity $|\mathbf{B}|$ for unknots $\mathcal{T}_{p,1}$ and $\mathcal{T}_{1,q}$ ($p, q = \{2, 3, 4, 5, 6, 7, 8\}$, left), and knots $\mathcal{T}_{p,2}$ and $\mathcal{T}_{2,q}$ ($p, q = \{3, 5, 7, 9, 11, 13, 15\}$, right); $R = 1$ and $\lambda = 0.75$. Knots/unknots are equally spaced on the x-axis. Induction point at the origin of the reference system. Interpolation is for visualization purposes only.

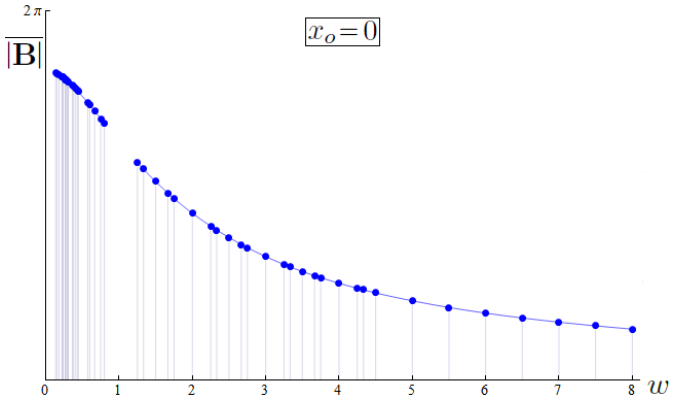

Figure 2.5: Intensity per unit length $\overline{|\mathbf{B}|}$ against winding number w for several torus knots/unknots with $w < 1$ and $w > 1$ ($R = 1$ and $\lambda = 0.75$). Induction point at the origin of the reference system. Interpolation is for visualization purposes only.

in the exterior of the torus (Figure 2.3g), with $|\mathbf{B}| \to 0$ as $x_o \to \infty$ (Figure 2.3h). Note that the induction of a poloidal source field has very different behaviours for different $\mathbf{x}_o$.

Diagrams in Figure 2.4 show $|\mathbf{B}|$ at the origin of the reference system for several torus knots/unknots ($R = 1$ and $\lambda = 0.75$) equally spaced on the x-axis. For knots/unknots with $w < 1$, $|\mathbf{B}|$ at the origin is proportional to total length (see Figure 1.8) and linear in p. In the limit $p \to \infty$ (q fixed), $\mathbf{B}$ develops a strong poloidal component, and hence $|\mathbf{B}| \to \infty$. When $w > 1$, since poloidal wraps on opposite sides of the torus have opposite source field orientation, their induction effects at the origin cancel out: by comparing the plots of $\mathcal{T}_{1,q}$ and $\mathcal{T}_{2,q}$ (Figure 2.4a and b), we see that the contribution from poloidal wraps is absent as the intensity of the induced field for unknots with 1 toroidal coil is half of that due to knots with 2 toroidal coils. Let us consider the *intensity per unit length*, given by

$$\overline{|\mathbf{B}|}(\mathcal{T}_{p,q}) = 2\pi R \cdot \frac{|\mathbf{B}|(\mathcal{T}_{p,q})}{L(\mathcal{T}_{p,q})} \ , \tag{2.14}$$

where $|\mathbf{B}|(\mathcal{T}_{p,q})$ and $L(\mathcal{T}_{p,q})$ denote the intensity of the field induced by $\mathcal{T}_{p,q}$ and the total length of $\mathcal{T}_{p,q}$, respectively. Figure 2.5 shows $\overline{|\mathbf{B}|}$ at the origin for several knots/unknots. This study can find applications to the problem of plasma confinement in experimental devices with toroidal geometry like tokamaks and stellarators [31, 26, 24].

2.6 Plots of mean B intensity

Let us consider the values of $|\mathbf{B}|$ for some unknots $\mathcal{T}_{p,1}$, for a given position x_o of the induction point on the x-axis. Let us denote by $|\mathbf{B}|_m$ the arithmetic mean of these values over the unknots considered. Diagrams in Figure 2.6 show $|\mathbf{B}|_m$ for several positions x_o of the induction point, where the mean is taken over 7 unknots within the classes $\mathcal{T}_{p,1}$ and $\mathcal{T}_{1,q}$, respectively, and 7 knots within the classes $\mathcal{T}_{p,2}$ and $\mathcal{T}_{2,q}$, respectively. The yellow region shows the positions where x_o is inside the mathematical torus. The presence of two maxima of $|\mathbf{B}|_m$ at $x_o = 0.3$ and $x_o = 1.7$ (inside the torus, next to its boundary) is a general feature of all the classes $\mathcal{T}_{i,q}$ (i fixed) (Figure 2.6b and d). For classes $\mathcal{T}_{p,i}$ (i fixed), $|\mathbf{B}|_m$ has generically a maximum at $x_o = 1.7$, but it has a different behaviour for $x_o \in [0, 0.3]$ depending on the parity of i (Figure 2.6a and c). This seems to be due to the dominant contribution of the local geometry of $\mathcal{T}_{p,i}$ in a neighbourhood of x_o.
This study can find applications to magnetic confinement of plasma, where the problem of the maintenance of the magnetic field's intensity within a safety range is crucial, and where the shaping of the device and the magnetic geometry are central for the control and optimization of plasma fusion [8, 67, 11].

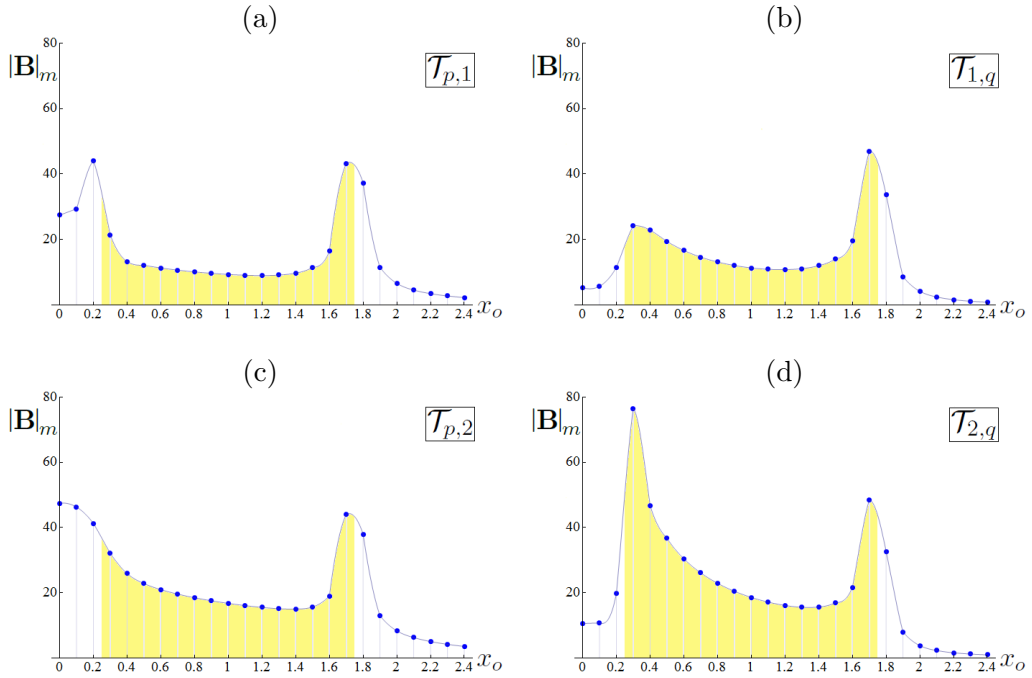

Figure 2.6: Mean intensity $|\mathbf{B}|_m$ against position x_o of the induction point on the x-axis. The mean is taken over (a) $\mathcal{T}_{p,1}$ and (b) $\mathcal{T}_{1,q}$ ($p, q = \{2, 3, 4, 5, 6, 7, 8\}$), (c) $\mathcal{T}_{p,2}$ and (d) $\mathcal{T}_{2,q}$ ($p, q = \{3, 5, 7, 9, 11, 13, 15\}$); $R = 1$ and $\lambda = 0.75$. Yellow region for positions x_o inside the mathematical torus. Interpolation is for visualization purposes only.

2.7 Helicity

Helicity has a peculiar role in fluid dynamics (including MHD) since it is an invariant of the Euler and ideal MHD equations and a robust quantity of non-ideal flows; it admits a topological interpretation in terms of linking numbers associated with magnetic/vortex lines in ideal fluids. Its conservation was proved by Woltjer [66] in the context of ideal MHD (magnetic helicity). Its topological characterization in terms of Gauss linking number was first established by Moffatt [36] in the context of vortex dynamics (kinetic helicity) for a collection of thin unknotted vortex filaments and then extended by Berger & Field [10], Moffatt & Ricca [39] to a general collection of knotted magnetic flux tubes. A recent breakthrough by Liu & Ricca [28] provides a relationship between helicity and another isotopy invariant, the HOMFLYPT polynomial, stronger than the Gauss linking number in detecting topological properties of fluid knots.
If $\mathbf{B} = \mathbf{B}(\mathbf{x})$ is a magnetic vector field over a volume $V = V(\mathbf{x})$ and conditions [54] are satisfied, being $\mathbf{A} = \mathbf{A}(\mathbf{x})$ the vector potential of $\mathbf{B}$, subject to the Coulomb

gauge, then magnetic helicity is given by

$$H = \int_{V(\mathbf{x})} \mathbf{A} \cdot \mathbf{B} \, d\mathbf{x} \ . \tag{2.15}$$

Note that $\mathbf{A} = \mathcal{BS}(\mathbf{B})$. By the analogy $\boldsymbol{\omega} \leftrightarrow \mathbf{B}$, kinetic helicity is simply obtained by replacing $\mathbf{A} \cdot \mathbf{B}$ with $\mathbf{u} \cdot \boldsymbol{\omega}$, where $\boldsymbol{\omega}$ is the vorticity field defined over V and $\mathbf{u} = \mathcal{BS}(\boldsymbol{\omega})$ is the rotational velocity field, with $\nabla \cdot \mathbf{u} = 0$. By the analogy $\boldsymbol{\omega} \leftrightarrow \mathbf{j}$, by replacing $\mathbf{u} \cdot \boldsymbol{\omega}$ with $\mathbf{B} \cdot \mathbf{j}$, we obtain the helicity of the electric current $\mathbf{j}$ (where $\mathbf{B} = \mathcal{BS}(\mathbf{j})$ is the induced magnetic field), a useful quantity for understanding physics of solar processes, but not an invariant of the MHD equations [55, 44].

If $\mathbf{B}$ is confined to a single thin flux tube $\mathcal{T}$ centred on $\mathcal{T}_{p,q}$, with flux Φ and satisfying the assumptions of section 2.2, then eq. (2.15) becomes

$$H = \int_{\mathcal{T}(\mathbf{x})} \mathcal{BS}(\mathbf{B}) \cdot \mathbf{B} \, d\mathbf{x} \ , \tag{2.16}$$

and H is related to the Călugăreanu self-linking number Lk (eqs. (1.64) and (1.65)), according to [39]

$$H = \Phi^2 Lk \ . \tag{2.17}$$

In order to have a non-dimensional quantity, we shall consider

$$\overline{H} = \frac{H}{\Phi^2} \ . \tag{2.18}$$

Since we have supposed $\mathbf{B}$ directed along the tangent of $\mathcal{T}_{p,q}$, the intrinsic twist $\mathscr{N}$ (given by the number of full rotations of the field lines of $\mathcal{T}$ around its centreline $\mathcal{T}_{p,q}$) is zero and no contribution comes from the distribution of the field lines of $\mathcal{T}$. Hence, by eq. (1.65) we have $Lk = SL$ and, in particular,

$$\overline{H} = SL \ , \tag{2.19}$$

where SL is the Pohl self-linking number of $\mathcal{T}_{p,q}$ (see eq. (1.61)).

We have three different approaches to calculate $\overline{H}$. For ease of presentation, let us consider $|\overline{H}|$, the negative values being due to the handedness associated with the parametrization of $\mathcal{T}_{p,q}$ chosen, and let us take $\lambda = 0.5$.

1. By eq. (2.19) and Corollary 1.13, we have the analytical result:

$$|\overline{H}| = \begin{cases} q(p-1) & \text{if } w < 1 \\ pq & \text{if } w > 1 \end{cases} \ . \tag{2.20}$$

2. By eqs. (2.19) and (1.61) we compute the quantity $|\overline{H}^g| = |Wr + \mathscr{T}|$ as the sum of the numerical data on the writhing number Wr and the normalized total torsion $\mathscr{T}$ of $\mathcal{T}_{p,q}$ (see sections 1.10 and 1.8).

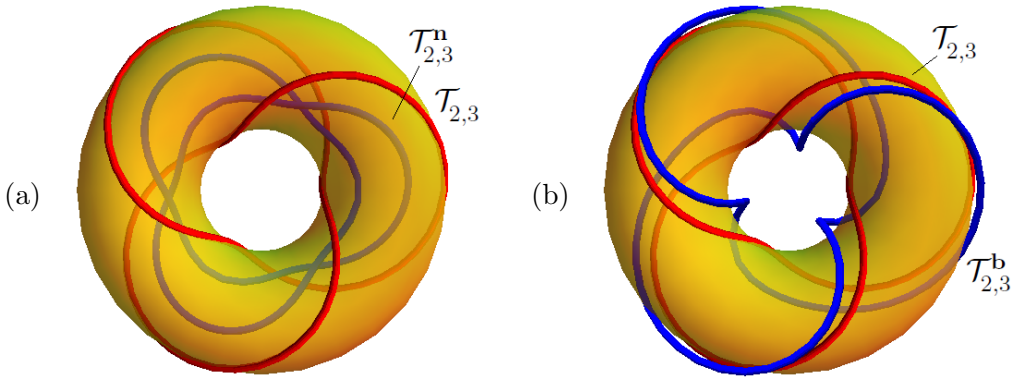

Figure 2.7: Torus knot $\mathcal{T}_{2,3}$ (red) for $R = 1$, $\lambda = 0.5$ and curves (a) $\mathcal{T}^{\mathbf{n}}_{2,3}$ and (b) $\mathcal{T}^{\mathbf{b}}_{2,3}$ (blue) for $\varepsilon = 0.3$.

3. We evaluate the integral in the right-hand side of eq. (2.16). Since this integral is singular, due to the singularity of the Biot-Savart operator $\mathcal{BS}$ when evaluated on $\mathcal{T}$, we de-singularize it by the following easy technique. Let us consider the second curve $\mathcal{T}^{\mathbf{n}}_{p,q} = \mathcal{T}^{\mathbf{n}}_{p,q}(\varepsilon) = \mathcal{T}_{p,q} + \varepsilon\mathbf{n}$, where $\mathcal{T}_{p,q}$ is parametrized by eqs. (1.2), $\mathbf{n}$ is its unit normal vector and ε is a small real number (see Figure 2.7a). We write the Biot-Savart integral (eq. (2.8)) by identifying $\mathcal{T}$ with $\mathcal{T}^{\mathbf{n}}_{p,q}$ instead of $\mathcal{T}_{p,q}$, and the helicity integral (eqs. (2.16)) by identifying $\mathcal{T}$ with $\mathcal{T}_{p,q}$. Thus, we have

$$\begin{aligned}\overline{H}^{\mathbf{n}} &= \frac{1}{4\pi}\int_0^{2\pi p} \dot{\mathbf{x}}(\alpha)\cdot\left(\int_0^{2\pi p} \dot{\mathbf{x}}^{\mathbf{n}}(\alpha^*)\times\frac{\mathbf{x}(\alpha)-\mathbf{x}^{\mathbf{n}}(\alpha^*)}{|\mathbf{x}(\alpha)-\mathbf{x}^{\mathbf{n}}(\alpha^*)|^3}\,d\alpha^*\right)d\alpha \\ &= \frac{1}{4\pi}\int_0^{2\pi p}\int_0^{2\pi p}\frac{(\dot{\mathbf{x}}(\alpha)\times\dot{\mathbf{x}}^{\mathbf{n}}(\alpha^*))\cdot(\mathbf{x}(\alpha)-\mathbf{x}^{\mathbf{n}}(\alpha^*))}{|\mathbf{x}(\alpha)-\mathbf{x}^{\mathbf{n}}(\alpha^*)|^3}\,d\alpha d\alpha^*\ ,\end{aligned} \tag{2.21}$$

where $\overline{H}^{\mathbf{n}} = \overline{H}^{\mathbf{n}}(\varepsilon)$, $\mathbf{x}(\alpha)$ and $\mathbf{x}^{\mathbf{n}}(\alpha^*)$ are points on $\mathcal{T}_{p,q}$ and $\mathcal{T}^{\mathbf{n}}_{p,q}$, respectively, $\dot{\mathbf{x}}$ (resp. $\dot{\mathbf{x}}^{\mathbf{n}}$) denotes derivative with respect to α (resp. α^*) and a standard vector equality is used to obtain the second line from the first. When $\varepsilon \to 0$, $\mathcal{T}^{\mathbf{n}}_{p,q} \to \mathcal{T}_{p,q}$ and $\overline{H}^{\mathbf{n}} \to \overline{H}$. Indeed, this technique is the direct application of Călugăreanu's definition of Lk as the limit for $\varepsilon \to 0$ of the Gauss linking number between $\mathcal{T}_{p,q}$ and $\mathcal{T}^{\mathbf{n}}_{p,q}$ (see eq. (1.64)), and of the Călugăreanu-White-Fuller theorem (see eq. (1.65)) realizing Lk as $Lk = SL + \mathscr{N}$. Note that the contribution given by the rotation of $\mathcal{T}^{\mathbf{n}}_{p,q}$ around $\mathcal{T}_{p,q}$ is zero, coherently with the assumption $\mathscr{N} = 0$ (see section 1.13 for a proof that the normal framing gives $\mathscr{N} = 0$). We then numerically evaluate $|\overline{H}^{\mathbf{n}}|$ for $\varepsilon = 0.1$.
Since the binormal framing gives $\mathscr{N} = 0$ as well, we can also consider the curve $\mathcal{T}^{\mathbf{b}}_{p,q} = \mathcal{T}^{\mathbf{b}}_{p,q}(\varepsilon) = \mathcal{T}_{p,q} + \varepsilon\mathbf{b}$, where $\mathbf{b}$ the unit binormal vector of $\mathcal{T}_{p,q}$

(see Figure 2.7b) and, by applying the same technique, we obtain

$$\overline{H}^{\mathbf{b}} = \frac{1}{4\pi}\int_0^{2\pi p}\int_0^{2\pi p} \frac{\left(\dot{\mathbf{x}}(\alpha)\times\dot{\mathbf{x}}^{\mathbf{b}}(\alpha^*)\right)\cdot\left(\mathbf{x}(\alpha)-\mathbf{x}^{\mathbf{b}}(\alpha^*)\right)}{\left|\mathbf{x}(\alpha)-\mathbf{x}^{\mathbf{b}}(\alpha^*)\right|^3}\, d\alpha d\alpha^* \ , \quad (2.22)$$

where $\overline{H}^{\mathbf{b}} = \overline{H}^{\mathbf{b}}(\varepsilon)$, $\mathbf{x}^{\mathbf{b}}(\alpha^*)$ is a point on $\mathcal{T}^{\mathbf{b}}_{p,q}$, $\dot{\mathbf{x}}^{\mathbf{b}}$ denotes derivative with respect to α^*, and when $\varepsilon \to 0$, $\overline{H}^{\mathbf{b}} \to \overline{H}$. We numerically evaluate $|\overline{H}^{\mathbf{b}}|$ for $\varepsilon = 0.1$.
More generally, any choice of the type $\mathcal{T}_{p,q} + \varepsilon\mathbf{N}$, where $\mathbf{N}$ is a linear combination of $\mathbf{n}$ and $\mathbf{b}$ with *constant* coefficient all along $\mathcal{T}_{p,q}$, gives $\mathscr{N} = 0$ and can be used to calculate $|\overline{H}|$ by applying the technique described. However note that these curves have different lengths: in general, $\mathcal{T}^{\mathbf{n}}_{p,q}$ is obtained through a shrinking deformation of $\mathcal{T}_{p,q}$, whereas $\mathcal{T}^{\mathbf{b}}_{p,q}$ through an expansion.

In Figure 2.8 we compare the methods in 2. and 3. with the theoretical result eq. (2.20), by showing the log-plot of $\Delta^g = |\overline{H} - \overline{H}^g|$ (blue), $\Delta^{\mathbf{n}} = |\overline{H} - \overline{H}^{\mathbf{n}}|$ (red) and $\Delta^{\mathbf{b}} = |\overline{H} - \overline{H}^{\mathbf{b}}|$ (black) for torus knots (a) $\mathcal{T}_{p,2}$ and (b) $\mathcal{T}_{2,q}$ ($p, q = \{3, 5, 7, 9, 11, 13, 15\}$, $R = 1$ and $\lambda = 0.5$). All three methods give very satisfactory results and generally the error is smaller than 2% of the expected value for all knots/unknots tested. Results are particularly good for knots/unknots of low complexity. Still, note that $\overline{H}^{\mathbf{n}}$ and $\overline{H}^{\mathbf{b}}$ depends on the choice of ε. By taking $\varepsilon < O(10^{-1})$, the features of $\overline{H}^{\mathbf{n}}$ and $\overline{H}^{\mathbf{b}}$ are qualitatively preserved, but numerical values can be quite different from the expected ones, certainly due to the numerical error in evaluating the Biot-Savart integral over a curve very close to $\mathcal{T}_{p,q}$. For this approach, hence, a careful balance between an ε too small, which may cause numerical error, and too large, which may produce an unlinking of the two curves, is needed.

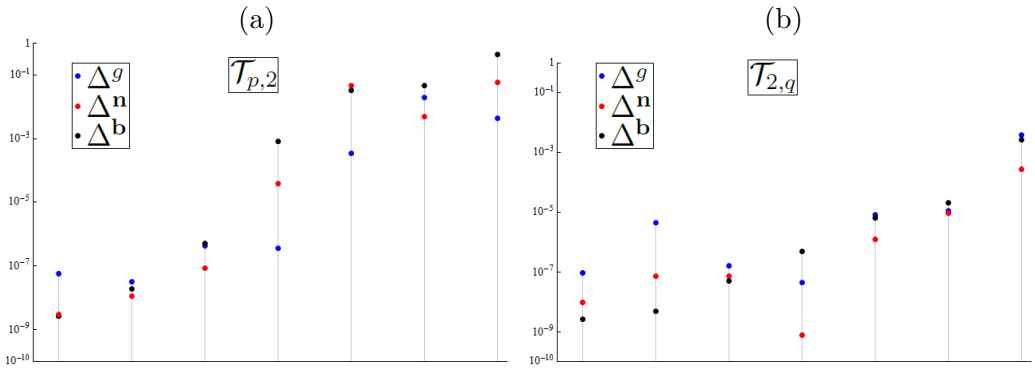

Figure 2.8: Log-plot of $\Delta^g = |\overline{H} - \overline{H}^g|$ (blue), $\Delta^{\mathbf{n}} = |\overline{H} - \overline{H}^{\mathbf{n}}|$ (red) and $\Delta^{\mathbf{b}} = |\overline{H} - \overline{H}^{\mathbf{b}}|$ (black) for torus knots (a) $\mathcal{T}_{p,2}$ and (b) $\mathcal{T}_{2,q}$ ($p, q = \{3, 5, 7, 9, 11, 13, 15\}$, $R = 1$ and $\lambda = 0.5$); $\varepsilon = 0.1$. Knots are equally spaced on the x-axis.

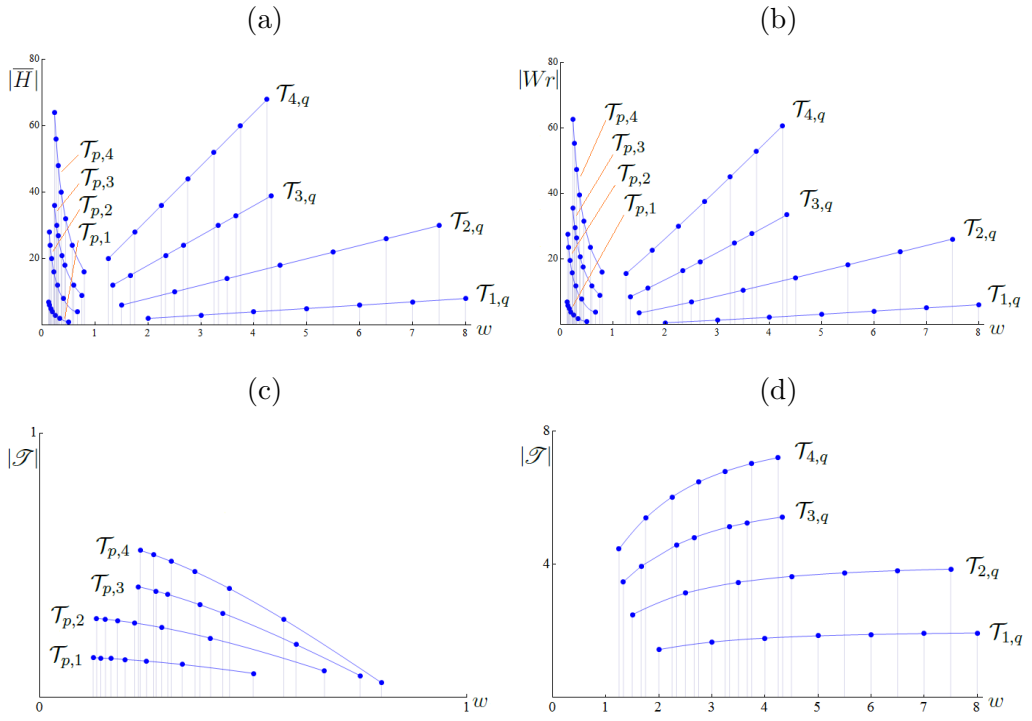

Figure 2.9: (a) non-dimensional helicity $|\overline{H}|$, (b) writhing number $|Wr|$ and (c)–(d) normalized total torsion $|\mathscr{T}|$ (absolute values) against winding number w of several torus knots/unknots ($R = 1$ and $\lambda = 0.5$; $\mathcal{T}_{p,1}$ and $\mathcal{T}_{1,q}$, $p, q = \{2, 3, 4, 5, 6, 7, 8\}$; $\mathcal{T}_{p,2}$ and $\mathcal{T}_{2,q}$, $p, q = \{3, 5, 7, 9, 11, 13, 15\}$; $\mathcal{T}_{p,3}$ and $\mathcal{T}_{3,q}$, $p, q = \{4, 5, 7, 8, 10, 11, 13\}$; $\mathcal{T}_{p,4}$ and $\mathcal{T}_{4,q}$, $p, q = \{5, 7, 9, 11, 13, 15, 17\}$). Interpolation is for visualization purposes only.

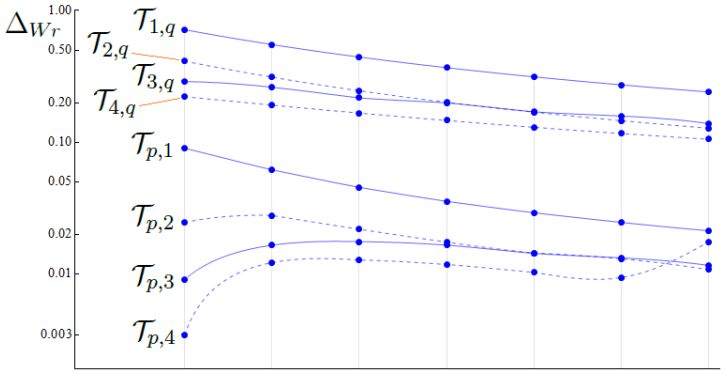

Figure 2.10: Log-plot of $\Delta_{Wr} = (|\overline{H}| - |Wr|)/|\overline{H}|$ for the torus knots/unknots $\mathcal{T}_{p,1}$–$\mathcal{T}_{p,4}$ and $\mathcal{T}_{1,q}$–$\mathcal{T}_{4,q}$ as in Figure 2.9. Knots/unknots are equally spaced on the x-axis. Interpolation lines are only for visualization purposes.

Figure 2.9a shows $|\overline{H}|$ against w for several torus knots/unknots. Qualitative features of $|\overline{H}|$ are fully captured by the writhing number $|Wr|$ (confront Figure 2.9b). For toroidal knots/unknots the contribution from $|\mathscr{T}|$ is negligible (Figure 2.9c) and $|\overline{H}|$ is well approximated by $|Wr|$: indeed the error $\Delta_{Wr} = (|\overline{H}| - |Wr|)/|\overline{H}|$ is generally far smaller then 9%. Conversely, the mean error over the poloidal knots/unknots considered is 25%. See Figure 2.10 for the log-plot of Δ_{Wr} for the knots/unknots $\mathcal{T}_{p,1}$–$\mathcal{T}_{p,4}$ and $\mathcal{T}_{1,q}$–$\mathcal{T}_{4,q}$ as in Figure 2.9 (knots/unknots are equally spaced on the x-axis).

2.8 Magnetic energy

Let $\mathbf{B} = \mathbf{B}(\mathbf{x})$ be a magnetic vector field confined to a domain $\mathcal{D} \subseteq \mathbb{R}^3$ of volume $V = V(\mathbf{x})$ in a perfectly conducting, incompressible fluid, and such that $\mathbf{B} \cdot \boldsymbol{\nu} = 0$ on $\partial\mathcal{D}$ (where $\boldsymbol{\nu}$ is the unit normal to $\partial\mathcal{D}$). The magnetic energy is given by

$$M = \frac{1}{2} \int_{V(\mathbf{x})} \mathbf{B}^2 \, d\mathbf{x} \ , \tag{2.23}$$

and a lower bound for M is given by [7, 37, 38]

$$M \geq v \, |H| \ , \tag{2.24}$$

where H is the magnetic helicity (eq. 2.15) and v depends on the geometry of $\mathcal{D}$. For example, if $\mathcal{D}$ is given by a collection of linked thin magnetic flux tube such that each component of the link has Călugăreanu self-linking number $Lk = 0$, then we have [49]

$$v = \left(\frac{2}{\pi}\right)^{1/3} \frac{1}{V^{1/3}} \ . \tag{2.25}$$

If $\mathbf{B}$ is confined to a single thin flux tube centred on $\mathcal{T}_{p,q}$ (parametrized by eqs. (1.2)), with flux Φ and satisfying the assumptions of section 2.20, then eq. (2.23) becomes

$$M = \frac{\Phi^2}{2} \int_0^{2\pi p} |\dot{\mathbf{x}}(\alpha)| d\alpha = \frac{\Phi^2}{2} L \ , \tag{2.26}$$

where L is the total length of $\mathcal{T}_{p,q}$ (eq. (1.37)). In order to have a non-dimensional quantity, we consider

$$\overline{M} = \frac{M}{2\pi R \Phi^2} \ . \tag{2.27}$$

By Theorem (1.10) and by eqs. (2.26) and (2.27), we have

Theorem 2.1. *Let $\overline{M}$ be the non-dimensional magnetic energy of a $\mathcal{T}_{p,q}$ parametrized by eqs. (1.2). Then*

$$\overline{M} \approx \begin{cases} \dfrac{\lambda q}{2} & \text{if } q \gg p \text{ } (p \text{ given}) \, ; \\ \dfrac{(1+\lambda)p}{2} & \text{if } p \gg q \text{ } (q \text{ given}) \, . \end{cases} \tag{2.28}$$

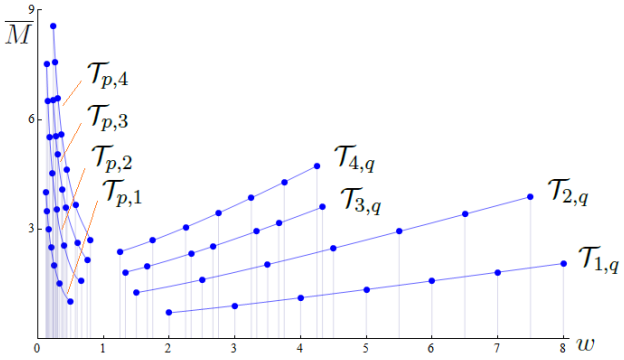

Figure 2.11: Non-dimensional magnetic energy $\overline{M}$ against winding number w for several torus knots/unknots ($R = 1$ and $\lambda = 0.5$; $\mathcal{T}_{p,1}$ and $\mathcal{T}_{1,q}$, $p, q = \{2, 3, 4, 5, 6, 7, 8\}$; $\mathcal{T}_{p,2}$ and $\mathcal{T}_{2,q}$, $p, q = \{3, 5, 7, 9, 11, 13, 15\}$; $\mathcal{T}_{p,3}$ and $\mathcal{T}_{3,q}$, $p, q = \{4, 5, 7, 8, 10, 11, 13\}$; $\mathcal{T}_{p,4}$ and $\mathcal{T}_{4,q}$, $p, q = \{5, 7, 9, 11, 13, 15, 17\}$). Interpolation is for visualization purposes only.

Moreover, by the bounds on L (eq. (1.48)) and by eqs. (2.26) and (2.27), we have

$$\frac{p}{2}\sqrt{(1-\lambda)^2+\lambda^2 w^2} \leq \overline{M} \leq \frac{p}{2}\sqrt{(1+\lambda)^2+\lambda^2 w^2}\ , \tag{2.29}$$

and can prove the following result:

Theorem 2.2. *Let $\overline{M}$ be the non-dimensional magnetic energy of a magnetic $\mathcal{T}_{p,q}$ parametrized by eqs. (1.2), with non-dimensional helicity $\overline{H}$, in a perfectly conducting, incompressible fluid under steady conditions. Then we have*

$$\overline{M} \geq v\,|\overline{H}|\ , \quad \text{with} \quad v = \frac{1}{2}\sqrt{\frac{(1-\lambda)^2}{q^2}+\frac{\lambda^2}{p^2}}\ . \tag{2.30}$$

Proof. By eqs. (1.62) and (2.19), if $\lambda > \lambda_{cr}$ we have $|\overline{H}| = pq$. Thus, by the left-hand side of eq. (2.29) we obtain

$$\overline{M} \geq \frac{p}{2}\sqrt{(1-\lambda)^2+\lambda^2 w^2} = \frac{1}{2}\sqrt{\frac{(1-\lambda)^2}{q^2}+\frac{\lambda^2}{p^2}}\,|\overline{H}|\ . \tag{2.31}$$

Conversely, if $\lambda < \lambda_{cr}$ we have $|\overline{H}| = q(p-1)$, and by the left-hand side of eq. (2.29) we obtain

$$\begin{aligned} \overline{M} &\geq \frac{p}{2}\sqrt{(1-\lambda)^2+\lambda^2 w^2} \\ &\geq \frac{p-1}{2}\sqrt{(1-\lambda)^2+\lambda^2 w^2} = \frac{1}{2}\sqrt{\frac{(1-\lambda)^2}{q^2}+\frac{\lambda^2}{p^2}}\,|\overline{H}|\ . \end{aligned} \tag{2.32}$$

□

Figure 2.11 shows $\overline{M}$ against w for several torus knots/unknots ($R = 1$ and $\lambda = 0.5$). Comparison between Figure 2.9 and 2.11 shows that $|Wr|$ capture some qualitative features of $\overline{M}$; in particular, for $\mathcal{T}_{p,2}$ and $\mathcal{T}_{2,q}$ $|Wr|$ and $\overline{M}$ have the same functional behaviour. In Figure 2.12 we show the log-plot of $\Delta_{lb} = (\overline{M} - lb)/\overline{M}$, where lb denotes the lower bound for $\overline{M}$ given by eq. (2.30). When $w > 1$ and the knots/unknots complexity is high, lb becomes actually a good approximation to $\overline{M}$. When $w < 1$, Δ_{lb} is on average 56% of $\overline{M}$ for the knots/unknots considered.

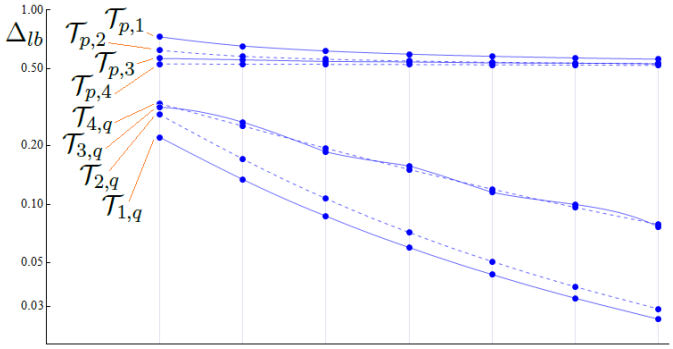

Figure 2.12: Log-plot of $\Delta_{lb} = (\overline{M} - lb)/\overline{M}$ for the torus knots/unknots $\mathcal{T}_{p,1}$–$\mathcal{T}_{p,4}$ and $\mathcal{T}_{1,q}$–$\mathcal{T}_{4,q}$ as in Figure 2.11. Knots/unknots are equally spaced on the x-axis. Interpolation is for visualization purposes only.

Chapter 3

The Biot-Savart integral: local and global contributions

In this chapter we compare the winding number effects on the local and global contributions of the Biot-Savart induction, by providing asymptotic expansions of the integrand function. For this purpose, we introduce the pseudo-toroidal reference system, by proving that it is orthonormal and by writing the toroidal, poloidal and radial components of the integrand for a given location of the induction point. By comparing the asymptotic expansion of these components with their global contributions, obtained by numerical integration, we show that leading order local terms do not generally provide sufficient information to capture global induction effects. Nevertheless, we show that for some orders of magnitude of the winding number local and global behaviours are in good agreement.

3.1 Pseudo-toroidal reference system

Let us consider the *pseudo-toroidal coordinates* (α, β, r), related to the cartesian coordinates by

$$\mathbf{x} = \mathbf{x}(\alpha, \beta, r) = \begin{cases} x = (R + r\cos\beta)\cos\alpha \\ y = (R + r\cos\beta)\sin\alpha \\ z = r\sin\beta \end{cases}, \tag{3.1}$$

where $\alpha, \beta \in [0, 2\pi)$ are toroidal and poloidal angles, $R, r > 0$ are the toroidal and poloidal radii of the torus; we set $R = 1$ and we take $r < R$ for the coordinate system to be well-defined. By this coordinate system, we can describe every point $\mathbf{x}$ in the interior of the degenerate torus with $r = R$, except for its centreline. If we allow $r \geq R$, the coordinate system is *not* monodromic. However, if we fix α and β, then we can take $0 < r < \infty$ and monodromy is satisfied.

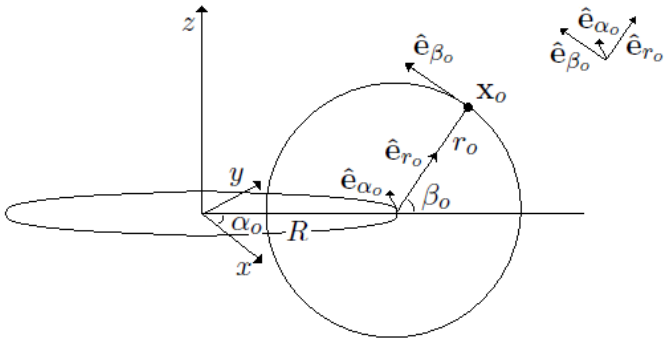

Figure 3.1: Pseudo-toroidal basis $\{\hat{\mathbf{e}}_{\alpha_o}, \hat{\mathbf{e}}_{\beta_o}, \hat{\mathbf{e}}_{r_o}\}$ at the point $\mathbf{x}_o(\alpha_o, \beta_o, r_o)$.

By differentiating eqs. (3.1), we obtain

$$d\mathbf{x} = \begin{cases} dx = -(R + r\cos\beta)\sin\alpha\, d\alpha - r\cos\alpha\sin\beta\, d\beta + \cos\alpha\cos\beta\, dr \\ dy = (R + r\cos\beta)\cos\alpha\, d\alpha - r\sin\alpha\sin\beta\, d\beta + \sin\alpha\cos\beta\, dr \\ dz = r\cos\beta\, d\beta + \sin\beta\, dr \end{cases} . \quad (3.2)$$

Hence, by denoting $\{\hat{\mathbf{e}}_1, \hat{\mathbf{e}}_2, \hat{\mathbf{e}}_3\}$ the canonical cartesian basis in $\mathbb{R}^3$, we have

$$\begin{aligned} d\mathbf{x} &= d\alpha\,[-(R + r\cos\beta)\sin\alpha\,\hat{\mathbf{e}}_1 + (R + r\cos\beta)\cos\alpha\,\hat{\mathbf{e}}_2] \\ &\quad + d\beta\,[-r\cos\alpha\sin\beta\,\hat{\mathbf{e}}_1 - r\sin\alpha\sin\beta\,\hat{\mathbf{e}}_2 + r\cos\beta\,\hat{\mathbf{e}}_3] \\ &\quad + dr\,[\cos\alpha\cos\beta\,\hat{\mathbf{e}}_1 + \sin\alpha\cos\beta\,\hat{\mathbf{e}}_2 + \sin\beta\,\hat{\mathbf{e}}_3] \\ &= d\alpha\,\mathbf{e}_\alpha + d\beta\,\mathbf{e}_\beta + dr\,\mathbf{e}_r\ , \end{aligned} \quad (3.3)$$

where

$$\mathbf{e}_\alpha = \begin{pmatrix} -(R + r\cos\beta)\sin\alpha \\ (R + r\cos\beta)\cos\alpha \\ 0 \end{pmatrix}, \quad \mathbf{e}_\beta = \begin{pmatrix} -r\cos\alpha\sin\beta \\ -r\sin\alpha\sin\beta \\ r\cos\beta \end{pmatrix}, \quad \mathbf{e}_r = \begin{pmatrix} \cos\alpha\cos\beta \\ \sin\alpha\cos\beta \\ \sin\beta \end{pmatrix} \quad (3.4)$$

are the basis vector of the pseudo-toroidal reference system. Note that these vectors are function of the coordinates (α, β, r) of the point $\mathbf{x}$. The metric tensor is given by

$$g_{ij} = \begin{pmatrix} (R + r\cos\beta)^2 & 0 & 0 \\ 0 & r^2 & 0 \\ 0 & 0 & 1 \end{pmatrix}, \qquad i, j = \alpha, \beta, r\ . \quad (3.5)$$

Hence, the system is orthogonal and we have

$$|\mathbf{e}_\alpha| = R + r\cos\beta, \quad |\mathbf{e}_\beta| = r, \quad |\mathbf{e}_r| = 1, \quad (3.6)$$

where the first equality holds true because $R+r\cos\beta > 0$ for all β. By normalizing eqs. (3.4), we obtain the orthonormal basis vectors

$$\hat{\mathbf{e}}_\alpha = \begin{pmatrix} -\sin\alpha \\ \cos\alpha \\ 0 \end{pmatrix}, \quad \hat{\mathbf{e}}_\beta = \begin{pmatrix} -\cos\alpha\sin\beta \\ -\sin\alpha\sin\beta \\ \cos\beta \end{pmatrix}, \quad \hat{\mathbf{e}}_r = \begin{pmatrix} \cos\alpha\cos\beta \\ \sin\alpha\cos\beta \\ \sin\beta \end{pmatrix}. \tag{3.7}$$

Let us consider a point $\mathbf{x}_o$, given by

$$\mathbf{x}_o = R \begin{pmatrix} (1+\lambda_o\cos\beta_o)\cos\alpha_o \\ (1+\lambda_o\cos\beta_o)\sin\alpha_o \\ \lambda_o\sin\beta_o \end{pmatrix}, \tag{3.8}$$

where $\lambda_o = r_o/R$, $\lambda_o \in (0,1)$. Let us set the orthonormal basis eqs. (3.7) at the point $\mathbf{x}_o$ and denote it by $\{\hat{\mathbf{e}}_{\alpha_o}, \hat{\mathbf{e}}_{\beta_o}, \hat{\mathbf{e}}_{r_o}\}$ (see Figure 3.1). By projecting $\mathbf{x}_o$ on $\{\hat{\mathbf{e}}_{\alpha_o}, \hat{\mathbf{e}}_{\beta_o}, \hat{\mathbf{e}}_{r_o}\}$, we obtain the *toroidal, poloidal and radial components* of $\mathbf{x}_o$, given by

$$\mathbf{x}_o \cdot \hat{\mathbf{e}}_{\alpha_o} = 0, \quad \mathbf{x}_o \cdot \hat{\mathbf{e}}_{\beta_o} = -R\sin\beta_o, \quad \mathbf{x}_o \cdot \hat{\mathbf{e}}_{r_o} = R(\cos\beta_o + \lambda_o). \tag{3.9}$$

Let us now denote the integrand function of $\mathcal{BS}$ (eq. (2.8)) by

$$d\mathcal{BS}(\alpha) = \frac{\mathbf{t}(\alpha) \times (\mathbf{x}_o - \mathbf{x}_k(\alpha))}{|\mathbf{x}_o - \mathbf{x}_k(\alpha)|^3} \, |\dot{\mathbf{x}}_k(\alpha)| d\alpha \,, \tag{3.10}$$

where we take $\mathbf{x}_o$ as in eq. (3.9) and $\lambda_o > \lambda$ (note that $d\mathcal{BS}$ depends on R, λ, w, and α_o, β_o, λ_o). By projecting $d\mathcal{BS}$ on $\{\hat{\mathbf{e}}_{\alpha_o}, \hat{\mathbf{e}}_{\beta_o}, \hat{\mathbf{e}}_{r_o}\}$, we obtain the toroidal, poloidal and radial components of $d\mathcal{BS}$, denoted by

$$d\mathcal{BS}_{\alpha_o} = d\mathcal{BS} \cdot \hat{\mathbf{e}}_{\alpha_o} \,, \quad d\mathcal{BS}_{\beta_o} = d\mathcal{BS} \cdot \hat{\mathbf{e}}_{\beta_o} \,, \quad d\mathcal{BS}_{r_o} = d\mathcal{BS} \cdot \hat{\mathbf{e}}_{r_o} \,. \tag{3.11}$$

Notice that, since $d\mathcal{BS}$ is singular only when $\mathbf{x}_o \in \mathcal{T}_{p,q}$, by taking $\lambda_o > \lambda$ we have no singularity.

3.2 Toroidal, poloidal and radial contributions from Biot-Savart integration

The toroidal, poloidal and radial components of the induced field $\mathbf{B}$ are given by

$$B_{\alpha_o} = \int_0^{2\pi p} d\mathcal{BS}_{\alpha_o} \,, \quad B_{\beta_o} = \int_0^{2\pi p} d\mathcal{BS}_{\beta_o} \,, \quad B_{r_o} = \int_0^{2\pi p} d\mathcal{BS}_{r_o} \,. \tag{3.12}$$

Numerical integration of eqs. (3.12) plotted against the winding number w is shown in Figures 3.2 and 3.3. When $\beta_o = 0$, the component B_{β_o} is dominant,

and as $w \to \infty$ (dominant poloidal source field) B_{β_o} tends to an almost constant value, whereas as $w \to 0$ (dominant toroidal source field) B_{β_o} increases. Indeed, a poloidal source field induces a toroidal field, mostly confined inside the mathematical torus, while weak and almost independent of q on the outside. Conversely, a toroidal source field induces a poloidal B_{β_o}. When $\beta_o = \pi/2$, contributions from

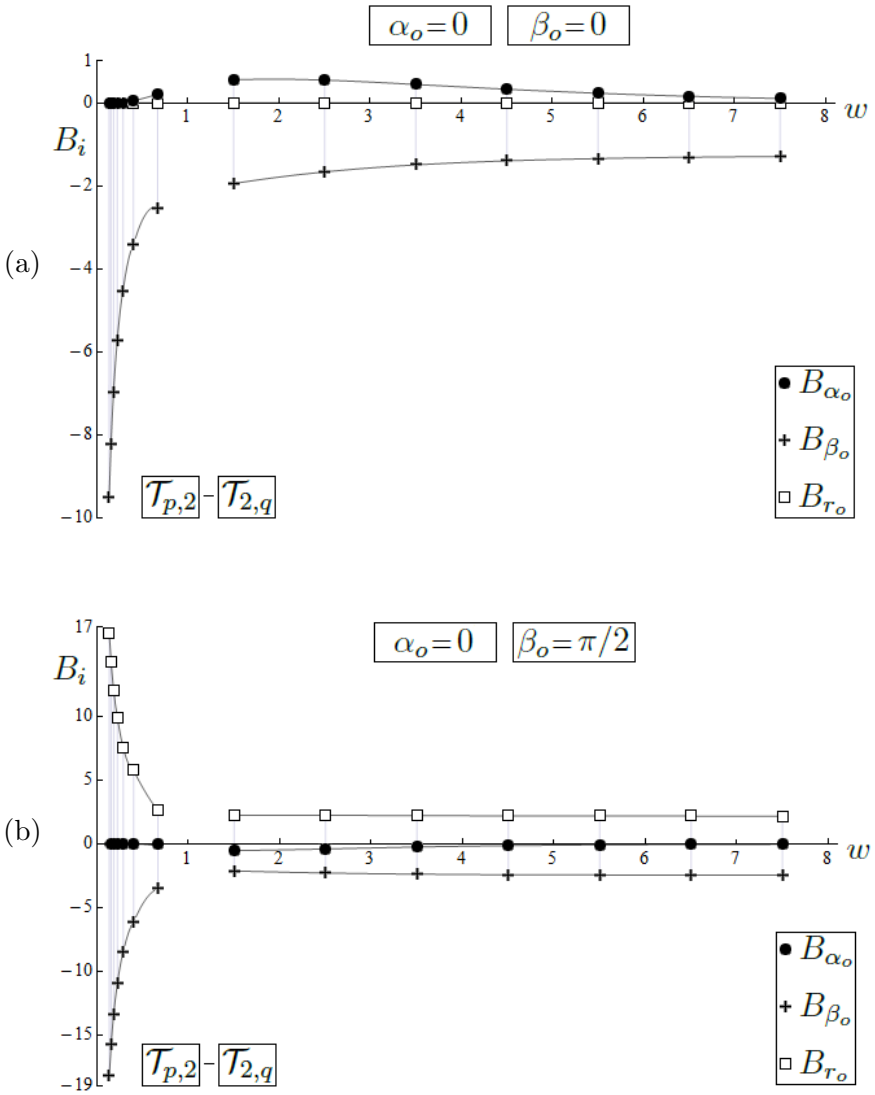

Figure 3.2: Components B_{α_o} (solid dot), B_{β_o} (cross shape) and B_{r_o} (empty square) of the induced field $\mathbf{B}$ against winding number w of knots $\mathcal{T}_{p,2}$ and $\mathcal{T}_{2,q}$ ($R = 1$, $\lambda = 0.5$, $p, q = \{3, 5, 7, 9, 11, 13, 15\}$) for induction points with $\lambda_o = 1$ and (a) $\alpha_o = 0$, $\beta_o = 0$, (b) $\alpha_o = 0$, $\beta_o = \pi/2$. Interpolation is for visualization purposes only.

B_{β_o} and B_{r_o} are of the same order. When ($\alpha_o = 0$, $\beta_o = 0$), B_{r_o} is zero for every $\mathcal{T}_{p,q}$ (Figure 3.2a): this is due to the antisymmetric configuration of every $\mathcal{T}_{p,q}$ with respect to the cross-sectional plane at $\alpha_o = 0$. Results in Figure 3.2a are in good agreement with the observed higher intensity $|\mathbf{B}|$ for dominant toroidal source fields (see, for example, Figure 2.3h).

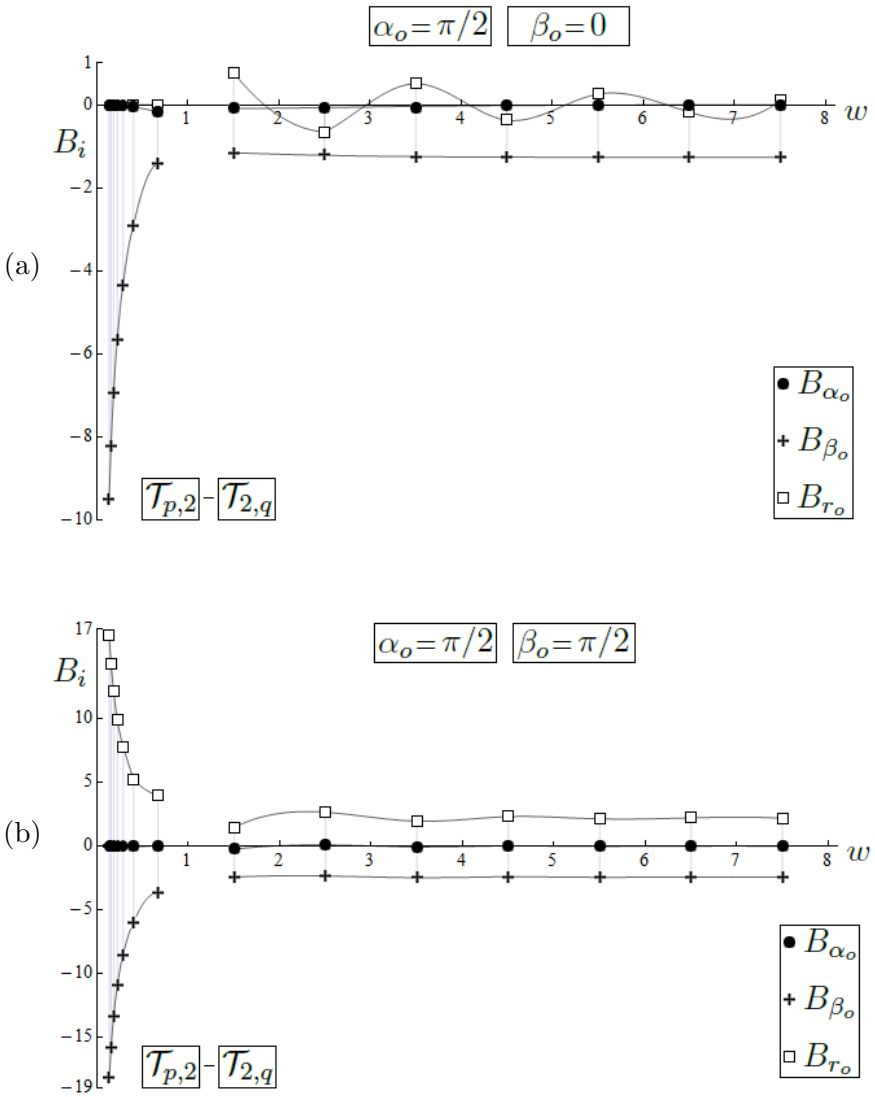

Figure 3.3: Components B_{α_o} (solid dot), B_{β_o} (cross shape) and B_{r_o} (empty square) of the induced field $\mathbf{B}$ against winding number w of knots $\mathcal{T}_{p,2}$ and $\mathcal{T}_{2,q}$ ($R = 1$, $\lambda = 0.5$, $p, q = \{3, 5, 7, 9, 11, 13, 15\}$) for induction points with $\lambda_o = 1$ and (a) $\alpha_o = \pi/2$, $\beta_o = 0$, (b) $\alpha_o = \pi/2$, $\beta_o = \pi/2$. Interpolation is for visualization purposes only.

3.3 Asymptotic expansions and local contributions

Let us suppose $\alpha_o = \beta_o = 0$. By eqs. (3.11) we have

$$\begin{aligned} d\mathcal{BS}_{\alpha_o}(\alpha) &= N_{\alpha_o}(\alpha) \cdot D(\alpha)\, d\alpha \ , \\ d\mathcal{BS}_{\beta_o}(\alpha) &= N_{\beta_o}(\alpha) \cdot D(\alpha)\, d\alpha \ , \\ d\mathcal{BS}_{r_o}(\alpha) &= N_{r_o}(\alpha) \cdot D(\alpha)\, d\alpha \ , \end{aligned} \tag{3.13}$$

where

$$\begin{aligned} D(\alpha) &= 2^{-3/2}\, R^{-1} \\ &\cdot \left\{ 1 + \frac{\lambda^2}{2} + \frac{\lambda_o^2}{2} + \lambda_o - \cos\alpha\,[1 + \lambda_o + \lambda\cos w\alpha(1+\lambda_o)] + \lambda\cos w\alpha \right\}^{-3/2} , \end{aligned} \tag{3.14}$$

and

$$\begin{aligned} N_{\alpha_o}(\alpha) &= -w\lambda\cos\alpha\,(\lambda + \cos w\alpha) - \lambda\sin\alpha\sin w\alpha\,(1 + \lambda\cos w\alpha) \\ &\quad + w\lambda\cos w\alpha\,(1+\lambda_o) \ , \end{aligned} \tag{3.15}$$

$$\begin{aligned} N_{\beta_o}(\alpha) &= 1 - \cos\alpha\,[1 + \lambda_o + \lambda\cos w\alpha\,(1+\lambda_o)] + \lambda\cos w\alpha\,(2 + \lambda\cos w\alpha) \\ &\quad + w\lambda\sin\alpha\sin w\alpha\,(1+\lambda_o) \ , \end{aligned} \tag{3.16}$$

$$N_{r_o}(\alpha) = -\lambda\cos\alpha\sin w\alpha\,(1 + \lambda\cos w\alpha) + w\lambda\sin\alpha\,(\lambda + \cos w\alpha) \ . \tag{3.17}$$

We shall produce the Taylor series centred at $\alpha = 0$ of eqs. (3.13). Let us first calculate the Taylor series of $D(\alpha)$. We have (primes denote derivatives with respect to α):

$$\begin{cases} D(0) = \dfrac{1}{R(\lambda_o - \lambda)^3} \ , \\ D'(0) = 0 \ , \\ D''(0) = -\dfrac{3(1 + \lambda + \lambda_o + \lambda\lambda_o + w^2\lambda\lambda_o)}{R(\lambda_o - \lambda)^5} \ , \\ D'''(0) = 0 \ . \end{cases} \tag{3.18}$$

Thus, we obtain

$$D(\alpha) = \frac{1}{R(\lambda_o - \lambda)^3} - \frac{3(1 + \lambda + \lambda_o + \lambda\lambda_o + w^2\lambda\lambda_o)}{2R(\lambda_o - \lambda)^5}\,\alpha^2 + O(\alpha^4) \ . \tag{3.19}$$

Let us now calculate the Taylor series of $N_{\alpha_o}(\alpha)$, $N_{\beta_o}(\alpha)$ and $N_{r_o}(\alpha)$. We have:

$$\begin{cases} \cos\alpha = 1 - \dfrac{\alpha^2}{2} + O(\alpha^4)\,, & \sin\alpha = \alpha - \dfrac{\alpha^3}{6} + O(\alpha^4)\,, \\ \cos w\alpha = 1 - \dfrac{w^2}{2}\alpha^2 + O(\alpha^4)\,, & \sin w\alpha = w\alpha - \dfrac{w^3}{6}\alpha^3 + O(\alpha^4)\,, \\ \cos^2 w\alpha = 1 - w^2\alpha^2 + O(\alpha^4)\,, & \sin^2 w\alpha = w^2\alpha^2 + O(\alpha^4)\,, \\ \cos\alpha\cos w\alpha = 1 - \dfrac{1+w^2}{2}\alpha^2 + O(\alpha^4)\,, & \sin\alpha\sin w\alpha = w\alpha^2 + O(\alpha^4)\,, \\ \cos\alpha\sin w\alpha = w\alpha - \dfrac{3w+w^3}{6}\alpha^3 + O(\alpha^4)\,, & \sin\alpha\cos w\alpha = \alpha - \dfrac{1+3w^2}{6}\alpha^3 + O(\alpha^4)\,, \\ \cos\alpha\cos^2 w\alpha = 1 - \dfrac{1+2w^2}{2}\alpha^2 + O(\alpha^4)\,, & \cos\alpha\sin^2 w\alpha = w^2\alpha^2 + O(\alpha^4)\,, \\ \cos\alpha\cos w\alpha\sin w\alpha = w\alpha - \dfrac{3w+4w^3}{6}\alpha^3 + O(\alpha^4)\,, & \sin\alpha\cos w\alpha\sin w\alpha = w\alpha^2 + O(\alpha^4)\,. \end{cases} \tag{3.20}$$

Thus, we obtain

$$\begin{aligned} N_{\alpha_o}(\alpha) &= w\lambda\,(\lambda_o - \lambda) \\ &\quad - \frac{w\lambda\,(1+\lambda) + w^3\lambda\lambda_o}{2}\,\alpha^2 + O(\alpha^4)\,, \end{aligned} \tag{3.21}$$

$$\begin{aligned} N_{\beta_o}(\alpha) &= \left(\lambda - \lambda_o + \lambda^2 - \lambda\lambda_o\right) \\ &\quad + \frac{(1+\lambda+\lambda_o+\lambda\lambda_o) + w^2\lambda\,(1-2\lambda+3\lambda_o)}{2}\,\alpha^2 + O(\alpha^4)\,, \end{aligned} \tag{3.22}$$

$$N_{r_o}(\alpha) = \frac{w\lambda\,(1+\lambda) + w^3\lambda\,(-1+2\lambda)}{3}\,\alpha^3 + O(\alpha^4)\,. \tag{3.23}$$

By multiplying eq. (3.19) with eqs. (3.21)– (3.23), respectively, we obtain

$$d\mathcal{BS}_{\alpha_o}(\alpha) = \left[\frac{w\lambda}{R(\lambda_o-\lambda)^2} - \frac{wA(\lambda,\lambda_o) + w^3B(\lambda,\lambda_o)}{2R(\lambda_o-\lambda)^4}\,\alpha^2 + O(\alpha^4)\right] d\alpha\,, \tag{3.24}$$

$$d\mathcal{BS}_{\beta_o}(\alpha) = \left[-\frac{1+\lambda}{R(\lambda_o-\lambda)^2} + \frac{C(\lambda,\lambda_o) + w^2D(\lambda,\lambda_o)}{2R(\lambda_o-\lambda)^4}\,\alpha^2 + O(\alpha^4)\right] d\alpha\,, \tag{3.25}$$

$$d\mathcal{BS}_{r_o}(\alpha) = \left[\frac{wE(\lambda) - w^3F(\lambda)}{3R(\lambda_o-\lambda)^3}\,\alpha^3 + O(\alpha^4)\right] d\alpha\,, \tag{3.26}$$

where

$$\begin{cases} A(\lambda,\lambda_o) = \lambda\left(3+2\lambda+4\lambda_o-\lambda^2+4\lambda\lambda_o\right) , \\ B(\lambda,\lambda_o) = \lambda\lambda_o\left(2\lambda+\lambda_o\right) , \\ C(\lambda,\lambda_o) = \left(3+5\lambda+4\lambda_o+2\lambda^2+\lambda_o^2+6\lambda\lambda_o+\lambda\lambda_o^2+2\lambda^2\lambda_o\right) , \\ D(\lambda,\lambda_o) = \lambda\left(-\lambda+4\lambda_o+2\lambda^2+3\lambda_o^2-2\lambda\lambda_o\right) , \\ E(\lambda) = \lambda\left(1+\lambda\right) , \\ F(\lambda) = \lambda\left(1-2\lambda\right) . \end{cases} \tag{3.27}$$

Let us first consider eq. (3.24) and discuss case by case $w<1$ and $w>1$. For given R, λ and λ_o such that $R=O(1)$, $\lambda_o=O(1)$ and $0<\lambda<O(\lambda_o)$, to the leading order, we have:

$$\begin{aligned} &1.\quad w<1: && d\mathcal{BS}_{\alpha_o} \sim \frac{w\lambda}{R(\lambda_o-\lambda)^2} \ ; \\ &2.\quad 1<w<O(1/\alpha^{2/3}): && d\mathcal{BS}_{\alpha_o} \sim \frac{w\lambda}{R(\lambda_o-\lambda)^2} \ ; \\ &3.\quad 1<w=O(1/\alpha^{2/3}): && d\mathcal{BS}_{\alpha_o} \sim \frac{w\lambda}{R(\lambda_o-\lambda)^2} - \frac{B(\lambda,\lambda_o)}{2R(\lambda_o-\lambda)^4} \ ; \\ &4.\quad 1<w=O(1/\alpha): && d\mathcal{BS}_{\alpha_o} \sim \frac{w\lambda}{R(\lambda_o-\lambda)^2} - \frac{wB(\lambda,\lambda_o)}{2R(\lambda_o-\lambda)^4} \ . \end{aligned} \tag{3.28}$$

We shall not consider the case when $w>O(1/\alpha)$. Indeed, since the remainder term in the Taylor expansion contains powers of w, eq. (3.24) will not be a good approximation of $d\mathcal{BS}_{\alpha_o}$ for large w. Moreover, for $w>O(1/\alpha^{2/3})$ terms of order $k\geq 4$ in α (not written in eq. (3.24)) may also be relevant at leading order. In general, for each order k of α we have a term of type $l_k w^{k+1}\alpha^k$, where $l_k=l_k(R,\lambda,\lambda_o)$. Thus, for example, if $w=O(1/\alpha)$, in 4. we have an additional term $l_k w$ for each $k\geq 4$. Let us define

$$L = L(R,\lambda,\lambda_o) = \sum_{k=0}^{\infty} l_k \ ; \tag{3.29}$$

we cannot prove that L is finite.
Let us take $R=1$, $\lambda=0.5$ and $\lambda_o=1$, and compare behaviours of $d\mathcal{BS}_{\alpha_o}$ and $\mathbf{B}_{\alpha_o}$ (see Figure 3.2a, solid dot). We have:

$$\begin{aligned} &1'.\quad w<1: && d\mathcal{BS}_{\alpha_o} \sim 2w \ ; \\ &2'.\quad 1<w<O(1/\alpha^{2/3}): && d\mathcal{BS}_{\alpha_o} \sim 2w \ ; \\ &3'.\quad 1<w=O(1/\alpha^{2/3}): && d\mathcal{BS}_{\alpha_o} \sim 2w-8 \ ; \\ &4'.\quad 1<w=O(1/\alpha): && d\mathcal{BS}_{\alpha_o} \sim Lw \ . \end{aligned} \tag{3.30}$$

By $1'.$, we have

$$d\mathcal{BS}_{\alpha_o} \sim 2w \to 0 \quad \text{as} \quad w\to 0 \ , \tag{3.31}$$

thus, behaviours of $d\mathcal{BS}_{\alpha_o}$ and $\mathbf{B}_{\alpha_o}$ (see Figure 3.2a, solid dot) are in good agreement for knots $\mathcal{T}_{p,2}$. Conversely, for knots $\mathcal{T}_{2,q}$ the leading order local terms generally overestimate the global contribution and non-local contributions need to be taken into account as well.

Let us now consider eq. (3.25) and discuss the cases $w < 1$ and $w > 1$. For given R, λ and λ_o such that $R = O(1)$, $\lambda_o = O(1)$ and $0 < \lambda < O(\lambda_o)$, to the leading order, we have:

$$\begin{aligned}
&5.\quad w < 1: && d\mathcal{BS}_{\beta_o} \sim -\frac{1+\lambda}{R(\lambda_o-\lambda)^2}\ ;\\
&6.\quad 1 < w < O(1/\alpha): && d\mathcal{BS}_{\beta_o} \sim -\frac{1+\lambda}{R(\lambda_o-\lambda)^2}\ ;\\
&7.\quad 1 < w = O(1/\alpha): && d\mathcal{BS}_{\beta_o} \sim -\frac{1+\lambda}{R(\lambda_o-\lambda)^2} + \frac{D(\lambda,\lambda_o)}{2R(\lambda_o-\lambda)^4}\ .
\end{aligned} \tag{3.32}$$

We shall not consider the case $w > O(1/\alpha)$, where knot complexity is too high for eq. (3.25) to be a good approximation of $d\mathcal{BS}_{\beta_o}$. When $w = O(1/\alpha)$ terms of order $k \geq 4$ in α (not written in eq. (3.25)) are relevant to leading order, as well. Indeed, for each order k of α we have a term of type $m_k w^k \alpha^k$, where $m_k = m_k(R, \lambda, \lambda_o)$. Thus, in 7. we have an additional term m_k for each $k \geq 4$. Let us define

$$M = M(R, \lambda, \lambda_o) = \sum_{k=0}^{\infty} m_k\ ; \tag{3.33}$$

we cannot prove that M is finite.
Let us now take $R = 1$, $\lambda = 0.5$ and $\lambda_o = 1$. We have:

$$\begin{aligned}
&5'.\quad w < 1: && d\mathcal{BS}_{\beta_o} \sim -6\ ;\\
&6'.\quad 1 < w < O(1/\alpha): && d\mathcal{BS}_{\beta_o} \sim -6\ ;\\
&7'.\quad 1 < w = O(1/\alpha): && d\mathcal{BS}_{\beta_o} \sim M\ .
\end{aligned} \tag{3.34}$$

By $5'$., behaviours of $d\mathcal{BS}_{\beta_o}$ and $\mathbf{B}_{\beta_o}$ (see Figure 3.2a, cross shape) disagree for $w < 1$ and higher order local terms together with non-local contributions need to be considered. Conversely, by $6'$. local and global behaviours for $1 < w < O(1/\alpha)$ are in agreement.

Finally let us consider eq. (3.26) for given R, λ and λ_o such that $R = O(1)$, $\lambda_o = O(1)$ and $0 < \lambda < O(\lambda_o)$. For $w < 1$ or $1 < w < O(1/\alpha)$ the leading order term is of third order in α and its integration over a small interval centred at $\alpha = 0$ gives zero, in agreement with the values of $\mathbf{B}_{r_o}$ (see Figure 3.2a, empty square). If $w = O(1/\alpha)$, the leading order term is given by the sum of the contribution of each term of type $n_k w^k \alpha^k$ of the Taylor expansion (where $n_k = n_k(R, \lambda, \lambda_o)$), and we have $d\mathcal{BS}_{r_o} \sim N$, where $N = N(R, \lambda, \lambda_o) = \sum_{k=0}^{\infty} n_k$ and we cannot prove that it is finite. In this case higher order terms are clearly relevant as well, and

w is too large for eq. (3.26) to be a good approximation of $d\mathcal{BS}_{r_o}$.

Let us consider eqs. (3.24) and (3.25) truncated at the second order and denote them, respectively by $d\mathcal{BS}^{(2)}_{\alpha_o}$ and $d\mathcal{BS}^{(2)}_{\beta_o}$. Let us consider the quantities

$$B^{loc}_{\alpha_o} = \int_{-\pi/30}^{\pi/30} d\mathcal{BS}^{(2)}_{\alpha_o} \,, \qquad B^{loc}_{\beta_o} = \int_{-\pi/30}^{\pi/30} d\mathcal{BS}^{(2)}_{\beta_o} \,. \tag{3.35}$$

In Figure 3.4 we compare the local and global contributions B^{loc}_i and B_i ($i = \alpha_o, \beta_o$) by showing the log-plot of $\Delta_i = |(B^{loc}_i - B_i)/B_i|$. For knots $\mathcal{T}_{2,q}$, $B^{loc}_{\beta_o}$ is on average 47% of B_{β_o}, whereas for knots $\mathcal{T}_{p,2}$, it is 24%. $B^{loc}_{\alpha_o}$ generally overestimate B_{α_o} for both classes of knots. In particular, Δ_{α_o} becomes very large for $\mathcal{T}_{p,2}$ when $w \to 0$ because B_{α_o} is two to three orders smaller than $B^{loc}_{\alpha_o}$.

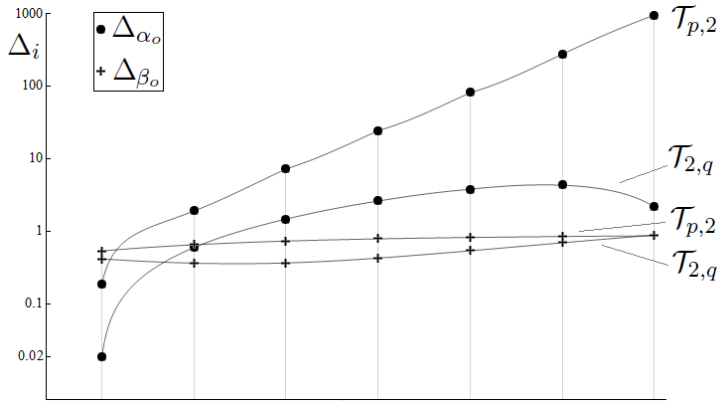

Figure 3.4: Log-plot of Δ_{α_o} (solid dot) and Δ_{β_o} (cross shape) for torus knots $\mathcal{T}_{p,2}$ and $\mathcal{T}_{2,q}$ ($R = 1$, $\lambda = 0.5$ and $p, q = \{3, 5, 7, 9, 11, 13, 15\}$) at the induction point $\alpha_o = 0$, $\beta_o = 0$, $\lambda_o = 1$. Knots are equally spaced on the x-axis. Interpolation lines are for visualization purposes only.

Chapter 4

Self-induction effects by asymptotic analysis

In this chapter we investigate the influence of the winding number on the self-induction of the Biot-Savart integral at a point asymptotically near to the source field. Since this study is important for vortex motion in ideal flows, we analyse the binormal component of the self-induced velocity, responsible for the vortex motion in the ambient fluid. The logarithmic singularity developing as the induction point approaches the source point is regularized by applying the analytical technique of Moore & Saffman (1972). While to leading order the self-induction is proportional to local curvature, we derive an integral formula for next terms, including higher-order local terms and non-local terms, and we study its dependence on the winding number by showing that the dominant contribution is generally given by non-local effects.

4.1 Asymptotic formula and leading order terms

The analysis of the Biot-Savart self-induction effects has important applications in the study of vortex dynamics. Here we investigate the winding number effects on the induction of torus knotted vortex filaments for a point asymptotically near to the source field. For this, we consider a thin vortex filament of constant, circular cross-section centred on $\mathcal{T}_{p,q}$ ($\mathbf{t}_k$ unit tangent), with vorticity $\boldsymbol{\omega} = \omega_0 \mathbf{t}_k$ (ω_0 constant) and vortex flux Φ. By identifying the vortex filament with its centre-line, the self-induced velocity of $\mathcal{T}_{p,q}$ (parametrized by eqs. (1.2)) is given by

$$\mathbf{u}(\mathbf{x}_o) = \frac{\Phi}{4\pi} \int_0^{2\pi p} \frac{\mathbf{t}_k(\alpha) \times (\mathbf{x}_o - \mathbf{x}_k(\alpha))}{|\mathbf{x}_o - \mathbf{x}_k(\alpha)|^3} \, |\dot{\mathbf{x}}_k(\alpha)| d\alpha \ , \tag{4.1}$$

in the limit case when $\mathbf{x}_o \to \mathbf{x}_k \in \mathcal{T}_{p,q}$. The logarithmic singularity that develops as $\mathbf{x}_o$ approaches the source field is the main cause of difficulties in the analysis of eq. (4.1), and several de-singularization techniques have been developed to

regularize the integral (see, for example, [46] for a comparison of different desingularization techniques applied to the case of helical vortex filaments). Here we shall apply the analytical prescription proposed by Moore & Saffman [40], that has been proven to give correct results to leading orders [46].

An asymptotic formula of $\mathbf{u}$ for a thin vortex filament of general cross-section and vorticity distribution was derived by Levi-Civita as an application of his results on asymptotic potential theory (see [27], chapter 4, for a comprehensive treatment of several results published from 1908 to 1912; see also [48]). Given a point $\mathbf{Q}$ on the vortex centre-line $\mathscr{C}$, with Frenet frame $(\mathbf{t}, \mathbf{n}, \mathbf{b})$ and local radius of curvature ρ, the induced velocity at a point $\mathbf{x}_o$ asymptotically near to $\mathbf{Q}$ is given by (cfr. [27], p. 26, eq. (6))

$$\mathbf{u}(\mathbf{x}_o) = \frac{\Phi}{2\pi\delta}\mathbf{q} + \frac{\Phi}{4\pi\rho}k\mathbf{b} + \mathbf{G} \ , \tag{4.2}$$

where $\delta \ll 1$ is a length parameter that depends on the filament cross-section and on $\mathbf{x}_o$, $\mathbf{q}$ is a unit vector orthogonal to $\mathbf{t}$, function only of $\mathbf{x}_o$, k is a dimensionless term that depends on the shape of the filament cross-section at $\mathbf{x}_o$ and on the vorticity distribution on it, and $\mathbf{G}$ denotes the finite-term contribution due to non-local effects.
By assuming the cross-section to be *circular* of radius ε, eq. (4.2) reduces to

$$\mathbf{u}(\mathbf{x}_o) = \frac{\Phi}{2\pi\varepsilon}\mathbf{q} + \frac{\Phi}{4\pi\rho}\left[\ln\left(\frac{\rho}{\varepsilon}\right) + F\right]\mathbf{b} + \mathbf{G} \ , \tag{4.3}$$

where F depends on the vorticity distribution over the cross-section and on the local geometry of $\mathscr{C}$. Finally, by assuming the vorticity distribution *constant* over the cross-section, F and $\mathbf{G}$ become function only of the local and non-local geometry, respectively. Equation (4.3) was then independently re-derived by Batchelor in 1967 (see [9], p. 510). The first term of eq. (4.3) yields a circulatory motion about $\mathscr{C}$ and gives no contribution to the displacement of the vortex in the fluid; the second term is the leading order term responsible for the vortex displacement. By taking the binormal component of the drift velocity $\mathbf{v}(\mathbf{x}_o) = \mathbf{u}(\mathbf{x}_o) - \Phi/(2\pi\varepsilon)\mathbf{q}$, that to leading order is responsible for the vortex propagation, we have

$$v_b(\mathbf{x}_o) = \mathbf{v}(\mathbf{x}_o)\cdot\mathbf{b} = \frac{\Phi}{4\pi\rho}\ln\left(\frac{\rho}{\varepsilon}\right) + C \ , \tag{4.4}$$

where $C = \Phi/(4\pi\rho)F + \mathbf{G}\cdot\mathbf{b}$. is a function of the (local and non local) geometry of $\mathscr{C}$. Following [46], we can apply the Moore & Saffman prescription to eq. (4.1) to study $C = C(w)$ in the case $\mathscr{C} = \mathcal{T}_{p,q}$.

4.2 Application of Moore & Saffman's prescription

Let us consider $\mathbf{x}_o \in \mathcal{T}_{p,q}$ of coordinates $\alpha_o = \beta_o = 0$ and $\lambda_o = \lambda$ (see eq. (3.8)), that is $\mathbf{x}_o = (R(1+\lambda), 0, 0)$. This choice is guided by the particular symmetry

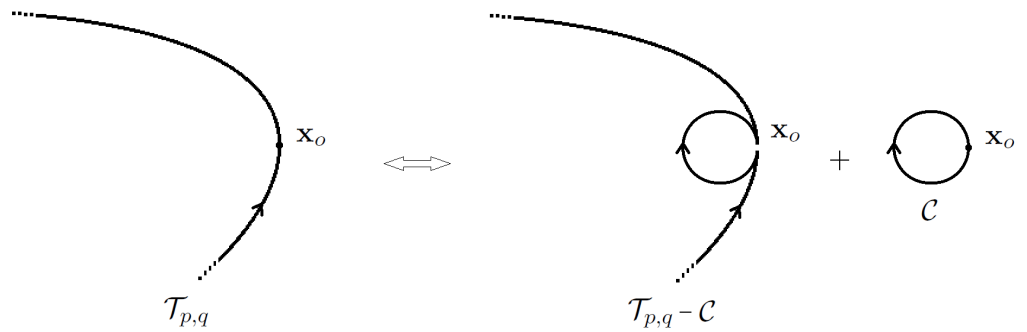

Figure 4.1: Geometric presentation of the Moore & Saffman's prescription. To the contribution due to $\mathcal{T}_{p,q}$ is first subtracted and then added the contribution of the vortex ring $\mathcal{C}$ osculating $\mathcal{T}_{p,q}$ at $\mathbf{x}_o$.

of torus knots/unknots: evaluations for $\mathbf{x}_o$ are valid for any point $\mathbf{x}'_o$ with $\alpha'_o = 2k\pi/w$, $k = 0, ..., q-1$, as well; however features of any other $\mathbf{x}'_o$ are related to features of $\mathbf{x}_o$ by general deformations.
We regularize the Biot-Savart integral eq. (4.1) by applying the prescription by Moore & Saffman. The de-singularization is obtained by subtracting and adding to eq. (4.1) the contribution of a circular vortex ring $\mathcal{C}$ that osculates the original vortex filament $\mathcal{T}_{p,q}$ at $\mathbf{x}_o$, with equal vorticity $\boldsymbol{\omega}$ and equal local vortex core (Figure 4.1): we have

$$\mathbf{v}(\mathbf{x}_o) = \frac{\Phi}{4\pi}\left[\int_{\mathcal{T}_{p,q}} \frac{\mathbf{t}_k \times (\mathbf{x}_o - \mathbf{x}_k)}{|\mathbf{x}_o - \mathbf{x}_k|^3}\, d\mathbf{x}_k - \int_{\mathcal{C}} \frac{\mathbf{t}_c \times (\mathbf{x}_o - \mathbf{x}_c)}{|\mathbf{x}_o - \mathbf{x}_c|^3}\, d\mathbf{x}_c\right] + \mathbf{v}_c(\mathbf{x}_o)\ , \quad (4.5)$$

where $\mathbf{x}_c$ and $\mathbf{t}_c$ denote point and unit tangent vector on $\mathcal{C}$, and, by Kelvin's formula (see, for example, [54])

$$\mathbf{v}_c(\mathbf{x}_o) = v_c \mathbf{b}_o = \frac{\Phi}{4\pi\rho_o}\left[\ln\left(\frac{\rho_o}{\varepsilon}\right) + \ln 8 - \frac{1}{4}\right]\mathbf{b}_o\ , \quad (4.6)$$

where ρ_o and $\mathbf{b}_o$ are the radius of curvature and the unit binormal of $\mathcal{T}_{p,q}$ at $\mathbf{x}_o$, respectively. Note that the circulatory motion term $\Phi/(2\pi\varepsilon)\mathbf{q}$ is the same for $\mathcal{T}_{p,q}$ and $\mathcal{C}$.

Let us first calculate the parametric equations for the osculating circle. At $\mathbf{x}_o$ the Frenet frame of $\mathcal{T}_{p,q}$ is given by

$$\mathbf{t}_o = \frac{1}{A(\lambda,w)}\begin{pmatrix}0\\1+\lambda\\ \lambda w\end{pmatrix}, \quad \mathbf{n}_o = \begin{pmatrix}-1\\0\\0\end{pmatrix}, \quad \mathbf{b}_o = \frac{1}{A(\lambda,w)}\begin{pmatrix}0\\-\lambda w\\1+\lambda\end{pmatrix}, \quad (4.7)$$

where $A(\lambda, w) = \sqrt{(1+\lambda)^2 + \lambda^2 w^2}$, and the local radius of curvature is given by

$$\rho_o = \frac{R\left[(1+\lambda)^2 + \lambda^2 w^2\right]}{1+\lambda+\lambda w^2}\ . \quad (4.8)$$

The osculating circle has centre

$$\mathbf{O} = \mathbf{x}_o + \rho_o \mathbf{n}_o = \left(\frac{R\lambda w^2}{1+\lambda+\lambda w^2}, 0, 0 \right), \tag{4.9}$$

and it is the locus of the points $\mathbf{x}_c = \mathbf{O} + \rho_o \left(\mathbf{t}_o \sin\theta - \mathbf{n}_o \cos\theta \right)$, that is

$$\mathbf{x}_c(\theta) : \begin{cases} x = \dfrac{R}{1+\lambda+\lambda w^2} \left[\lambda w^2 + F^2(\lambda, w) \cos\theta \right] \\ y = \dfrac{R}{1+\lambda+\lambda w^2} \left[(1+\lambda) A(\lambda, w) \sin\theta \right] \\ z = \dfrac{R}{1+\lambda+\lambda w^2} \left[\lambda w A(\lambda, w) \sin\theta \right] \end{cases} , \quad \theta \in [0, 2\pi) . \tag{4.10}$$

Hence, we have $|\dot{\mathbf{x}}_c| = \rho_o$ and

$$\mathbf{t}_c = \frac{\dot{\mathbf{x}}_c}{|\dot{\mathbf{x}}_c|} = \begin{pmatrix} \sin\theta \\ \dfrac{1+\lambda}{A(\lambda, w)} \cos\theta \\ \dfrac{\lambda w}{A(\lambda, w)} \cos\theta \end{pmatrix}, \tag{4.11}$$

from which we find correctly $\mathbf{t}_c(\theta = 0) = \mathbf{t}_o$.
By eqs. (1.2) and (4.10), eq. (4.5) is now given by

$$\begin{aligned} \mathbf{v}(\mathbf{x}_o) = & \frac{\Phi}{4\pi} \left[\int_0^{2\pi p} \frac{\mathbf{t}_k(\alpha) \times (\mathbf{x}_o - \mathbf{x}_k(\alpha))}{|\mathbf{x}_o - \mathbf{x}_k(\alpha)|^3} \, |\dot{\mathbf{x}}_k(\alpha)| d\alpha \right] \\ & - \frac{\Phi}{4\pi} \left[\int_0^{2\pi} \frac{\mathbf{t}_c(\theta) \times (\mathbf{x}_o - \mathbf{x}_c(\theta))}{|\mathbf{x}_o - \mathbf{x}_c(\theta)|^3} \, |\dot{\mathbf{x}}_c| d\theta \right] + \mathbf{v}_c(\mathbf{x}_o) \ . \end{aligned} \tag{4.12}$$

We are interested in the contribution of $\mathbf{v}$ along the binormal direction, hence by eqs. (4.12) and (4.6), and by simply renaming θ as α, we have

$$\begin{aligned} v_b(\mathbf{x}_o) = \mathbf{v} \cdot \mathbf{b}_o = & \frac{\Phi}{4\pi} \left[\int_0^{2\pi p} \mathbf{b}_o \cdot \frac{\mathbf{t}_k(\alpha) \times (\mathbf{x}_o - \mathbf{x}_k(\alpha))}{|\mathbf{x}_o - \mathbf{x}_k(\alpha)|^3} \, |\dot{\mathbf{x}}_k(\alpha)| d\alpha \right] \\ & - \frac{\Phi}{4\pi} \left[\int_0^{2\pi} \mathbf{b}_o \cdot \frac{\mathbf{t}_c(\alpha) \times (\mathbf{x}_o - \mathbf{x}_c(\alpha))}{|\mathbf{x}_o - \mathbf{x}_c(\alpha)|^3} \, |\dot{\mathbf{x}}_c| d\alpha \right] + v_c(\mathbf{x}_o) \ . \end{aligned} \tag{4.13}$$

Let us now set

$$\begin{cases} d\mathcal{BS}_k := \dfrac{\mathbf{b}_o \cdot \mathbf{t}_k(\alpha) \times (\mathbf{x}_o - \mathbf{x}_k(\alpha)) \, |\dot{\mathbf{x}}_k(\alpha)|}{|\mathbf{x}_o - \mathbf{x}_k(\alpha)|^3} = \dfrac{N}{D} \ , \\ d\mathcal{BS}_c := \dfrac{\mathbf{b}_o \cdot \mathbf{t}_c(\alpha) \times (\mathbf{x}_o - \mathbf{x}_c(\alpha)) \, |\dot{\mathbf{x}}_c|}{|\mathbf{x}_o - \mathbf{x}_c(\alpha)|^3} = \dfrac{N'}{D'} \ , \end{cases} \tag{4.14}$$

where $\mathbf{t}_k(\alpha)\,|\dot{\mathbf{x}}_k(\alpha)|$ is given by the first of eqs. (1.5). We take Taylor's expansions of eqs. (4.14) at $\alpha = 0$ to compare the local behaviour of $d\mathcal{BS}_k$ and $d\mathcal{BS}_c$ near the osculation point $\mathbf{x}_o$. For this, we apply the following technique first to $d\mathcal{BS}_k$:

1. We take the Taylor expansions of N and D, given by

$$\begin{cases} N = n_2\alpha^2 + n_4\alpha^4 + \dots\,, \\ D = d_3\alpha^3 + d_5\alpha^5 + \dots\,, \end{cases} \tag{4.15}$$

   where $n_i = n_i(R, \lambda, w)$ and $d_i = d_i(R, \lambda, w)$.

2. We search for a Taylor expansion of N/D in the form

$$N/D = \dots + \frac{c_{-3}}{\alpha^3} + \frac{c_{-2}}{\alpha^2} + \frac{c_{-1}}{\alpha} + c_0 + c_1\alpha + c_2\alpha^2 + c_3\alpha^3 + \dots\,, \tag{4.16}$$

   with $c_i = c_i(R, \lambda, w)$ to be found.

3. We write the equation $N = (N/D) \cdot D$, where N is given by the first of eqs. (4.15), and $(N/D) \cdot D$ by the product of the formal expression eq. (4.16) and the second of eqs. (4.15). By matching the coefficients term by term we obtain a set of 7 equations in the c_is in terms of the known coefficients n_is and d_is, finding that the only non-zero c_is are c_{-1}, c_1 and c_3.

4. By recursion, we can prove that $c_i = 0$ for $i < -1$ and for $i \geq 0$, i even.

By applying the same technique to $d\mathcal{BS}_c$ as well, we obtain

$$\begin{cases} d\mathcal{BS}_k = \dfrac{c_{-1}}{\alpha} + c_1\alpha + c_3\alpha^3 + \dots\,, \\ d\mathcal{BS}_c = \dfrac{c'_{-1}}{\alpha} + c'_1\alpha + c'_3\alpha^3 + \dots\,, \end{cases} \tag{4.17}$$

with, in particular,

$$c_{-1} = c'_{-1} = \frac{1}{2\rho_o}\,, \tag{4.18}$$

thus proving that to leading order $d\mathcal{BS}_k$ and $d\mathcal{BS}_c$ have the same singular behaviour near $\mathbf{x}_o$, and hence that the Moore & Saffman technique indeed regularize eq. (4.1). Moreover, since the higher order terms are all odd powers of α, the integration of the expansion of $d\mathcal{BS}_k - d\mathcal{BS}_c$ over a neighbourhood of $\mathbf{x}_o$ (i.e. a small interval centred at $\alpha = 0$) gives 0, proving that $\mathcal{C}$ is locally a good approximation for $\mathcal{T}_{p,q}$ (note that $d\mathcal{BS}_k$ and $d\mathcal{BS}_c$ have periods $2\pi p$ and 2π, respectively).

4.3 Winding number effects on next terms

We prove the following symmetry properties of $d\mathcal{BS}_c$ and $d\mathcal{BS}_k$ in order to simplify eq. (4.13):

$$\begin{cases} d\mathcal{BS}_c(\pi-\alpha) = d\mathcal{BS}_c(\pi+\alpha)\ , \\ d\mathcal{BS}_k(\pi p-\alpha) = d\mathcal{BS}_k(\pi p+\alpha)\ . \end{cases} \tag{4.19}$$

Let us prove the first of eqs. (4.19): by eqs. (4.11) and (4.10), and by using the equalities $\cos(\pi-\alpha)=\cos(\pi+\alpha)$ and $\sin(\pi-\alpha)=-\sin(\pi+\alpha)$, we obtain

$$\begin{pmatrix} t_c^x \\ t_c^y \\ t_c^z \end{pmatrix}(\pi-\alpha) = \begin{pmatrix} -t_c^x \\ t_c^y \\ t_c^z \end{pmatrix}(\pi+\alpha), \quad \begin{pmatrix} x_o^x - x_c^x \\ -x_c^y \\ -x_c^z \end{pmatrix}(\pi-\alpha) = \begin{pmatrix} x_o^x - x_c^x \\ x_c^y \\ x_c^z \end{pmatrix}(\pi+\alpha), \tag{4.20}$$

where superscripts denote the x, y, z components of $\mathbf{t}_c$, $\mathbf{x}_o$ and $\mathbf{x}_c$. Hence, by the second of eqs. (4.14) we have $N'(\pi-\alpha) = N'(\pi+\alpha)$ and $D'(\pi-\alpha) = D'(\pi+\alpha)$. By applying the same method to the first of eqs. (1.5) and to (1.2), and by using the equalities $\cos(\pi p-\alpha)=\cos(\pi p+\alpha)$, $\sin(\pi p-\alpha)=-\sin(\pi p+\alpha)$, $\cos[w(\pi p-\alpha)]=\cos[w(\pi p+\alpha)]$ and $\sin[w(\pi p-\alpha)]=-\sin[w(\pi p+\alpha)]$, we obtain for $\mathbf{t}_k(\alpha)\,|\dot{\mathbf{x}}_k(\alpha)|$ and $\mathbf{x}_o-\mathbf{x}_k$ equations similar to (4.20), and the second of eqs. (4.19) is proven, as well.

By eqs. (4.19), eq. (4.13) now becomes

$$\begin{aligned} v_b(\mathbf{x}_o) &= 2\cdot\frac{\Phi}{4\pi}\left[\int_0^{\pi p}\mathbf{b}_o\cdot\frac{\mathbf{t}_k(\alpha)\times(\mathbf{x}_o-\mathbf{x}_k(\alpha))}{|\mathbf{x}_o-\mathbf{x}_k(\alpha)|^3}\,|\dot{\mathbf{x}}_k(\alpha)|d\alpha\right] \\ &\quad -2\cdot\frac{\Phi}{4\pi}\left[\int_0^{\pi}\mathbf{b}_o\cdot\frac{\mathbf{t}_c(\alpha)\times(\mathbf{x}_o-\mathbf{x}_c(\alpha))}{|\mathbf{x}_o-\mathbf{x}_c(\alpha)|^3}\,|\dot{\mathbf{x}}_c|d\alpha\right] + v_c(\mathbf{x}_o) \\ &= \frac{\Phi}{4\pi}(I_1+I_2)+v_c(\mathbf{x}_o)\ , \end{aligned} \tag{4.21}$$

where

$$\begin{aligned} I_1 &= 2\int_0^{\pi}\mathbf{b}_o\cdot\left[\frac{\mathbf{t}_k(\alpha)\times(\mathbf{x}_o-\mathbf{x}_k(\alpha))}{|\mathbf{x}_o-\mathbf{x}_k(\alpha)|^3}\,|\dot{\mathbf{x}}_k(\alpha)| - \frac{\mathbf{t}_c(\alpha)\times(\mathbf{x}_o-\mathbf{x}_c(\alpha))}{|\mathbf{x}_o-\mathbf{x}_c(\alpha)|^3}\,|\dot{\mathbf{x}}_c|\right]d\alpha\ , \\ I_2 &= 2\int_{\pi}^{\pi p}\mathbf{b}_o\cdot\frac{\mathbf{t}_k(\alpha)\times(\mathbf{x}_o-\mathbf{x}_k(\alpha))}{|\mathbf{x}_o-\mathbf{x}_k(\alpha)|^3}\,|\dot{\mathbf{x}}_k(\alpha)|d\alpha\ . \end{aligned} \tag{4.22}$$

By normalizing eqs. (4.21) and (4.6) by the reference velocity $\Phi/(4\pi R)$, we obtain

$$\overline{v}_b(\mathbf{x}_o) = \frac{4\pi R}{\Phi}v_b(\mathbf{x}_o) = R(I_1+I_2)+\frac{R}{\rho_o}\left[\ln\left(\frac{\rho_o}{\varepsilon}\right)+\ln 8-\frac{1}{4}\right], \tag{4.23}$$

and by eq. (4.4) we have that $\overline{v}_b$ takes the form

$$\overline{v}_b(\mathbf{x}_o) = \frac{R}{\rho_o}\ln\left(\frac{\rho_o}{\varepsilon}\right)+\overline{C}\ , \tag{4.24}$$

where $\overline{C} = C(4\pi R/\Phi)$ is thus given by

$$\overline{C} = R(I_1 + I_2) + \frac{R}{\rho_o}\left(\ln 8 - \frac{1}{4}\right). \tag{4.25}$$

Figures 4.2–4.4 show $K = R/\rho_o\,(\ln 8 - 1/4)$ and I_1, I_2, and $\overline{C}$, respectively, against w for several knots/unknots with $R = 1$ and three different values of λ. I_1 measures he difference between $\mathcal{T}_{p,q}$ and its osculating circle $\mathcal{C}$ over $[-\pi, \pi]$. For toroidal $\mathcal{T}_{p,q}$ $I_1 \approx 0$, whereas as q increases $|I_1|$ increases as well, with a neat rate for small λ and an oscillatory rate for larger λ. I_2 gives the "non-local" effects. For dominant toroidal $\mathcal{T}_{p,q}$, contribution from I_2 for small λ is one order larger than $\lambda = 0.5$, whereas $I_2 \approx 0$ (as I_1) for larger λ. For $\mathcal{T}_{1,q}$, $I_2 = 0$ by definition for every λ (see eq. (4.22)). For $\lambda > 0.5$, given $i_1 < i_2$ it is $I_2(\mathcal{T}_{i_1,q}) < I_2(\mathcal{T}_{i_2,q})$, however for $\lambda \leq 0.5$ the existence of a critical w for which $I_2(\mathcal{T}_{i_1,q}) > I_2(\mathcal{T}_{i_2,q})$ seems to be a generic feature due to the effects of different knot geometries.
The dominant contribution to $\overline{C}$ is generally given by the non-local term I_2 for most of the knots/unknots tested (confront Figures 4.3 and 4.4). For dominant poloidal $\mathcal{T}_{p,q}$ with small λ, contributions from I_1 and K generally cancel out, hence $\overline{C} \approx I_2$, whereas for large λ it is $I_1 \approx -K + 1$, hence $\overline{C} \approx I_2 + 1$. For dominant toroidal $\mathcal{T}_{p,q}$, since $I_1 \approx 0$ and $K \approx 1$, it is $\overline{C} \approx I_2 + 1$, and for large λ, since $I_2 \approx 0$, it is $\overline{C} \approx 1$.

Numerical simulations of the time evolution of torus knotted vortex filaments in the context of the Euler equations has been performed in [52], where the evolutions under the Biot-Savart law and the localised induction approximation are compared, and a stabilizing effect of the Biot-Savart law due to global geometric contributions is discovered. The translational velocity and kinetic energy of vortex torus knots/unknots, calculated by numerical integration of the Biot-Savart law, are related in [30] to knot complexity, given by the winding number. Here we have derived for the first time by analytical means an integral formula for higher-order terms of the binormal component of the self-induced velocity at a given point, and we have confirmed the importance of global geometric contributions by showing the dominance of non-local terms. Moreover, since for $w > 1$ and λ small, $\overline{C}$ is generally small (Figure 4.4a), the main contribution to the drift velocity is given by the leading order term (eq. (4.4)), in good agreement with [30], where small-amplitude vortex torus knots/unknots with $w > 1$ are found to move essentially as fast as the reference vortex ring of same size and vorticity.

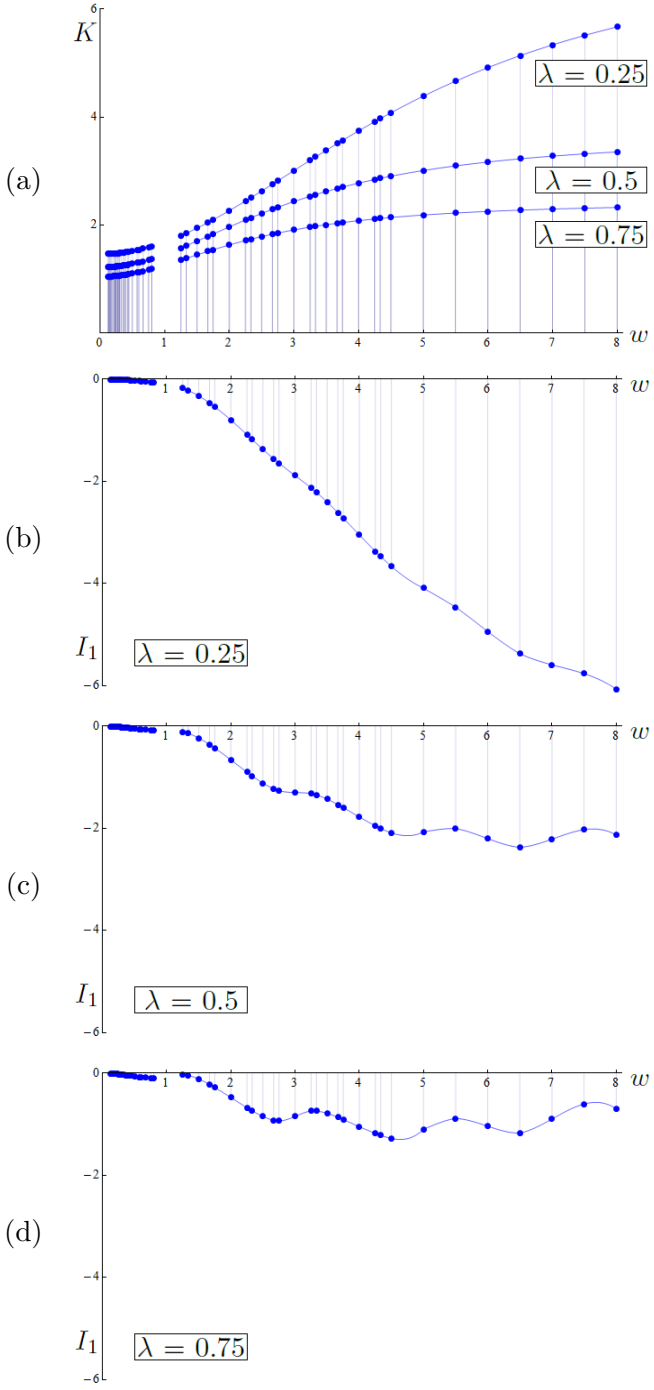

Figure 4.2: (a) K and (b)–(d) I_1 against w of several torus knots/unknots with $R = 1$ and different λ. $\mathcal{T}_{p,1}$ and $\mathcal{T}_{1,q}$ $(p, q = 2, 3, 4, 5, 6, 7, 8)$; $\mathcal{T}_{p,2}$ and $\mathcal{T}_{2,q}$ $(p, q = 3, 5, 7, 9, 11, 13, 15)$; $\mathcal{T}_{p,3}$ and $\mathcal{T}_{3,q}$ $(p, q = 4, 5, 7, 8, 10, 11, 13)$; $\mathcal{T}_{p,4}$ and $\mathcal{T}_{4,q}$ $(p, q = 5, 7, 9, 11, 13, 15, 17)$. Interpolation is for visualization purposes only.

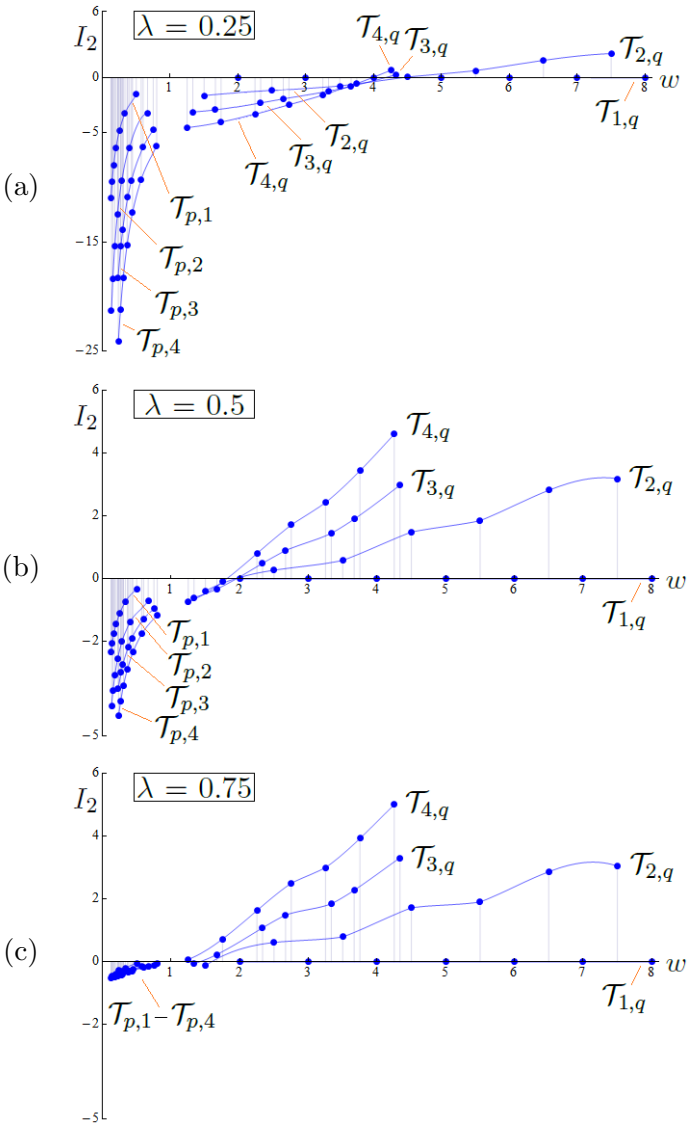

Figure 4.3: I_2 against w of several torus knots/unknots with $R = 1$ and different λ. $\mathcal{T}_{p,1}$ and $\mathcal{T}_{1,q}$ $(p, q = 2, 3, 4, 5, 6, 7, 8)$; $\mathcal{T}_{p,2}$ and $\mathcal{T}_{2,q}$ $(p, q = 3, 5, 7, 9, 11, 13, 15)$; $\mathcal{T}_{p,3}$ and $\mathcal{T}_{3,q}$ $(p, q = 4, 5, 7, 8, 10, 11, 13)$; $\mathcal{T}_{p,4}$ and $\mathcal{T}_{4,q}$ $(p, q = 5, 7, 9, 11, 13, 15, 17)$. Interpolation is for visualization purposes only.

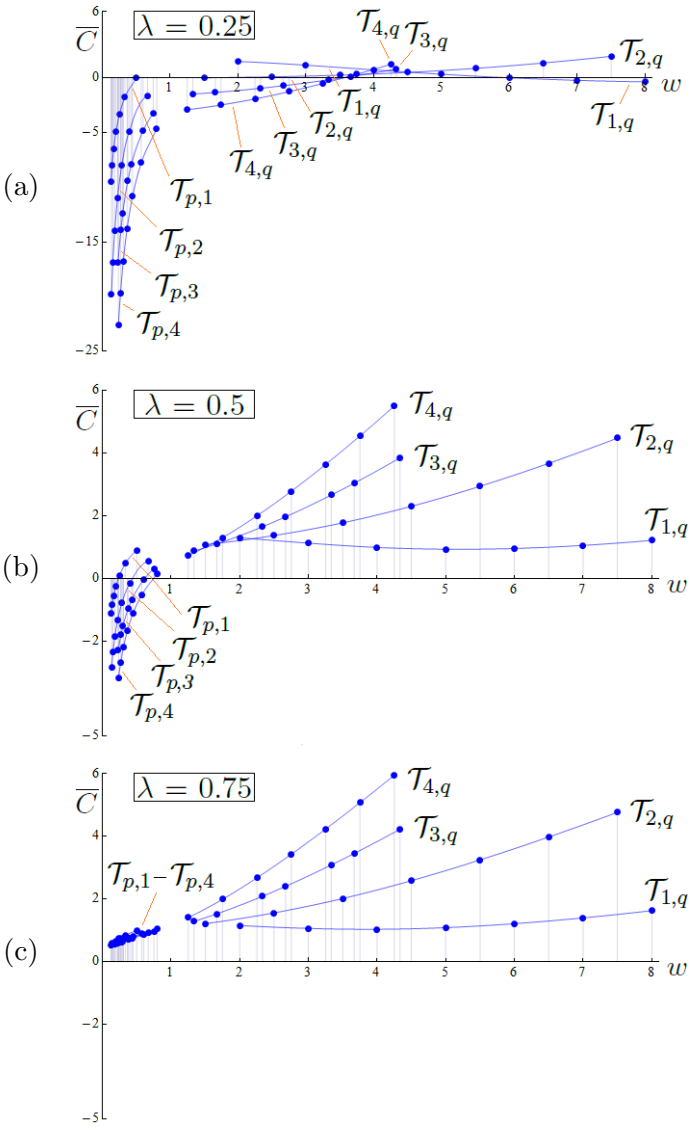

Figure 4.4: $\overline{C}$ against w of several torus knots/unknots with $R = 1$ and different λ. $\mathcal{T}_{p,1}$ and $\mathcal{T}_{1,q}$ $(p, q = 2, 3, 4, 5, 6, 7, 8)$; $\mathcal{T}_{p,2}$ and $\mathcal{T}_{2,q}$ $(p, q = 3, 5, 7, 9, 11, 13, 15)$; $\mathcal{T}_{p,3}$ and $\mathcal{T}_{3,q}$ $(p, q = 4, 5, 7, 8, 10, 11, 13)$; $\mathcal{T}_{p,4}$ and $\mathcal{T}_{4,q}$ $(p, q = 5, 7, 9, 11, 13, 15, 17)$. Interpolation is for visualization purposes only.

References

[1] Adams, C. *et al.* (2010) The spiral index of knots. *Math. Proc. Camb. Phil. Soc.* **149**, 297–315.

[2] Aguirre, J., Giné, J. & Peralta-Salas, D. (2008) Integrability of magnetic fields created by current distributions. *Nonlinearity* **21**, 51–69.

[3] Aguirre, J. & Peralta-Salas, D. (2007) Realistic examples of chaotic magnetic fields created by wires. *Europhys. Lett.* **80**, 60007 (6pp).

[4] Aldinger, J., Klapper, I. & Tabor, M. (1995) Formulae for the calculation and estimation of writhe. *J. Knot Theory Ramification* **4**, 343–372.

[5] Ampère, A.M. (1820) Mémoire présenté à l'académie royale des sciences, le 2 octobre 1820 où se trouve compris le résumé de ce qui avait été lu à la même académie les 18 et 25 septembre 1820, sur les effets des courants électriques. *Ann. Chim. Phys.* **15**, 59–75.

[6] Ampère, A.M. (1820) Suite du mémoire sur l'action mutuelle entre deux courants électriques, un courant électrique et un aimant ou le globe terrestre, et entre deux aimants. *Ann. Chim. Phys.* **15**, 170–218.

[7] Arnold, V.I. (1974) The asymptotic Hopf invariant and its applications. In *Proc. Summer School in Diff. Eqs. at Dilizhan*, 229–256. Armenian Academy of Sciences, Erevan (Armenia). [In Russian], [transl. English (1986) *Sel. Math. Sov.* **5**, 327–345].

[8] Ball, J. *et al.* (2014) Intrinsic momentum transport in up-down asymmetric tokamaks. *Plasma Phys. Control. Fusion* **56**, 095014 (20pp).

[9] Batchelor, G.K. (1967) *An Introduction to Fluid Dynamics*, Cambridge University Press, Cambridge.

[10] Berger, M.A. & Field, G.B. (1984) The topological properties of magnetic helicity. *J. Fluid Mech.* **147**, 133–148.

[11] Betti, R. (2014) Magnetic fields lock in the heat for fusion. *Physics* **7**, 105 (4pp).

[12] Biot, J.B. & Savart, F. (1820) Expériences électromagnétiques. *J. Phys. Chim. Hist. Nat. Arts* **91**, 151–152.

[13] Biot, J.B. & Savart, F. (1820) Note sur le magnétisme de la pile de Volta. *Ann. Chim. Phys.* **15**, 222–223.

[14] Călugăreanu, G. (1959) L'intégrale de Gauss et l'analyse des nœuds tridimensionnels. *Rev. Math. Pures Appl.* **4**, 5–20.

[15] Călugăreanu, G. (1961) Sur les classes d'isotopie des nœuds tridimensionnels et leurs invariants. *Czechoslovak Math. J.* **11**, 588–625.

[16] Coleman B.D. & Swigon D. (2004) Theory of self-contact in Kirchhoff rods with applications to supercoiling of knotted and unknotted DNA plasmids. *Phil. Trans. R. Soc. Lond. A* **362**, 1281–1299.

[17] Fàry, I. (1949) Sur la courbure totale d'une courbe gauche faisant un nœud. *Bull. Soc. Math. France* **77**, 128–138.

[18] Fenchel, W. (1951) On the differential geometry of closed space curves. *Bull. Amer. Math. Soc.* **57**, 44–54.

[19] Fuller, F.B. (1971) The writhing number of a space curve. *Proc. Natl. Acad. Sci. USA* **68**, 815–819.

[20] Fuller, F.B. (1978) Decomposition of the linking number of a closed ribbon: a problem from molecular biology. *Proc. Natl. Acad. Sci. USA* **75**, 3557–3561.

[21] Fuller Jr, E.J. (1999) *The Geometric And Topological Structure Of Holonomic Knots*. PhD Thesis, University of Georgia, Athens, 42–54.

[22] Fuller Jr, E.J. (2003) The self-linking of torus knots. Preprint.

[23] Gascon, F.G. & Peralta-Salas, D. (2005) Some properties of the magnetic fields generated by symmetric configurations of wires. *Phys. D* **206**, 109–120.

[24] Harris, J.H. (2004) Small to mid-sized stellarator experiments: topology, confinement and turbulence. *Plasma Phys. Control. Fusion* **46**, B77–B90.

[25] Kac, M. (1966) Can one hear the shape of a drum? *Am. Math. Mon.* **73**, 1–23.

[26] Klinger, T. *et al.* (2013) Towards assembly completion and preparation of experimental campaigns of Wendelstein 7-X in the perspective of a path to a stellarator fusion power plant. *Fus. Eng. Des.* **88**, 461–465.

[27] Levi-Civita, T. (1932) Attrazione Newtoniana dei tubi sottili e vortici filiformi (Newtonian attraction of slender tubes and filiform vortices), *Annali R. Scuola Norm. Sup. Pisa* **1**, 1–33; 229–250.

[28] Liu, X. & Ricca, R.L. (2015) On the derivation of the HOMFLYPT polynomial invariant for fluid knots. *J. Fluid Mech.* **773**, 34–48.

[29] Love, A.E.H. (1920) *A Treatise On The Mathematical Theory Of Elasticity*, 4^{th} edition. Cambridge University Press, pp. 387–388.

[30] Maggioni, F., Alamri, S.Z., Barenghi, C.F. & Ricca, R.L. (2010) Velocity, energy and helicity of vortex knots and unknots. *Phys. Rev. E* **82**, 26309 (9 pp).

[31] Maingi, R. (2014) Enhanced confinement scenarios without large edge localized modes in tokamaks: control, performance, and extrapolability issues for ITER. *Nucl. Fusion* **54**, 114016 (34pp).

[32] Manuar, O. & Jaggard, D.L. (1995) Backscatter signatures of knots. *Opt. Lett.* **20**, 115–117.

[33] Manuar, O. & Jaggard, D.L. (2001) Knots, symmetry, and scattering. *IEEE Trans. Ant. Prop.* **49**, 1299–1304.

[34] Massey, W.S. (1977) *Algebraic Topology. An Introduction.* Springer-Verlag, New York, 136–141.

[35] Milnor, J. (1953) On total curvatures of closed space curves. *Math. Scan.* **1**, 289–296.

[36] Moffatt, H.K. (1969) The degree of knottedness of tangled vortex lines. *J. Fluid Mech.* **35**, 117–129.

[37] Moffatt, H.K. (1985) Magnetostatic equilibria and analogous Euler flows of arbitrarily complex topology. Part I. Fundamentals. *J. Fluid Mech.* **159**, 359–378.

[38] Moffatt, H.K. (1992) Relaxation under topological constraints. In *Topological Aspects Of The Dynamics Of Fluids And Plasmas* (ed. H.K. Moffatt *et al.*). Kluwer, Dordrecht, 3–28.

[39] Moffatt, H.K. & Ricca, R.L. (1992) Helicity and the Călugăreanu invariant. *Proc. R. Soc. A* **439**, 411–429.

[40] Moore, D.W. & Saffman, P.G. (1972) The motion of a vortex filament with axial flow. *Phil. Trans. R. Soc. Lond. A* **272**, 403–429.

[41] Murasugi, K. (1991) On the braid index of alternating links. *Trans. Amer. Math. Soc.* **326**, 237–260.

[42] Oersted, M.J.C. (1820) Sur un effet que le courant de la pile excite dans l'aguille aimantée. *Journal de physique, de chimie, d'histoire naturelle et des arts* **91**, 72–76.

[43] O'Hara, J. (1991) Energy of a knot. *Topology* **30**, 241–247.

[44] Pevtsov, A.A., Berger, M.A., Nindos, A., Norton, A.A. & Van Driel-Gesztelyi, L. (2014) Magnetic helicity, tilt, and twist. *Space Sci. Rev.* **186**, 285–324.

[45] Pohl, W.F. (1968) The self-linking number of a closed space curve. *J. Math. Mech.* **17**, 975–985.

[46] Ricca, R.L. (1994) The effects of torsion on the motion of a helical vortex filament. *J. Fluid Mech.* **273**, 241–259.

[47] Ricca, R.L. (1995) The energy spectrum of a twisted flexible string under elastic relaxation. *J. Phys.* A **28**, 2335–2352.

[48] Ricca, R.L. (1996) The contributions of Da Rios and Levi-Civita to asymptotic potential theory and vortex filament dynamics. *Fluid Dyn. Res.* **18**, 245–268.

[49] Ricca, R.L. (2008) Topology bounds energy of knots and links. *Proc. R. Soc. A* **464**, 293–300.

[50] Ricca, R.L. & Maggioni, F. (2008) Multiple folding and packing in DNA modeling. *Comput. Math. Appl.* **55**, 1044–1053.

[51] Ricca, R.L. & Moffatt, H.K. (1992) The helicity of a knotted vortex filament. In *Topological Aspects Of The Dynamics Of Fluids And Plasmas* (ed. H.K. Moffatt *et al.*). Kluwer, Dordrecht, 225–236.

[52] Ricca, R.L., Samuels, D.C. & Barenghi, C.F., (1999) Evolution of vortex knots. *J. Fluid Mech.* **391**, 29–44.

[53] Rodrigues Costa, S.I. (1990) On closed twisted curves. *Proc. Am. Math. Soc.* **109**, 205–214.

[54] Saffman, P.G. (1992) *Vortex Dynamics*. Cambridge University Press, Cambridge.

[55] Seehafer, N. (1990) Electric current helicity in the solar atmosphere. *Sol. Phys.* **125**, 219–232.

[56] Société Française de Physique (ed.) (1885) *Collection De Mémoires Relatifs A La Physique* **2**. Gauthier-Villars, Paris.

[57] Tait, P.G. (1877) Note on the measure of beknottedness. *Proc. Royal Soc. Edin.* **9**, 289–298.

[58] Tait, P.G. (1877) On knots I. *Trans. Roy. Soc. Edin.* **28**, 145–190.

[59] Tait, P.G. (1884) On knots II. *Trans. Roy. Soc. Edin.* **32**, 327–342.

[60] Tait, P.G. (1885) On knots III. *Trans. Roy. Soc. Edin.* **32**, 493–506.

[61] von der Mosel, H. (1999) Elastic knots in Euclidean 3-space. *Ann. Inst. H. Poincaré* **16**, 137–166.

[62] Weyl, H. (1911) Über die asymptotische Verteilung der Eigenwerte. *Nachrichten der Königlichen Gesellschaft der Wissenschaften zu Göttingen* **2**, 110–117.

[63] Werner, D.H. (1999) Radiation and scattering from thin toroidally knotted wires. *IEEE Trans. Ant. Prop.* **47**, 1351–1363.

[64] White, J H. (1969) Self-linking and the Gauss integral in higher dimensions. *Am. J. Math.* **91**, 693–728.

[65] Wolfram Research, Inc. (2010) *Mathematica*® (Version 8.0). Champaign, IL.

[66] Woltjer, L. (1958) A theorem on force-free magnetic fields. *Proc. Natl. Acad. Sci. USA* **44**, 489–491.

[67] Xanthopoulos, P. *et al.* (2014) Controlling turbulence in present and future stellarators. *Phys. Rev. Lett.* **113**, 155001 (4pp).